MASTER OF SCIENCE IN ELECTRICAL AND ELECTRONIC ENGINEERING

Development of an Adaptive Neuro-Fuzzy Controller for Speed Control of Induction Motor Drives

By

Md. Riyasat Azim

Department of Electrical and Electronic Engineering
Islamic University of Technology (IUT)
Gazipur-1704, Bangladesh.
July, 2012.

CERTIFICATE OF APPROVAL

The thesis titled "Development of an Adaptive Neuro-Fuzzy Controller for Speed Control of Induction Motor Drives" submitted by Md. Riyasat Azim, Student number: 092610 of Academic Year 2009-2010 has been found as satisfactory and accepted as partial fulfillment of the requirement for the degree of Masters of Science in Electrical and Electronic Engineering on 26 July, 2012.

Board of Examiners

1.

…….

Dr. Md. Ashraful Hoque — Chairman (Supervisor)
Professor,
Department of Electrical and Electronic Engineering,
Islamic University of Technology (IUT), Boardbazar, Gazipur.

2.

…….

Dr. Md. Shahid Ullah — Member (Ex-Officio)
Professor and Head,
Department of Electrical and Electronic Engineering,
Islamic University of Technology (IUT), Boardbazar, Gazipur.

3.

…….

Dr. Md. Ruhul Amin — Member
Professor,
Department of Electrical and Electronic Engineering,
Islamic University of Technology (IUT), Boardbazar, Gazipur.

4.

…….

Dr. Muhammad Fayyaz Khan — Member (External)
Professor,
Department of Electrical and Electronic Engineering,
United International University (UIU), Dhanmondi, Dhaka.

Declaration of Candidate

It is hereby declared that this Thesis or any part of it has not been submitted elsewhere for the award of any Degree or Diploma.

Dr. Md. Ashraful Hoque
Supervisor and Professor,
Department of Electrical and Electronic Engineering,
Islamic University of Technology (IUT), Boardbazar,
Gazipur-1704, Bangladesh.

Md. Riyasat Azim
Student No. - 092610
A.Y.: 2009-2010

DEDICATION

This thesis is dedicated to my beloved parents, my loving sister and all well wishers helping me to accomplish this work.

Acknowledgements

First I would like to thank my creator who provided me this opportunity to study in Islamic University of Technology and then blessed me with the most precious gift of physical and mental health during the whole study period. Then my supervisor Dr. Md. Ashraful Hoque, who played the vital role by giving valuable guidelines and technical support. He is the person who played the instrumental role behind this work and his motivation in every possible stage is the key to the completion of this thesis. This work might not have been possible without his guidance. I am thankful to Dr. Kazi Khairul Islam and Dr. Md. Ruhul Amin for their valuable suggestions and guideline during my research which encouraged me to improve the work further. Then, I am also indebted to Dr. Md. Shahid Ullah, Head of the Electrical and Electronic Engineering Department for rendering the administrative support and also for his useful suggestions.

I am also grateful to Md. Golam Sarowar and Md. Ashik Ahmed for their cooperation in my research. I want to give many thanks to other graduate students, faculty members and staffs of my department at Islamic University of Technology.

Last but not least, I like to thank my parents and sister, colleagues and friends for their supplications, patience and moral encouragement to do this job well in time.

Md. Riyasat Azim

Abstract

Robust and precise speed control is of critical importance in high performance drive applications. Control schemes for AC machines are complicated as compared to DC machines since they exhibit nonlinear relationships between process variables e.g. speed and manipulated variables e.g. current, torque etc. Direct torque control (DTC) scheme offers faster and simpler control of AC machines with high dynamic performance but without extensively using coordinate transformations and hence with lesser computational burden on the processor. Artificial intelligent controllers (AIC) are capable of overcoming the limitations of the mathematical model dependent conventional fixed gain and existing adaptive controllers. In this thesis, an adaptive neuro-fuzzy inference system (ANFIS) based controller is proposed to improve the dynamic behavior of DTC based induction motor drive which offers the combined advantages of the flexibility of fuzzy logic and adaptability of neural networks. Hence the developed adaptive neuro-fuzzy controller can be utilized to minimize the effects of unavoidable system disturbances such as, system parameter variations, sudden impact of load changes etc. Since the use of intelligent controllers are very limited in the drives industry due to the relevant computational burden on the microprocessor, therefore, in order to reduce the computational burden, linear linguistic variables with an optimum number of membership functions have been selected for the adaptive neuro-fuzzy controller developed in this thesis. The effectiveness of the proposed NFC based DTC scheme of the IM drive is consolidated through the development of a simulation model using MATLAB/Simulink. The results obtained from the simulation of the proposed system are compared with the results from simulation of the same system using conventional proportional integral (PI) controller. The results have shown promising improvements both in the transient and steady state responses of the system. Further, as an integral part of the thesis, a fuzzy logic controlled dynamic voltage restorer (DVR) system has been developed in order to protect the induction motor drive system from the power quality problems (like- voltage sag, swell etc.). The DVR system was developed and simulated in MATLAB/Simulink environment to verify its functionality. The simulation results have confirmed the ability of the DVR system to perform at an expected level when used in conjunction with the induction motor drive. The DVR system kept the induction motor drive performance intact under both symmetrical and asymmetrical system fault conditions.

Table of Contents

List of Figures

List of Tables

List of Symbols

K_p	Proportional gain
K_i	Integral gain
e_T	Torque error
$\overline{i_r}$	Rotor current phasor in rotor reference frame
$\overline{i_r}'$	Rotor current phasor in stator reference frame
$\overline{v_r}$	Rotor voltage in rotor reference frame
$\overline{v_r}'$	Rotor voltage in stator reference frame
ψ	Magnetic flux linkage
$\psi_{s\alpha}\psi_{s\beta}$	Real and imaginary component of stator magnetic flux linkage
$\psi_{sd}\psi_{sq}$	Real and imaginary component of rotor magnetic flux linkage
ψ_{sr}	Radial component of stator flux linkage
ψ_{st}	Tangential component of stator flux linkage
ψ_{so}	Residual flux linkage
$\psi_{sa}, \psi_{sb}, \psi_{sc}$	Flux linkage of phase a, b, c
ψ_s, ψ_r	Net stator and rotor flux
v_a, v_b, v_c	a, b, c phase voltages
i_a, i_b, i_c	a, b, c phase currents
$v_{s\alpha}, v_{s\beta}$	Real and imaginary component of stator voltage
$i_{s\alpha}, i_{s\beta}$	Real and imaginary component of stator current
R_s	Per phase stator resistance
R_r	Per phase rotor resistance
L_{sl}	Stator leakage inductance
L_{sm}	Stator magnetizing inductance
L_m	Mutual inductance
L_{rl}	Rotor leakage inductance
L_{rm}	Rotor magnetizing inductance
ω_m	Motor mechanical speed
ω_s	Synchronous speed of the induction motor
$\omega_m{}^*$	Reference or command speed of the motor
$\Delta\omega$	Difference between reference speed and actual speed
θ_m	Mechanical position angle of the rotor
γ	Angle between stator and rotor flux linkages
P	No. of pole pairs of the motor
T_e	Estimated torque
T_c	Command or reference torque
T_L	Load torque
J	Rotor inertia constant

B_m	Friction damping coefficient
H_ψ	Output of the flux hysteresis comparator
E_ψ	Flux error
$2HB_\psi$	Bandwidth of the flux hysteresis comparator
H_{Te}	Output of the torque hysteresis comparator
$2HB_{Te}$	Bandwidth of the flux hysteresis comparator
E_{Te}	Torque error

Chapter 1

Introduction

About fifty years elapsed from Faraday's initial discovery of electro-magnetic induction in 1831 to the development of the first induction machine by Nikola Tesla in 1888. He succeeded, after many years, at development of an electrical machine that didn't require brushes for its operation. This development marked a revolution in electrical engineering and gave a decisive impulse to the widespread use of polyphase generation and distribution systems. Moreover, the choice of mains frequency (50 Hz and 60 Hz) was established in the late 19th century because Tesla found it suitable for his induction machines. Now a day more than 60% of all the electrical energy generated in the world is used by the induction machines. Nevertheless induction machines (and AC machines in general) have been mostly used at fixed speed for more than a century. On the other hand DC machines have been used for variable speed applications using the Ward-Leonard configuration. This however requires three machines (two DC machines and an induction motor) and is therefore bulky, expensive and requires careful maintenance.

With the advances of power electronics, new impulse was given to variable speed applications of both DC and AC machines. The former typically used thyristor controlled rectifiers to provide high performance torque, speed and flux control. The variable speed induction motor drives mainly use pulse width modulation (PWM) techniques to generate polyphase supply of a given frequency. Most of the induction motor drives are based on keeping a constant voltage/frequency (V/f) ratio in order to maintain a constant flux in the machine. Although the control of V/f drives is relatively simple, the torque and flux dynamic performance is extremely poor. As a consequence, great quantities of industrial applications that require good torque, speed or position control still use DC machines. The advantages of induction machines are clear in terms of robustness and price; however it was not until the development and implementation of the vector control method [also called field oriented control (FOC)] that the induction machines were able to compete with DC machines in high performance applications. The principle behind

vector control methods is that the machine flux and torque are controlled independently, in a similar fashion to a separately excited DC machine. But at the same time it introduces the computational complexity of co-ordinate transformations and vector modulators. Considering the drawback of the field oriented control scheme, direct torque control (DTC) method was introduced which does not require the cumbersome co-ordinate transformations and vector modulators for its operation while performing at the same level of field oriented control. Because of its advantages, DTC became the focus of the research and development activities in the recent times.

Alongside these highly efficient control methods, advance controllers are gaining popularity in the modern industrial drive realm and artificial intelligence controllers are at the core of it. With the advancement and increased performance demand from the industrial drive systems, it became necessary to introduce controllers with high efficiency as well as precise and adaptive controllability. Because of these quintessential features, artificial intelligence methods were introduced in the process of controller development with the likes of fuzzy logic, neural networks and neuro-fuzzy systems are in the forefront of it. Because of their design flexibility, lesser dependence on system mathematical models and adaptability, these artificial intelligence controllers have become the focus of research activities in area of controller development in recent times.

1.1 Electric Motor Applications

Electric motors are the workhorse of the manufacturing industry and they also play a key-role in the transportation industry. Variable speed drives are used in all industries to control precisely the speed of electric motors driving loads ranging from pumps and fans to complex drives on paper machines, rolling mills, cranes, traction systems and similar drives. In order to understand the requirements for adjustable speed drives, an overview about the fields of electrical motor applications is mentioned. Of the total number of electrical machine applications, less than 10 % require an adjustable speed drive [1]. Due to the increased demand for flexibility in manufacturing and due to the urge for rational use of electrical energy, the percentage is rapidly growing [2].

• *Constant torque*: The requirement is to maintain torque constant independently of the speed. This is used in conveyors, mixers, screw feeders, extruders and positive displacement pumps for example, accounting for the majority of the electrical machine applications. These applications have high friction loads with little or no inertia, requiring starting torque much higher than rated.

• *Variable torque (continuously variable load):* Low torque is needed at low speeds and high torque at high speeds. This is used for centrifugal loads such as fans, pumps and blowers, being second place in number of applications. Speed can be controlled to adjust air or liquid flow.

• *Constant power:* High torque is needed at low speeds and low torque at high speeds. This is used in the machine tool industry, e.g. cutters and lathes, where usually DC motors are used. Motor applications for electric vehicles could also be classified under this category. Crucial factors, affecting the choice of an adjustable speed drive, include among others: rating, cost, speed range, efficiency, speed regulation, braking requirements, reliability, power factor, power supply availability, environmental considerations, [3]. The basic applications of electrical motors show that motion control of an electrical machine can be focused to one or more of the following objectives: Speed, torque and position control.

1.2 Alternating Current Motors

In the past, DC motors were used extensively in applications where high performance variable speed operation and controlled torque were required. In a separately excited DC motor, flux and torque can be easily controlled by the field and armature currents. The main drawback of the DC motors is the use of a commutator and brushes. This leads to constant maintenance, limited use in explosive environments and limited use in high-speed and high-voltage applications.

Alternating current motors present several advantages over their DC counterparts: they are more robust and smaller for the same power rating. This means lower rotating mass that can be translated into higher operating speeds and faster acceleration. The induction motor advantages also include the lack of electrical connections that can generate sparks or dust. Thus, they are suitable for explosive environments, clean-room areas and for low maintenance applications.

Among alternating current motors, induction motor and permanent magnet synchronous motor are the most prominent names. In comparison with the other AC machines, the induction motors

have the simplest of the constructions, hence the implementation of the speed control methods for the induction motors are simpler, efficient, precise and economic. In recent times, induction motors are gaining popularity in the adjustable speed drive market even more than before. However, a major impetus to the use of the permanent magnet synchronous motor (PMSM) has been caused by the introduction of neodymium-iron-boron materials in 1983. Magnets are used to produce the magnetic field rather than employing a magnetizing component of stator current as in the induction motor. Furthermore, there is no equivalent of the loss in the rotor bars of an induction motor. Significant advantages arise from the simplification in construction, the reduction of losses and the efficiency improvement. Currently, induction motors and PMSM are being used extensively in applications requiring high-dynamic and accurate control of both speeds and position.

Apart from induction motor drives and PMSM, there is a wide variety of different electrical AC motors available for use with variable speed drives, e.g. brushless DC motor, switched reluctance motor, synchronous reluctance motor. No single motor type is ideal for all applications. However, the former are usually used for high performance drive applications and they form the motor types considered extensively within literature.

In the last three decades, important advances in the power semiconductor and control technology areas have led to new adjustable speed-drives for AC motors. Unfortunately, AC motor mathematical models are much more complex than those of the DC motor and thus require more complex control schemes and more expensive power converters to achieve speed and torque control. Using advanced control approaches like field-oriented control (FOC) or direct torque control (DTC), a dynamic performance at least equivalent to that of a DC motor can be achieved.

1.3 Induction Motors

Induction motor is the most popular electromechanical energy conversion device for the industry due to its simple and robust construction. Depending on the demand, IMs are manufactured from fraction to thousands of horse powers. Based on the construction of the rotor, IMs are classified as wound rotor type and squirrel cage rotor type. Almost 90% of the industrial IMs are squirrel cage rotor type. The typical advantages of squirrel cage rotor type are rugged structure, no electrical connection to the rotating part, efficient high overload capability, low cost, compact,

least maintenance requirement and due to inaccessible rotor it can work even in the most volatile environment. The wound type IM has only edge that the rotor is accessible. This feature might be used to improve the starting torque. A cross-sectional view of the IM is shown in Fig.1.1, clearly showing the rotor and stator windings.

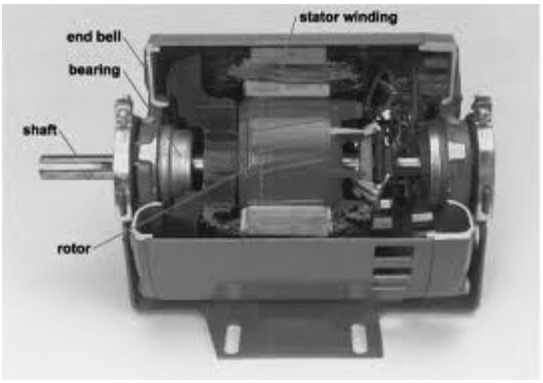

Fig.1.1: Induction Motor [2]

The rotor of a squirrel cage induction motor is shown in Fig.1.2.

Fig.1.2: Rotor of a squirrel cage Induction Motor [2]

AC induction motors are the most common motors used in industrial motion control systems, as well as in mains powered home appliances. Simple and rugged design, low-cost, low maintenance and direct connection to an AC power source are the main advantages of AC induction motors. AC induction motor design is quite simple and its speed depends upon the three basic parameters namely –

1. The fixed number of winding sets (known as poles) built into the motor, which determines the motor's base speed.

2. The frequency of the AC line voltage. Variable speed drives change this frequency to change the speed of the motor.
3. The amount of torque loading on the motor, which causes slip.

The induction motor has further advantages over the other types of AC machines because of it being the lowest cost motor for applications requiring more than about 1/2 HP (325 watts) of power. This is due to the simple design of the induction motors. For this reason, induction motors are overwhelmingly preferred for fixed speed applications in industrial applications and for commercial and domestic applications where AC line power can be easily attached. Over 90% of all motors are AC induction motors. They are found in air conditioners, washers, dryers, industrial machinery, fans, blowers, vacuum cleaners, and many, many other applications. The simple design of the induction motors also results in extremely reliable, low maintenance operation. Unlike the DC motor, there are no brushes to replace. If run in the appropriate environment for its enclosure, the induction motors can expect to need new bearings after several years of operation. If the application is well designed, an induction motor may not even need new bearings for more than a decade. Among the AC machines, the squirrel-cage induction motor has additional advantages: it is simple and rugged and is one of the cheapest machines available.

However, speed control and position control is complex and in the expensive side but only slightly in comparison with its DC counterpart of the same capability. The electronics required to handle an AC inverter drive are considerably more expensive than those required to handle a DC motor. However, if performance requirements can be met, meaning that the required speed range is over 1/3rd of base speed, AC inverters and AC motors are usually more cost-effective than DC motors and DC drives for applications larger than about 10 HP, because of cost savings in the AC motor. Because of all these advantages and industrial demand of the AC induction motors, this work focuses on the development of a precise speed control system for the induction motors using intelligent controller.

1.4 Control Methods for AC Machines

Control technology of AC motor drives has improved dramatically during the last two decades. This trend owes its progress to the new control techniques and philosophies developed by several researchers around the world. The implementation of those concepts was possible due to

technological developments such as the digital signal processor based controllers and the new power semiconductors.

Variable speed or adjustable torque control of electrical motor drives are crucial components in almost all modern industrial manufacturing processes. Traditionally variable speed electric machines were based on DC motors, but, for the last 20 years, the inverter-fed AC motors have largely taken over as the preferred solution for variable speed applications. For low performance applications, open loop voltage/frequency control strategies are employed. Considering high-performance motion control, field oriented control (FOC), or more recently direct torque control (DTC) are used. Using these techniques, both the induction motor and the permanent magnet synchronous motor (PMSM) can be applied even in high performance servo applications that were once the exclusive domain of the DC machines. Both FOC and DTC are strategies that allow torque and flux to be decoupled and controlled independently. Compared to the DC machine, the AC motor drive control strategy effectively becomes similar. Among the two most prominent strategies, DTC has the edge over the FOC since it offers lesser computational burden on the processor and it also offers simpler implementation and faster control. Moreover it is a comparatively newer method and modern research is focused around its development and real time implementation issues. Hence this work also concentrates in the DTC as the control strategy of the induction motor drive.

1.5 Literature Review

All the advancements in motor drives are thankful to the revolution of power electronics, signal processing techniques implemented on platforms using microprocessor and digital signal processors (DSPs). After 1970s these devices have made it economically possible to apply new algorithms for the motor control schemes. The only requirement to implement a high performance drive system is the availability of a voltage source with variable amplitude and frequency. Before the advancement of power electronics, the only option to change the motor field was to vary its number of poles. That method was very costly with very little flexibility. Alongside it is very much essential to implement a suitable and efficient control scheme for controlling the motor. The control scheme should be capable of providing high dynamic performance over a wide speed and torque limits at the same time it should be simple, fast and efficient thus providing a reduced response time for the controller.

1.5.1 Literature Review on Control Schemes

The ideal goal of a control scheme is that the machine follows the command trajectory and it operates within the rated parameters with maximum efficiency. The controller can be implemented to control either the speed of the motor or the torque of the motor depending upon the purpose it is being designed to serve. When variable speed drive (VSD) operates in the 'Torque Control' mode, its speed is left uncontrolled and is determined by the load. Similarly, in 'Speed Control' mode, the torque is left uncontrolled and is determined by the load. Principally, there are two major control strategies. The first primitive one is the scalar or non-vector control used for low performance drives. This scheme uses the stator voltage or current as the control parameter for speed or torque control respectively. The basic idea is to keep the stator field constant by varying the magnitude of the voltage/ current and frequency [4]. The main advantage of this scheme is the simplicity and it can be used in both feed forward and feedback loops. The major disadvantages are its low accuracy and its unsatisfactory response under transient conditions although its response is satisfactory under steady state conditions [5, 6]. Due to its simplicity, this scheme is still used by the industries.

Contrarily, in vector control scheme both the magnitude and the phase angle of the alternating current (manipulated variable) are controlled. It means the position vector of the manipulated variable is known after each sampling time for discrete control scheme. These characteristics, contrary to the scalar control system, enable the controller to control both the transient and steady state conditions of the system [7, 8]. In vector control of AC machines, the torque and flux producing components are decoupled (being orthogonal to each other) and are controlled independently like a separately excited DC machine [9]. These schemes do the same job but in a different way. They control the motor torque and flux in order to track the command trajectory irrespective to the system conditions and disturbances. Both schemes have been successfully implemented by the industry for high performance drives. The major drawback of the vector control schemes is the computational burden rendered by the vector coordinate transformations as well as the motor parameter dependence of the whole method [10].

For vector control of AC motors, the concept of field oriented control (FOC) was introduced by Blasekke in 1970s [11]. The stator current is transformed into its real (flux producing) and imaginary (torque producing) components. Orthogonal nature of these components makes it

feasible to control them independently [12, 13]. This scheme due to its accuracy is used in the high performance drives. The drawback compared to scalar control is that this scheme for its implementation needs a lot of computation for conversion of parameters to a reference frame. This drawback is not of significant importance after the common use of microprocessors. After its sensorless application by Toyo Electric Mfg. Co. Ltd. Japan, this technique became gradually more popular in the industry [14].

The direct torque control was introduced by Takahashi and Depenbrock in 1980s [15, 16]. The idea to control an IM using direct torque control is quite similar to the FOC in the sense that both the motor field and torque are controlled independently. The difference is that in FOC the motor torque and stator flux linkage are controlled indirectly by the imaginary and real component of the stator current respectively. While in DTC these quantities are controlled directly. Therefore, DTC is faster than FOC. The coordinate transformations and pulse width modulation (PWM) regulators are not necessary in DTC as those were in FOC. The DTC scheme is only sensitive to stator resistance which is a static component and undergoes comparatively smaller variations during operations as compared to rotor resistance. These aspects make DTC scheme simpler for computations [17, 18]. The DTC scheme for control of AC machines is becoming more popular since its first sensorless application introduced by ABB in 1995 [19]. According to ABB, the DTC is the ultimate and most advanced AC drive technology. The DTC is almost ten times faster for any AC or DC drive as compared to FOC. The dynamic speed accuracy is eight times than any open loop AC drive and comparable to a DC drive that is using feedback [20]. The current industry is looking for a simple, reliable, faster, efficient, low noise producing and economical motor drive scheme. The only available variable speed drive matching most of the desired requirements is an IM drive with DTC scheme.

1.5.2 Literature Review on Controllers

The mathematical model of an IM is nonlinear. Researchers have developed different controllers for this nonlinear model of the IM. The Proportional-Integral-Derivative (PID) controller was in use for governor design system since long time. But the first analysis of the PID controller was made by Minorshy [21]. Due to its simplicity and acceptable results this most primitive controller is still used in the industry. The derivative part of the controller creates problem in real time implementation. It amplifies noise and needs a low pass filter (LPF) for its operation.

Therefore the most common form of this controller is proportional-integral (PI) controller which excludes the derivative part. The working of the PI controller is explained in Fig. 1.3. The acronyms SP, PV and MV stands for the set/ reference point, process/ measured variable and manipulated variable respectively. Mathematically the output of the PI controller may be described by the following relation:

$$u = K_p.e(t) + K_i \int_0^t e(\tau)\, d\tau \tag{1.1}$$

Where, 'e' is the difference between the reference and measured values of the control variable. The PI controller is characterized by high overshoot and almost no steady state error. The overall performance of the conventional PI controller is compromising because it does not have any direct knowledge of the process. The fixed gain PI controller is inherently sensitive to parameter variations and disturbances of the system and is difficult to use in high performance drives [22].

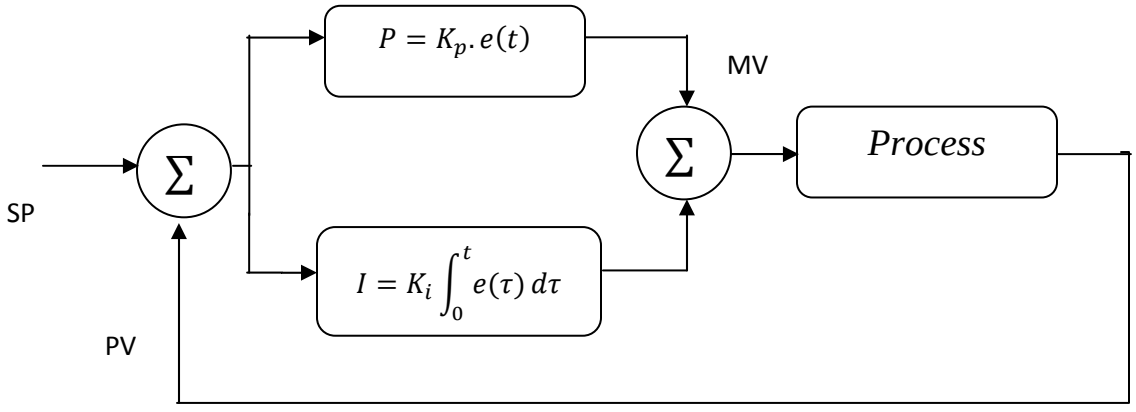

Fig.1.3: Closed Loop Block Diagram of a Conventional PI Controller

The researchers proposed different techniques to overcome the inherited problems with a PI controller [23, 24]. They tuned the parameters of a PI controller using both off-line [23] and online [24] methods. However the new controller introduced complex tuning rules and requires very long sampling time up to 50 ms, which is not acceptable for high performance drives.

The problem of sensitivity to system parameter change and disturbances was resolved by the introduction of adaptive controllers. The idea behind the adaptive controller is that they update the system parameters at each sampling time. Researchers have proposed mainly three types of adaptive controllers [25-27]. These controllers modify the control laws to mitigate the parameter

changes and system disturbances. This is achieved by changing the system gains in such a way to converge the tracking error between reference and the actual machine models.

Sliding mode control (SMC) is comparatively a simpler adaptive technique [28, 29]. Due to discrete nature of control system and limitation of sampling time this technique causes motor chattering around set points [30]. These vibrations cause stress on the load and can damage the motor bearings. The latest nonlinear control technique, called adaptive back-stepping (AB) control technique was introduced in 1990s [31]. This recursive technique is called back-stepping because it starts with some virtually stable system and progressively steps back to the actual system guaranteeing stability at each step [32]. This method was used along with field oriented control principle to control IM by Tan et. al. [33]. The major problem with this technique is the availability of finding an absolutely correct mathematical model of the IM.

The researchers [34-36] claimed that, under ideal conditions it is possible to design globally stable adaptive systems. But it was proved that for modeling errors (e.g. bonded disturbances and/or un-modeled dynamics), the adaptive scheme designed for ideal conditions may go unstable [37]. The main reason for this instability was the adaptive law for estimation of parameters that made the closed loop system nonlinear and more susceptible to modeling errors.

The precise dynamic control of IM is complicated by the nonlinear relation between the winding currents (manipulated variable) and rotor speed (process variable). The nonlinearity in the motor developed torque due to the magnetic saturation of the core adds further complexity for the controller [38]. The core advantage of the artificial intelligent (AI) controllers is that they don't need the exact mathematical model of the system and it can cope with system nonlinearities and disturbances [39]. The requirement for AI controllers for high performance variable speed drives proper functioning is the approximate system mathematical model to handle the system nonlinearities and disturbances [40-42].

The basic concept for the first type of artificial intelligent controllers (AIC), called the fuzzy logic controller (FLC) was introduced by Lotif Zadeh [43]. Both fuzzy sets and fuzzy logic are based on the pattern the human brain deals with inaccurate information. The performance of the fuzzy logic control and decision system depends on the input and output membership functions, the fuzzy logic rules and the fuzzy inference mechanism. Ideally, the FLC can handle any kind of system nonlinearities [44]. Many researchers developed different FLCs based on their experience

of the drive behavior, for the FOC/ DTC based IM drives [45-52]. Most of the times, in DTC scheme, the researchers have used FLC to replace the flux/ torque hysteresis controllers. The FLC has been used to improve the torque response of the DTC based IM drive by replacing the conventional hysteresis comparators [45-48]. The target is to convert the fixed hysteresis bandwidth to a variable parameter dependent on the torque/ speed variations. But the use of extensive membership functions and rules make the system cumbersome. Especially the author of [46] has used 180 fuzzy rules which are almost impossible to implement in real time. Most of the reported works on the FLC based drive system is provided in simulation only due to the high computational burden. Therefore in this thesis instead of a complicated FLC, the conventional simple linear hysteresis controller model is used to achieve the optimum torque ripple and switching frequency of the voltage source inverter (VSI).

The artificial neural networks (ANN) has preference over the FLC that they are capable of learning the desired mapping between the inputs and outputs of the drive system stability and they don't require too much knowledge about the system behavior as well [53]. The ANNs are modeled after the physical architecture of the brain to solve a problem. The accuracy of the performance of an ANN is based on the computational function of the neurons and the structure of the network [54]. The researchers have used ANN to produce the VSI input voltage vector from the error signals [55, 56]. The author of [55]has used two neural networks. The first ANN finds position of the stator flux linkage vector. Though, the DTC scheme for its operation just required the sector where the flux linkage vector is lying and not its actual position. The second ANN is used just to replace the conventional DTC table without modifying its functionality. The author of [56] has also used the artificial intelligence to produce the look up tables. Both the citations don't have real time results.

To improve the speed response, another work on DTC scheme has been reported by the researchers et. al.[57]. The authors in this work have used a hybrid controller, switching PI controller for steady state and a FLC for transient states. The switching mechanism is based on the magnitude of the speed error. The switching transition of the controller always create real time problem. Further PI controller is used in steady state which is highly sensitive to motor parameters and system disturbances. Even FLC has no learning mechanism and is designed based on trial and error.

1.6 Problem Identification and Thesis Motivation

After brief literature review, it is fair to say that induction motor is one of the most efficient motors in the drive technology. Faster response, quicker recovery from any disturbances and insensitivity to parameter variations are some of the main criteria in high performance drive system used in robotics, industrial processes and machine tools etc. As discussed in the literature review, the conventional controllers like – proportional integral (PI) controller, proportional integral derivative (PID) controllers are widely used in the control of both AC and DC machines. But these controllers are difficult to design since they are completely dependent on mathematical model of the system to be controlled. Moreover they are also sensitive to the parameter variations during the system operations and show no adaptability. Further, unknown load dynamics and other factors such as- noise, temperature adversely affect the performance of these controllers. The conventional adaptive controllers such as- model reference adaptive controller (MRAC), sliding mode controller (SMC), variable structure controller (VSC) and self tuning regulator (STR) are involved in the system with large number of unknown parameters. Moreover, these controllers are dependent upon system mathematical models. Hence unavailability of accurate system model often leads to cumbersome design approach for these controllers.

In modern times, an increasing interest in the application of artificial intelligence especially the hybrid combination of the neural network and fuzzy logic called the neuro-fuzzy systems in control applications has been observed. In high performance drive applications involving induction motors, the adaptive hybrid neuro fuzzy inference system can play a key role in speed control applications.

The primary motivation of this research work is to design a precise and efficient speed control of induction motor drive based on the adaptive neuro-fuzzy inference system (ANFIS). Since the direct torque control (DTC) scheme is simpler and faster than the field oriented control (FOC) scheme, it is declared as a control strategy for the induction motor drive speed control in this work. The biggest problem in this scheme is the large ripples in the torque and stator flux both in steady and transient states. As discussed in the literature, various researchers have suggested different schemes based on the complicated neuro-fuzzy techniques to reduce these ripples. Therefore, in this thesis, a new simple and very low computation intensive adaptive hybrid neuro

fuzzy inference system based speed controller is proposed and implemented in the speed control loop of a DTC based induction motor drive in order to achieve precise speed control and to reduce the motor torque and stator flux ripples. Moreover, a fuzzy logic controlled dynamic voltage restorer (DVR) is also developed in order to prevent power quality problems (i.e. voltage sag, swell, interruptions etc.) from interrupting the operation of the proposed ANFIS controller based direct torque control scheme based induction motor drive speed control system.

1.7 Thesis Organization

The remaining part of this thesis is organized in the following sequence.

Chapter -2 is devoted to the modeling of an induction motor for the direct torque control scheme. It covers the space phasor model of the induction motor as well as the mathematical relationships of torque and flux linkages in the motor.

Chapter-3 analyzes the conventional DTC scheme. Motor torque and flux linkages are elaborated and the factors affecting the production of these quantities are discussed.

Chapter-4 provides a detail discussion about the functioning of an adaptive hybrid neuro-fuzzy controller. Then a NFC has been proposed for improving the dynamic behavior of the DTC based IM drive. The detailed design of the proposed NFC including input/ output membership functions, the network structure and training methods of the network are also discussed in this chapter.

Chapter-5 discusses the simulation results obtained from the MATLAB/ Simulink simulation of the proposed system under various operation conditions.

Chapter-6 introduces the concept of the dynamic voltage restorer (DVR) for the induction motor drive and presents the development of the simulation model for the proposed DVR in Simulink platform and also discusses the results obtained from the simulations under different system fault conditions.

Chapter-7 summarizes the research work presented in this thesis and discusses the scope for future works also.

Chapter 2

Modeling of Induction Motor for Direct Torque Control

The design of any kind of controller is based on the plant/machine dynamic model. The tolerance levels for different machine models are entirely different due to machine ratings and design. The machine model should be simple so that it could be implemented easily and at the same time it should be so accurate to provide acceptable results. So, there exists a compromise between accuracy and economy. The transient and steady state behavior are entirely different in nature. The model must be capable of working in both states. Generally, an induction motor is modeled by using space-phasor or two axes theory [58]. In this thesis, the space-phasor theory is preferred since it provides more understanding of the physical image of the system.

For the induction motor, the following assumptions are made to derive the mathematical model:

- Rotor core never saturates
- Uniform air gap between rotor and stator windings
- Machine iron losses and effects are neglected
- Both stator and rotor windings are full pitched coils
- Slotting effects are neglected
- Unity winding factor
- Machine MMFs are pure sinusoidal centered on the magnetic axis of the respective winding.
- Zero Magnetic reluctance of the stator and rotor cores
- Flux density is radial in air gap between stator and rotor
- Symmetrical two pole machine
- Both rotor and stator have balanced three phase windings.

2.1 Induction Motor Space Phasor Model

2.1.1 Space Phasor Representation of Stator Flux Linkages

Space Phasor model of the induction machine is used to simplify the machine analysis for real time implementation and to have better understanding of the physical system [19]. The three phase stator current waveforms are shown in Fig.2.1. Corresponding to any instant of time (t) the three phase stator current phasor is shown in Fig.2.2 along with the α-β components.

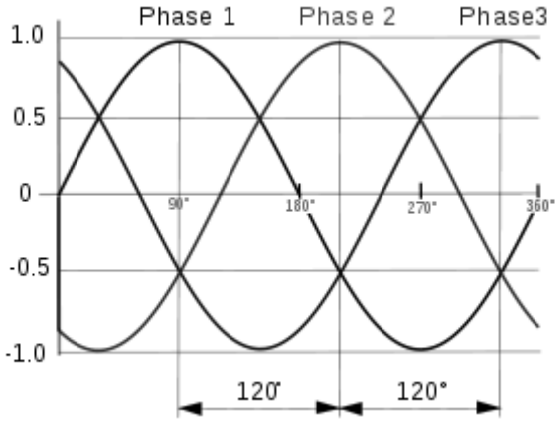

Fig.2.1: Three phase balanced current waveform [3]

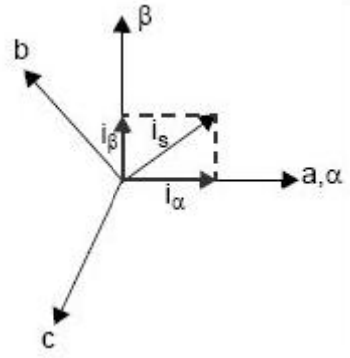

Fig.2.2: Three phase current phasor [3]

Where, α-β axes present the two phase stationary frame attached to the stator. The three phasors of IM flux linkages, produced by the stator currents are converted to a complex plane located in the cross section of the motor. The resultant flux linkage rotate with an angular speed equal to the three phase supply frequency. This single resultant space phasor can describe the rotating magnetic field like the regular three phases. This conversion of the system frame allows the

analysis in terms of complex algebra which is easier to comprehend. Similar analysis can be made for the other motor parameters like voltages etc.

Fig.2.3 (a) and (b) shows the stator currents in the three phase stator winding and stator and rotor current phasors of IM respectively. In both cases the net flux linkage rotates with the synchronous speed. For balanced three phase system, the resultant stator space phasor flux linkage can be expressed as follows:

$$\overrightarrow{\psi_s} = \frac{2}{3}\left[\overrightarrow{\psi_{sa}} + a\overrightarrow{\psi_{sb}} + a^2\overrightarrow{\psi_{sc}}\right] \tag{2.1.a}$$

or

$$\overrightarrow{\psi_s} = |\psi_s|\, e^{j\theta} \tag{2.1.b}$$

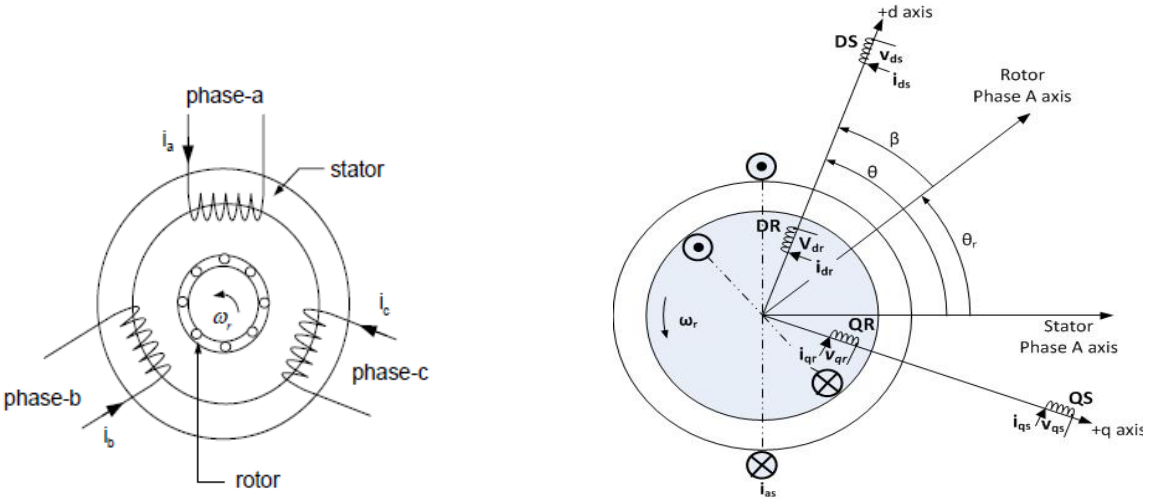

Fig.2.3: (a) Three phases of stator currents [4] (b) Equivalent phasor in two axes [4]

The α-β axes equivalent of IM stator winding is shown in Fig.2.3 (b). From α-β - axes equivalent of flux linkage vectors, the following mathematical relation can be easily deduced:

$$\overrightarrow{\psi_s} = \left[\overrightarrow{\psi_{sa}} + j\overrightarrow{\psi_{sb}}\right] \tag{2.2}$$

Comparing (2.1.a) and (2.2)

$$Re\left(\overrightarrow{\psi_s}\right) = Re\left\{\frac{2}{3}\left[\overrightarrow{\psi_{sa}} + a\overrightarrow{\psi_{sb}} + a^2\overrightarrow{\psi_{sc}}\right]\right\} = \overrightarrow{\psi_{s\alpha}} \tag{2.3}$$

$$Im(\overrightarrow{\psi_s}) = Im\{\frac{2}{3}[\overrightarrow{\psi_{sa}} + a\overrightarrow{\psi_{sb}} + a^2\overrightarrow{\psi_{sc}}]\} = \overrightarrow{\psi_{s\beta}} \quad (2.4)$$

Based on assumptions made in the opening paragraph of this chapter and considering only one stator and rotor winding for each phase, as single, multi-turn full pitch coils located on the two sides of the smooth air gap, the schematic diagram of IM is shown is shown in Fig.2.4. The phase windings of both stator and rotor are spaced 120 electrical degrees apart from each other. In the frame of reference attached to the stationary stator, the voltage equations for the stator are given as follows:

$$V_{sa} = R_s i_{sa} + \frac{d}{dt}(\psi_{sa}) \quad (2.5.a)$$

$$V_{sb} = R_s i_{sb} + \frac{d}{dt}(\psi_{sb}) \quad (2.5.b)$$

$$V_{sc} = R_s i_{sc} + \frac{d}{dt}(\psi_{sc}) \quad (2.5.c)$$

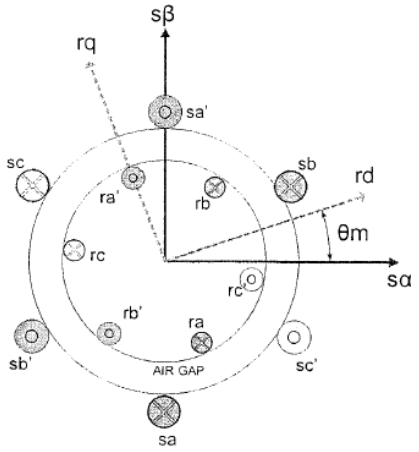

Fig.2.4: Schematic diagram of an IM winding [2]

Following the same pattern, the mathematical relations for the rotor voltages in the rotor's frame of reference can be expressed as:

$$V_{ra} = R_r i_{ra} + \frac{d}{dt}(\psi_{ra}) \quad (2.6.a)$$

$$V_{rb} = R_r i_{rb} + \frac{d}{dt}(\psi_{rb}) \quad (2.6.b)$$

$$V_{rc} = R_r i_{rc} + \frac{d}{dt}(\psi_{rc}) \quad (2.6.c)$$

Considering all the magnetic interactions between stator and rotor, the total flux linkage of each of the stator phase winding is given as follows:

$$\psi_{sa} = L_s i_{sa} + M_s i_{sb} + M_s i_{sc} + M_{sr} i_{ra} \cos\theta_m + M_{sr} i_{rb} \cos(\theta_m + \frac{2\pi}{3}) + M_{sr} i_{rc} \cos(\theta_m + \frac{4\pi}{3}) \quad (2.7.a)$$

$$\psi_{sb} = L_s i_{sb} + M_s i_{sa} + M_s i_{sc} + M_{sr} i_{rb} \cos\theta_m + M_{sr} i_{rc} \cos(\theta_m + \frac{2\pi}{3}) + M_{sr} i_{ra} \cos(\theta_m + \frac{4\pi}{3}) \quad (2.7.b)$$

$$\psi_{sc} = L_s i_{sc} + M_s i_{sa} + M_s i_{sb} + M_{sr} i_{rc} \cos\theta_m + M_{sr} i_{ra} \cos(\theta_m + \frac{2\pi}{3}) + M_{sr} i_{rb} \cos(\theta_m + \frac{4\pi}{3}) \quad (2.7.c)$$

Similarly for each of the rotor phase, the flux linkages are given as:

$$\psi_{ra} = L_r i_{ra} + M_r i_{rb} + M_r i_{rc} + M_{sr} i_{sa} \cos(-\theta_m) + M_{sr} i_{sb} \cos(-\theta_m + \frac{2\pi}{3}) + M_{sr} i_{sc} \cos(-\theta_m + \frac{4\pi}{3}) \quad (2.8.a)$$

$$\psi_{rb} = L_r i_{rb} + M_r i_{ra} + M_r i_{rc} + M_{sr} i_{sb} \cos(-\theta_m) + M_{sr} i_{sc} \cos(-\theta_m + \frac{2\pi}{3}) + M_{sr} i_{sa} \cos(-\theta_m + \frac{4\pi}{3}) \quad (2.8.b)$$

$$\psi_{rc} = L_r i_{rc} + M_r i_{ra} + M_r i_{rb} + M_{sr} i_{sc} \cos(-\theta_m) + M_{sr} i_{sa} \cos(-\theta_m + \frac{2\pi}{3}) + M_{sr} i_{sb} \cos(-\theta_m + \frac{4\pi}{3}) \quad (2.8.c)$$

Where, ψ, L and M represents flux linkage, self inductance and mutual inductance respectively. The first subscript (e.g. 'r' and's') stands for the rotor and stator of IM. θ_m represents the rotor mechanical angle with respect to the stationary stator frame.

Combining all equations from (2.1.a) to (2.8.c), the matrix form for the voltage mathematical model of IM can be obtained as:

$$\begin{bmatrix} V_{sa} \\ V_{sb} \\ V_{sc} \\ V_{ra} \\ V_{rb} \\ V_{rc} \end{bmatrix} = \begin{bmatrix} R_s + pL_s & pM_s & pM_s & pM_{sr}\cos\theta_m & pM_{sr}\cos\theta_1 & pM_{sr}\cos\theta_2 \\ pM_s & R_s + pL_s & pM_s & pM_{sr}\cos\theta_2 & pM_{sr}\cos\theta_m & pM_{sr}\cos\theta_1 \\ pM_s & pM_s & R_s + pL_s & pM_{sr}\cos\theta_1 & pM_{sr}\cos\theta_2 & pM_{sr}\cos\theta_m \\ pM_{sr}\cos\theta_m & pM_{sr}\cos\theta_2 & pM_{sr}\cos\theta_1 & R_r + pL_r & pM_r & pM_r \\ pM_{sr}\cos\theta_1 & pM_{sr}\cos\theta_m & pM_{sr}\cos\theta_2 & pM_r & R_r + pL_r & pM_r \\ pM_{sr}\cos\theta_2 & pM_{sr}\cos\theta_1 & pM_{sr}\cos\theta_m & pM_r & pM_r & R_r + pL_r \end{bmatrix} \begin{bmatrix} i_{sa} \\ i_{sb} \\ i_{sc} \\ i_{ra} \\ i_{rb} \\ i_{rc} \end{bmatrix} \quad (2.9)$$

Equation (2.9) can be written as:

$$\begin{bmatrix} V_{sa} \\ V_{sb} \\ V_{sc} \\ V_{ra} \\ V_{rb} \\ V_{rc} \end{bmatrix} = \begin{bmatrix} R_s & 0 & 0 & 0 & 0 & 0 \\ 0 & R_s & 0 & 0 & 0 & 0 \\ 0 & 0 & R_s & 0 & 0 & 0 \\ 0 & 0 & 0 & R_r & 0 & 0 \\ 0 & 0 & 0 & 0 & R_r & 0 \\ 0 & 0 & 0 & 0 & 0 & R_r \end{bmatrix} \begin{bmatrix} i_{sa} \\ i_{sb} \\ i_{sc} \\ i_{ra} \\ i_{rb} \\ i_{rc} \end{bmatrix} + p \begin{bmatrix} L_s & M_s & M_s & M_{sr}\cos\theta_m & M_{sr}\cos\theta_1 & M_{sr}\cos\theta_2 \\ pM_s & L_s & M_s & M_{sr}\cos\theta_2 & M_{sr}\cos\theta_m & M_{sr}\cos\theta_1 \\ pM_s & pM_s & L_s & M_{sr}\cos\theta_1 & M_{sr}\cos\theta_2 & M_{sr}\cos\theta_m \\ M_{sr}\cos\theta_m & M_{sr}\cos\theta_2 & M_{sr}\cos\theta_1 & L_r & M_r & M_r \\ M_{sr}\cos\theta_1 & M_{sr}\cos\theta_m & M_{sr}\cos\theta_2 & M_r & R_r + pL_r & pM_r \\ M_{sr}\cos\theta_2 & M_{sr}\cos\theta_1 & M_{sr}\cos\theta_m & M_r & M_r & L_r \end{bmatrix} \begin{bmatrix} i_{sa} \\ i_{sb} \\ i_{sc} \\ i_{ra} \\ i_{rb} \\ i_{rc} \end{bmatrix} \quad (2.10)$$

Where,

$$\theta_1 = \theta_m + \frac{2\pi}{3} \tag{2.11}$$

$$\theta_2 = \theta_m + \frac{4\pi}{3} \tag{2.12}$$

This model is non-linear since it contains the parameters like rotor position which is a non-linear function of time. Additionally, under saturation conditions, the inductances may vary with currents. This model is too complex because it contains a bundle of mutual inductances.

2.1.2 Space Phasor Model in Two Axes

Park's transformation can be used to convert a, b, c to α-β reference frame as:

$$\begin{bmatrix} V_{s0} \\ V_{s\alpha} \\ V_{s\beta} \end{bmatrix} = \frac{2}{3} \begin{bmatrix} 1/\sqrt{2} & 1/\sqrt{2} & 1/\sqrt{2} \\ \cos\theta & \cos(\theta - \frac{2\pi}{3}) & \cos(\theta + \frac{2\pi}{3}) \\ -\sin\theta & -\sin(\theta - \frac{2\pi}{3}) & -\sin(\theta + \frac{2\pi}{3}) \end{bmatrix} \begin{bmatrix} V_{sa} \\ V_{sb} \\ V_{sc} \end{bmatrix} \tag{2.13}$$

The inverse Park's transformation can be expressed as:

$$\begin{bmatrix} V_{sa} \\ V_{sb} \\ V_{sc} \end{bmatrix} = \frac{\sqrt{2}}{3} \begin{bmatrix} 1/\sqrt{2} & \cos\theta & -\sin\theta \\ 1/\sqrt{2} & \cos(\theta - \frac{2\pi}{3}) & -\sin(\theta - \frac{2\pi}{3}) \\ 1/\sqrt{2} & \cos(\theta + \frac{2\pi}{3}) & -\sin(\theta + \frac{2\pi}{3}) \end{bmatrix} \begin{bmatrix} V_{s0} \\ V_{s\alpha} \\ V_{s\beta} \end{bmatrix} \tag{2.14}$$

The rotor position angle is defined as:

$$\theta_m(t) = \int_0^t \omega_m \, dt + \theta_m(0) \tag{2.15}$$

Where, θ_m defines the position of the rotor and ω_m is the mechanical speed of the rotor.

Applying Park's transformation to (2.9),

$$\begin{bmatrix} V_{s\alpha} \\ V_{s\beta} \\ V_{rd} \\ V_{rq} \end{bmatrix} = \begin{bmatrix} R_s + pL_s & -p\theta L_s & pL_m & -L_m(p\omega_m + p\theta_m) \\ pL_s & R_s + pL_s & L_m(p\omega_m + p\theta_m) & pL_m \\ pL_m & L_m(p\theta_s - p\omega_m) & R_r + pL_r & p\theta_m L_r \\ L_m(p\theta_s - p\omega_m) & pL_m & p\theta_m L_r & R_r + pL_r \end{bmatrix} \begin{bmatrix} i_{s\alpha} \\ i_{s\beta} \\ i_{rd} \\ i_{rq} \end{bmatrix} \quad (2.16)$$

Since the end ring bars on a squirrel cage IM short circuit the conductors, therefore

$$V_{rd} = V_{rq} = 0$$

And for the synchronously rotating frame,

$$\omega_s = 0$$

Therefore,

$$\omega_r = -\omega_m$$

Applying these relationships to (2.16) we get,

$$\begin{bmatrix} V_{s\alpha} \\ V_{s\beta} \\ 0 \\ 0 \end{bmatrix} = \begin{bmatrix} R_s + pL_s & 0 & pL_m & 0 \\ 0 & R_s + pL_s & 0 & pL_m \\ pL_m & L_m p\omega_m & R_r + pL_r & p\theta_m L_r \\ -L_m p\omega_m & pL_m & -p\theta_m L_r & R_r + pL_r \end{bmatrix} \begin{bmatrix} i_{s\alpha} \\ i_{s\beta} \\ i_{rd} \\ i_{rq} \end{bmatrix} \quad (2.17)$$

This model is independent of the rotor position angle wm. It also involves comparatively fewer types of impedances than model in (2.9). Overall, this equation is much simpler compared to the relevant equation in three phasor form.

2.1.3. IM Space Phasor Model in Steady State

The stator and rotor voltage space phasor in the frame of reference attached to stationary stator can be written as:

$$\overrightarrow{V_s} = R_s \overrightarrow{\imath_s} + \frac{d}{dx}(\overrightarrow{\psi_s}) \quad (2.18)$$

$$\overrightarrow{V'_r} e^{-j\theta m} = R_r \overrightarrow{\imath'_r} e^{-j\theta m} + \frac{d}{dx}(\overrightarrow{\psi'_r} e^{-j\theta m}) \quad (2.19)$$

Equation (2.19) can be simplified as:

$$\overrightarrow{V'_r} = R_r\overrightarrow{\iota'_r} + \frac{d}{dx}\left(\overrightarrow{\psi'_r}\right) - j.p\omega_m\overrightarrow{\psi'_r} \tag{2.20}$$

Similarly, in general, the flux linkage space phasor with reference to the same stator frame of reference can be written as:

$$\overrightarrow{\psi_s} = L_s\overrightarrow{\iota_s} + L_m\overrightarrow{\iota'_r} \tag{2.21}$$

$$\overrightarrow{\psi'_r} = L_r\overrightarrow{\iota'_r} + L_m\overrightarrow{\iota_s} \tag{2.22}$$

Ideally, when an IM is supplied by a symmetrical sinusoidal supply, in steady state the space vectors behave like phasors. Hence the following mathematical relationships become valid in steady state condition.

$$\overrightarrow{V_s} = V_s \tag{2.23}$$

$$\frac{d}{dx}\left(\overrightarrow{\iota_s}\right) = j\omega_s I_s \tag{2.24}$$

$$\overrightarrow{V'_r} = V'_r e^{j\theta} \tag{2.25}$$

$$\frac{d}{dx}\left(\overrightarrow{\iota'_r}\right) = j\omega_r I'_r + jp\omega_m I'_r \tag{2.26}$$

The voltage equations (2.18) and (2.20) may be expressed as:

$$\overrightarrow{V_s} = R_s\overrightarrow{\iota_s} + \left(L_{sl} + \frac{3}{2L_{sm}}\right)\frac{d}{dt}\left(\overrightarrow{\iota_s}\right) + \frac{3}{2}L_{rm}\frac{d}{dt}\left(\overrightarrow{\iota'_r}\right) \tag{2.27}$$

$$\overrightarrow{V'_r} = R_r\overrightarrow{\iota'_r} + \left(L_{rl} + \frac{3}{2L_{rm}}\right)\frac{d}{dt}\left(\overrightarrow{\iota'_r}\right) + \frac{3}{2}L_{rm}\frac{d}{dt}\left(\overrightarrow{\iota'_r}\right) - jp\omega_m\{\left(L_{rl} + \frac{3}{2L_{rm}}\right)\overrightarrow{\iota'_r} + \frac{3}{2}L_{rm}\overrightarrow{\iota_s}\} \tag{2.28}$$

By applying the steady state equations from (2.23) to (2.26) and short circuit condition of the squirrel cage rotor, it is possible to achieve:

$$V_s = R_s I_s + j\omega_s\left(L_{sl} + \frac{3}{2L_{sm}}\right)I_s + j\frac{3}{2\omega_s L_{sm} I'_r} \tag{2.29}$$

$$0 = \frac{R_r}{s}I'_r + j\omega_s\left(L_{rl} + \frac{3}{2L_{sm}}\right)I'_r + j\frac{3}{2\omega_s L_{sm} I_s} \tag{2.30}$$

On the basis of these equations and using Kirchhoff's voltage law, the equivalent circuit for the IM under steady state can be drawn as Fig.2.5.

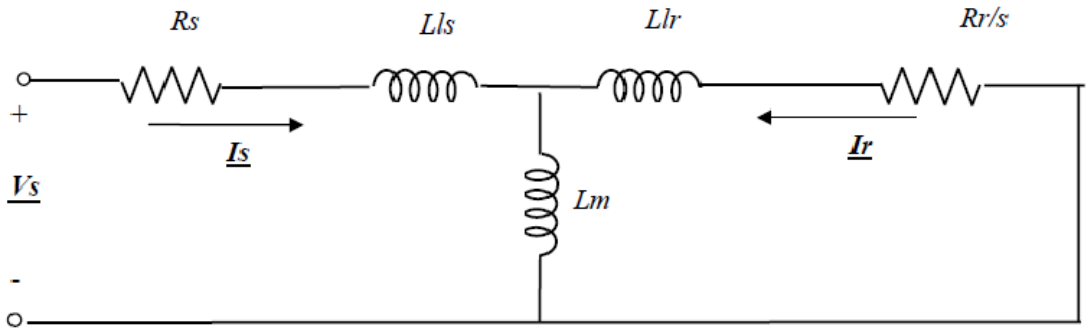

Fig.2.5: Model of Per Phase Equivalent Circuit of Induction Motor in Steady State

2.2 IM Torque Production

The developed torque of an IM for balanced three phases of IM is given by [19].

$$T_e = \frac{3}{2}(\overrightarrow{\psi_s} \, X \, \overrightarrow{\imath'_r}) \tag{2.31}$$

or

$$T_e = \frac{3}{2}\left(\frac{P}{2}\right)|\overrightarrow{\psi_s}||\overrightarrow{\imath'_r}| \sin\gamma \tag{2.32}$$

or

$$T_e = \frac{3}{2}\left(\frac{P}{2}\right)|\overrightarrow{\psi_s}||\overrightarrow{\psi_r}| \sin\gamma \tag{2.33}$$

Where, γ is the angle between the stator flux linkage, ψ_s and rotor flux linkage vectors, ψ_r . Equation (2.33) indicates that for maximum torque generation, the rotor and stator flux linkage vectors (ψ_s and ψ_r) must be orthogonal to each other. In DC machines, this feature is inherently existent. While in AC machines, this property of vectors needs to be created. In AC machines, both of these quantities are inter dependent and their position in space depends upon both the stator and rotor positions. The control of squirrel cage IM adds further complexity due to inaccessibility of rotor winding. So the requirement is to make these quantities decoupled and be controlled independently. This is achieved by both FOC and DTC.

From Faraday's electromagnetic theory for two coils mutually coupled in the magnetic field of each other:

$$\overrightarrow{\psi_s} = L_s\overrightarrow{\imath_s} + L_m\overrightarrow{\imath'_r} \tag{2.34}$$

$$\overrightarrow{\psi'_r} = L_r\overrightarrow{\imath'_r} + L_m\overrightarrow{\imath_s} \tag{2.35}$$

Decomposing these flux linkage equations into real and imaginary part and then plugging into torque equation, the following can be achieved.

$$T_e = \frac{3}{2}\left(\frac{P}{2}\right)(\psi_{s\beta}I_{s\alpha} + \psi_{s\alpha}I_{s\beta}) \tag{2.36}$$

This equation will be used for estimation of developed torque for the direct torque control scheme.

Chapter 3

Principles of Direct Torque Control of Induction Motor Drives

3.1. Introduction

Today there are basically two types of control techniques for speed control of ac drives used for high-performance applications: vector or field oriented control (FOC) and direct torque control (DTC). The most popular method, vector control was introduced more than 25 years ago in Germany by Hasse [6], Blaskke [11], and Leonhard. The vector control method, also called field oriented control (FOC) transforms the motor equations into a coordinate system that rotates in synchronism with the rotor flux vector. Under a constant rotor flux amplitude there is a linear relationship between the control variables and the torque. Transforming the ac motor equations into field coordinates makes the FOC method resemble the decoupled torque production in a separately excited dc motor. Over the years, FOC drives have achieved a high degree of maturity in a wide range of applications. They have established a substantial worldwide market which continues to increase [2].

No later than 20 years ago, when there was still a trend toward standardization of control systems based on the FOC method, direct torque control was introduced in Japan by Takahashi and Nagochi [4] and also in Germany by Depenbrock [5], [16], [27]. Their innovative studies depart from the idea of coordinate transformation and the analogy with dc motor control. These innovators proposed a method that relies on a control mechanism that does not require the decoupled control equations which are the characteristics of vector or field oriented control method. Their technique works very well with the on-off operation of inverter semiconductor power devices. After the innovation of the DTC method it has gained much momentum, but in areas of research. So far only one form of a DTC of ac drive has been marketed by an industrial company, but it is expected very soon that other manufacturers will come out with their own DTC drive products [19]. The basic concept behind the DTC of ac drive, as its name implies, is

to control the electromagnetic torque and flux linkage directly and independently by the use of six or eight voltage space vectors found in lookup tables. The possible eight voltage space vectors used in DTC are shown in Fig.3.1 [19].

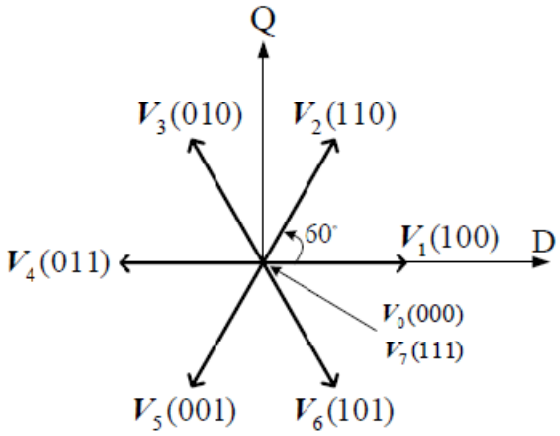

Fig.3.1: Eight possible voltage space vectors obtained from VSI [2].

The typical DTC includes two hysteresis controllers, one for torque error correction and one for flux linkage error correction. The hysteresis flux controller makes the stator flux rotate in a circular fashion along the reference trajectory for sine wave ac machines as shown in Fig.3.2. The hysteresis torque controller tries to keep the motor torque within a pre-defined hysteresis band.

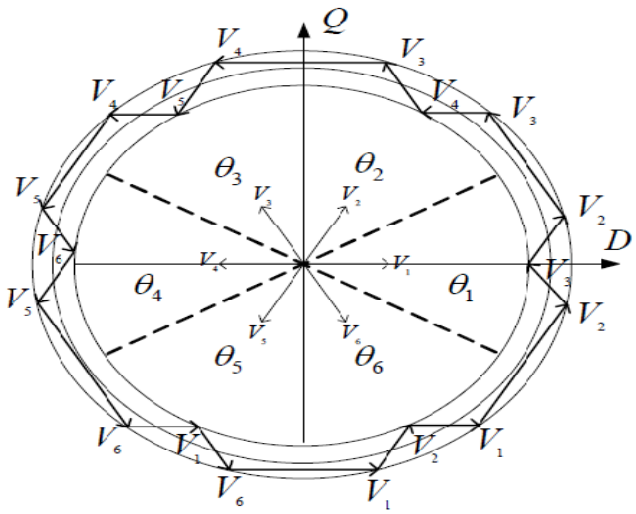

Fig.3.2: Circular trajectory of stator flux linkage in the stationary d-q reference frame [2].

At every sampling time the voltage vector selection block decides on one of the eight possible inverter switching states (S_a, S_b, S_c) to be applied to the motor terminals. The possible outputs of the hysteresis controller and the possible number of switching states in the inverter are finite, so a look-up table can be constructed to choose the appropriate switching state of the inverter. This selection is a result of both the outputs of the hysteresis controllers and the sector of the stator flux vector in the circular trajectory.

There are many advantages of direct torque control (DTC) over other high-performance torque control systems such as vector control. Some of these are summarized as follows:

- The only motor parameter that is required is stator resistance. The stator winding being static undergoes lesser variation during system operation as compared to the rotor resistance.
- The switching commands of the inverter are derived from a look-up table, simplifying the control system and also decreasing the processing time unlike a PWM modulator used in vector control or field oriented control (FOC).
- Instead of current control loops, stator flux linkage vector and torque estimation are required so that simple hysteresis controllers are used for torque and stator flux linkage control.
- Vector coordinate transformations are not applied extensively because stator quantities are enough to calculate the torque and stator flux linkage as feedback quantities to be compared with the reference values.
- The rotor position, which is essential for torque control in a vector control scheme, is not required in DTC for induction and synchronous reluctance motor DTC drives.
- The DTC scheme is capable of providing very accurate torque control even at low frequencies. With or without any feedback sensors and even at zero speed it can supply the full load torque [20].
- DTC scheme provides rapid starting of the drive system irrespective of the residual magnetism and mechanical load. The computational burden on the controller is also inferior as compared with that of the vector control schemes.

The DTC scheme, as its name indicates, is focused on the control of the torque and the stator flux linkage of the motor, therefore, a faster torque response is achieved over vector control. Furthermore, due to the fact that DTC does not need current controller, the time delay caused by the current loop is eliminated.

Although there are several advantages of the DTC scheme over vector control, it still has a few drawbacks which are explained below:

- A major drawback of the DTC scheme is the high torque and stator flux linkage ripples. Since the switching state of the inverter is updated once every sampling time, the inverter keeps the same state until the outputs of each hysteresis controller changes states. As a result, large ripples in torque and stator flux linkage occur.
- The switching frequency varies with load torque, rotor speed and the bandwidth of the two hysteresis controllers.
- Stator flux estimation is achieved by integrating the difference between the input voltage and the voltage drop across the stator resistance. The applied voltage on the motor terminal can be obtained either by using a dc-link voltage sensor, or two voltage sensors connected to the any two phases of the motor terminals. For current sensing there should be two current sensors connected on any two phases of the motor terminals. Offset in the measurements of dc-link voltage and the stator currents might happen, because for current and voltage sensing, however, temperature sensitive devices, such as operational amplifiers, are normally used which can introduce an unwanted dc offset. This offset may introduce large drifts in the stator flux linkage computation (estimation) thus creating an error in torque estimation (torque is proportional to the flux value) which can make the system become unstable.
- The stator flux linkage estimation has a stator resistance, so any variation in the stator resistance introduces error in the stator flux linkage computation, especially at low frequencies. If the magnitude of the applied voltage and back-EMF are low, then any change in the resistance will greatly affect the integration of the back-EMF.
- The DTC scheme for its proper functioning needs a very high frequency processor to keep the torque ripple within standard limits.

3.2. Critical Analysis of DTC Scheme

3.2.1. Principles of Classical DTC Scheme for Induction Motor Drive

The basic idea of direct torque control is to choose the appropriate stator voltage vector out of eight possible inverter states (according to the difference between the reference and actual torque and flux linkage) so that the stator flux linkage vector rotates along the stator reference frame (d-q frame) trajectory and produces the desired torque. The torque control strategy in the direct torque control of an induction motor is explained in Section 3.2.1.1. The flux control is discussed following the torque control section.

3.2.1.1. Torque Control Strategy in DTC Scheme of IM Drive

Before going through the control principles of DTC for IMs, an expression for the torque as a function of the stator and rotor flux will be developed. The torque equation used for DTC of IM drives can be derived from the phasor diagram of induction motor shown in Fig.3.3.

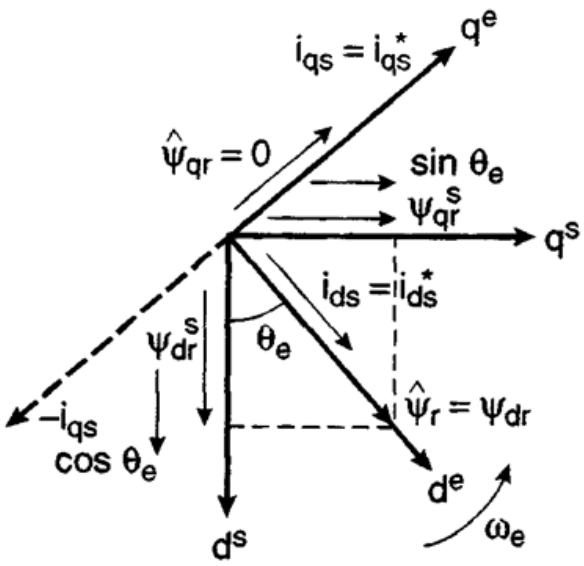

Fig.3.3: Phasor diagram of stator current and rotor flux quantities of induction machine in d-q frame [3].

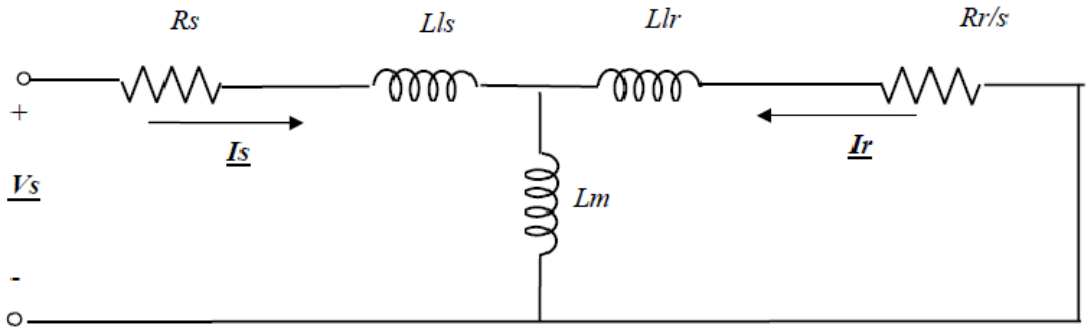

Fig.3.4: Per phase equivalent circuit for induction machine in stationary reference frame [3].

The torque expression can be expressed in the following form as

$$\overline{T_e} = \frac{3}{2}\left(\frac{P}{2}\right)\overline{\psi_s} X \overline{I_s} \tag{3.1}$$

Where, $\overline{\psi_s} = \psi_{qs}^s - j\psi_{ds}^s$ and $\overline{I_s} = i_{qs}^s - j\, i_{ds}^s$. In this equation $\overline{I_s}$ is to be replaced by rotor flux, $\overline{\psi_r}$. In the complex form, $\overline{\psi_s}$ and $\overline{\psi_r}$ can be expressed as a functions of currents as

$$\overline{\psi_s} = L_s\overline{I_s} + L_m\overline{I_r} \tag{3.2}$$

$$\overline{\psi_r} = L_r\overline{I_r} + L_m\overline{I_s} \tag{3.3}$$

By eliminating $\overline{I_r}$ from the equation (3.2)

$$\overline{\psi_s} = \frac{L_m}{L_r}\overline{\psi_r} + L_s{}'\overline{I_s} \tag{3.4}$$

Where, $L_s{}' = L_sL_r - L_m{}^2$. The corresponding expression of $\overline{I_s}$ is

$$\overline{I_s} = \frac{1}{L_s}\overline{\psi_s} - \frac{L_m}{L_rL_s}\overline{\psi_r} \tag{3.5}$$

Substituting the value of $\overline{I_s}$ into the torque equation,

$$\overline{T_e} = \frac{3}{2}\left(\frac{P}{2}\right)\frac{L_m}{L_rL_s}\overline{\psi_r} X \overline{\psi_s} \tag{3.6}$$

That is, the magnitude of the torque is

$$T_e = \frac{3}{2}\left(\frac{P}{2}\right)\frac{L_m}{L_rL_s}\left|\overline{\psi_r}\right|\left|\overline{\psi_s}\right| \sin\gamma \tag{3.7}$$

Where, γ is the angle between stator and rotor fluxes. If the rotor flux remains constant and the stator flux is changed incrementally by stator voltage $\overline{V_s}$ as shown, and the corresponding change of γ is $\Delta\gamma$, the incremental torque ΔT_e expression is given as

$$\Delta T_e = \frac{3}{2}\left(\frac{P}{2}\right)\frac{L_m}{L_r L_s}\left|\overline{\psi_r}\right|\left|\overline{\psi_s} + \Delta\overline{\psi_s}\right| \sin\Delta\gamma \tag{3.8}$$

As it can be seen from (3.8), if the load angle γ is increased then torque variation is increased. To increase the load angle γ the stator flux vector should turn faster than rotor flux vector. The rotor flux rotation depends on the mechanical speed of the rotor, so to decrease load angle γ the stator flux should turn slower than rotor flux. Therefore, according to the torque (3.7), the electromagnetic torque can be controlled effectively by controlling the amplitude and rotational speed of stator flux vector $\overline{\psi_s}$. To achieve the above phenomenon, appropriate voltage vectors are applied to the motor terminals. For counter-clockwise operation, if the actual torque is smaller than the reference value, then the voltage vectors that keep the stator flux vector $\overline{\psi_s}$ rotating in the same direction are selected. When the load angle γ between $\overline{\psi_s}$ and $\overline{\psi_r}$ increases the actual torque increases as well. Once the actual torque is greater than the reference value, the voltage vectors that keep stator flux vector $\overline{\psi_s}$ rotating in the reverse direction are selected instead of the zero voltage vectors. At the same time, the load angle γ decreases thus the torque decreases. A more detailed look at the selection of the voltage vectors and their effect on torque and flux results will be discussed later as well. Referring back to the discussion above, however, torque is controlled via the stator flux rotation speed, as shown in Fig. 3.5. If the speed of the stator flux is high then faster torque response is achieved.

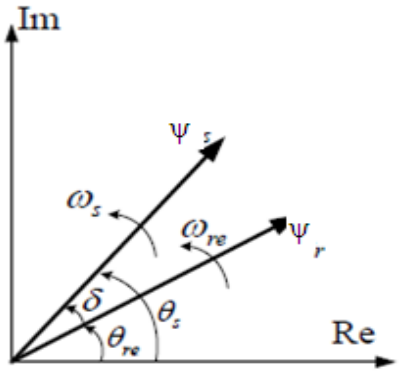

Fig.3.5: Rotor and stator flux linkage space vectors (rotor flux lagging stator flux) [21].

3.2.2. Flux Control Strategy in DTC of IM Drive

If the resistance term in the stator flux estimation algorithm is neglected, the variation of the stator flux linkage (incremental flux expression vector) will only depend on the applied voltage vector as shown in Fig.3.6 [40].

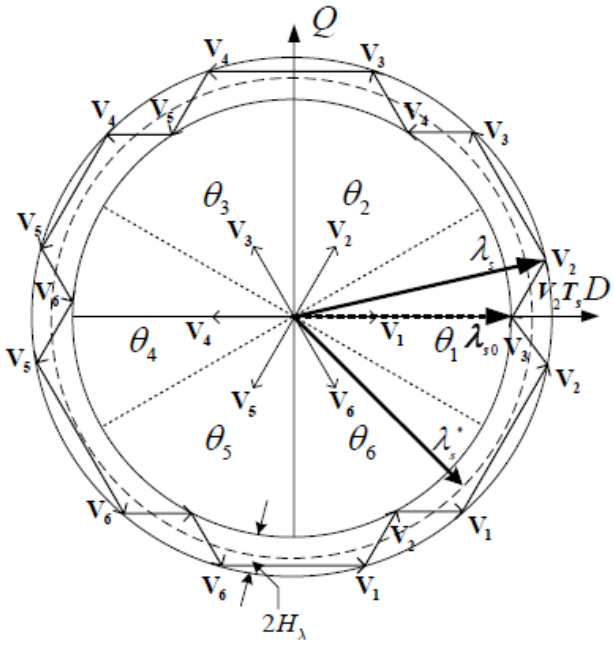

Fig.3.6: Incremental stator flux linkage space vector representation in the d-q reference frame [2].

For a short interval of time, namely the sampling time $T_s = \Delta t$ the stator flux linkage $\overline{\psi_s}$ position and amplitude can be changed incrementally by applying the stator voltage vector, $\overline{Vs}$. As discussed above, the position change of the stator flux linkage vector $\overline{\psi_s}$ will affect the torque. The stator flux linkage of an induction motor that is depicted in the stationary reference frame is written as

$$\psi_s = \int (V_s - R_s I_s) dt \tag{3.9}$$

During the sampling interval time or switching interval, one out of the eight voltage vectors is applied and each voltage vector applied during the pre-defined sampling interval is constant, therefore (3.9) can be rewritten as

$$\psi_s = V_s . t + R_s \int I_s dt + \psi_{s|t=0} \tag{3.10}$$

Where $\psi_{s|t=0}$ is the initial stator flux linkage at the instant of switching, V_s is the measured stator voltage, I_s is the measured stator current, and R_s is the estimated stator resistance. When the stator resistance term in stator flux estimation is removed implying that the end of the stator flux vector $\overline{\psi_s}$ will move in the direction of the applied voltage vector, as shown in Fig.3.6, we obtain

$$V_s = \frac{d}{dt}(\psi_s) \tag{3.11}$$

$$\Delta\psi_s = V_s \Delta t \tag{3.12}$$

The goal of controlling the flux in DTC is to keep its amplitude within a predefined hysteresis band. By applying a required voltage vector, stator flux linkage amplitude can be controlled. To select the voltage vectors for controlling the amplitude of the stator flux linkage the voltage plane is divided into six regions, as shown in Fig. 3.2.

In each region, two adjacent voltage vectors, which give the minimum switching frequency, are selected to increase or decrease the amplitude of stator flux linkage, respectively. For example, according to the Table - I, when the voltage vector V_2 is applied in Sector 1, then the amplitude of the stator flux increases when the flux vector rotates counter-clockwise. If V_3 is selected, then stator flux linkage amplitude decreases. The stator flux incremental vectors corresponding to each of the six inverter voltage vectors are shown in Fig.3.1.

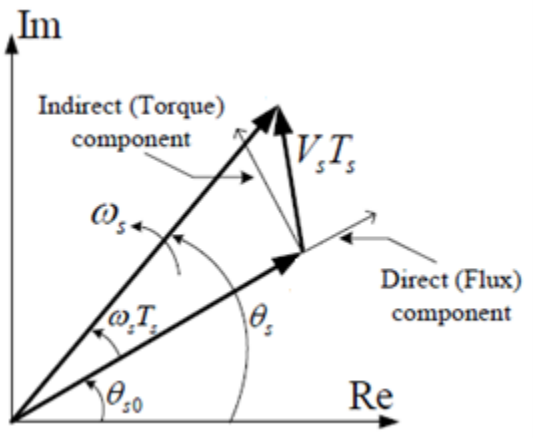

Fig.3.7: Representation of direct and indirect components of the stator flux linkage vector [21].

Fig.3.7 is a basic graph that shows how flux and torque can be changed as a function of the applied voltage vector is presented. According to the figure, the direct component of applied voltage vector changes the amplitude of the stator flux linkage and the indirect component

changes the flux rotation speed which changes the torque. If the torque needs to be changed abruptly then the flux does as well, so the closest voltage vector to the indirect component vector is applied. If torque change is not required, but flux amplitude is increased or decreased then the voltage vector closest to the direct component vector is chosen. Consequently, if both torque and flux are required to change then the appropriate resultant mid-way voltage vector between the indirect and direct components is applied [21]. It seems obvious from (3.9) that the stator flux linkage vector will stay at its original position when zero voltage vectors S_a *(000)* and S_a *(111)* are applied. This is true for an induction motor since the stator flux linkage is uniquely determined by the stator voltage.

3.2.3. Voltage Vector Selection in DTC of IM Drive

As discussed before, the stator flux is controlled by properly selected voltage vectors, and as a result the torque is achieved by stator flux rotation. The higher the stator vector rotation speed the faster torque response is achieved.

The estimation of the stator flux linkage components described previously requires the stator terminal voltages. In a DTC scheme it is possible to reconstruct those voltages from the dc-link voltage V_{dc} and the switching states (S_a, S_b , S_c) of a six-step voltage-source inverter (VSI) rather than monitoring them from the motor terminals. The primary voltage vector $\boldsymbol{v_s}$ is defined by the following equation:

$$v_s = \frac{2}{3}\left(v_a + v_b e^{j\left(\frac{2}{3}\right)\pi} + v_c e^{j\left(\frac{4}{3}\right)\pi}\right) \tag{3.13}$$

Where, v_a, v_b and v_c are the instantaneous values of the primary line-to-neutral voltages. When the primary windings are fed by an inverter, as shown in Fig.3.8, the primary voltages v_a, v_b and v_c are determined by the status of the three switches S_a, S_b and S_c. If the switch is at state 0 that means the phase is connected to the negative and if it is at 1 it means that the phase is connected to the positive leg.

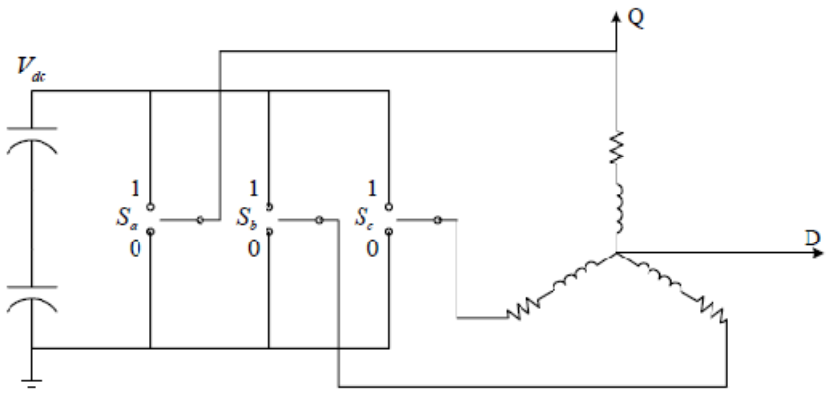

Fig.3.8: Voltage Source Inverter (VSI) connected to the R-L load [5].

For example, v_a is connected to V_{dc} if S_a is one, otherwise v_a is connected to zero. This is similar for v_b and v_c. The voltage vectors that are obtained this way are shown in Fig.3.1. There are six nonzero voltage vectors: $\boldsymbol{V}_1(100)$, $\boldsymbol{V_2}$ (110) , …, and $\boldsymbol{V_6}$ (101) and two zero voltage vectors: $\boldsymbol{V_7}$ (000) and $\boldsymbol{V_8}$ (111) . The six nonzero voltage vectors are 60 degrees apart from each other as in Fig.3.1.

The stator voltage space vector (expressed in the stationary reference frame) representing the eight voltage vectors can be shown by using the switching states and the dc-link voltage V_{dc} as

$$v_s(S_a, S_b, S_c) = \frac{2}{3} V_{dc}(S_a + S_b e^{j\left(\frac{2}{3}\right)\pi} + S_c e^{j(4/3)\pi}) \tag{3.14}$$

Where, V_{dc} is the dc-link voltage and the coefficient of 2/3 is the coefficient comes from the Park Transformation. Equation (3.14) can be derived by using the line-to-line voltages of the ac motor which can be expressed as, $v_{ab} = V_{dc}(S_a - S_b)$, $v_{ca} = V_{dc}(S_c - S_a)$ and $v_{bc} = V_{dc}(S_b - S_c)$. The stator phase voltages (line-to-neutral voltages) are required for (3.14). They can be obtained from the line-to-line voltages as $v_a = (v_{ab} - v_{ca})/3$, $v_b = (v_{bc} - v_{ab})/3$ and $v_c = (v_{ca} - v_{bc})/3$. If the line-to-line voltages in terms of the dc-link voltage V_{dc} and switching states are substituted into the stator phase voltages it gives

$$v_a = \frac{1}{3} V_{dc}(2S_a - S_b - S_c) \tag{3.15}$$

$$v_b = \frac{1}{3} V_{dc}(2S_b - S_a - S_c) \tag{3.16}$$

$$v_c = \frac{1}{3}V_{dc}(2S_c - S_b - S_a) \tag{3.17}$$

Equation (3.15) can be summarized by combining with (3.13) as

$$v_a = Re(v_s) = \frac{1}{3}V_{dc}(2S_a - S_b - S_c) \tag{3.18}$$

$$v_b = Re(v_s) = \frac{1}{3}V_{dc}(2S_b - S_a - S_c) \tag{3.19}$$

$$v_c = Re(v_s) = \frac{1}{3}V_{dc}(2S_c - S_b - S_a) \tag{3.20}$$

To determine the proper applied voltage vectors, information from the torque and flux hysteresis outputs, as well as stator flux vector position, are used so that circular stator flux vector trajectory is divided into six symmetrical sections according to the nonzero voltage vectors as shown in Fig.3.2.

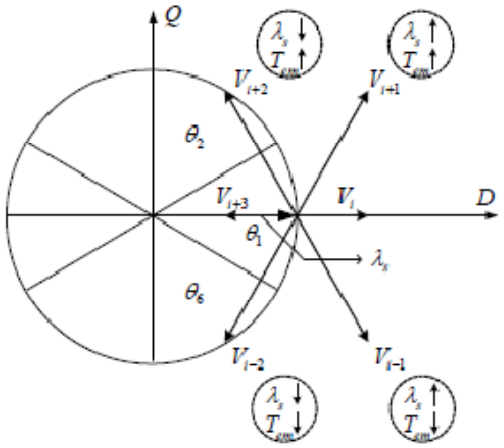

Fig.3.9: Voltage vector selection when the stator flux vector is located in sector *i* [21].

According to Fig.3.9, while the stator flux vector is situated in sector *i*, voltage vectors V_{i+1} and V_{i-1} have positive direct components, increasing the stator flux amplitude, and V_{i+2} and V_{i-2} have negative direct components, decreasing the stator flux amplitude. Moreover, V_{i+1} and V_{i+2} have positive indirect components, increasing the torque response, and V_{i-1} and V_{i-2} have negative

indirect components, decreasing the torque response. In other words, applying V_{i+1} increases both torque and flux but applying V_{i+2} increases torque and decreases flux amplitude [21].

The switching table for controlling both the amplitude and rotating direction of the stator flux linkage is given in Table I.

Table I: Switching table for inverter voltage vectors

Hψ	H_{Te}	$\theta(1)$	$\theta(2)$	$\theta(3)$	$\theta(4)$	$\theta(5)$	$\theta(6)$
1	1	V2	V3	V4	V5	V6	V1
	0	V0	V7	V0	V7	V0	V7
	-1	V6	V1	V2	V3	V4	V5
-1	1	V3	V4	V5	V6	V7	V8
	0	V7	V0	V7	V0	V7	V0
	-1	V5	V6	V1	V2	V3	V4

The voltage vector plane is divided into six sectors so that each voltage vector divides each region into two equal parts. In each sector, four of the six non-zero voltage vectors may be used. Zero vectors are also allowed. All the possibilities can be tabulated into a switching table. The switching table presented by Rahman et al [10] is shown in Table I.

3.3. Control Strategy of DTC of IM

The block diagram for direct torque and flux control for induction motor is shown in Fig.3.10. The speed control loop and the flux program as a function of speed are shown. The command stator flux, $\overline{\psi_s}^*$ and torque T_e^* are compared with respective estimated values and the errors are processed through the hysteresis band controllers as shown. The flux level hysteresis controller has two levels of digital output according to the following relations:

$$H_{\psi} = 1 \quad for\ E_{\psi} > +HB_{\psi} \tag{3.21}$$

$$H_{\psi} = -1 \quad for\ E_{\psi} < -HB_{\psi} \tag{3.22}$$

Where, $2HB_{\psi}$= total hysteresis bandwidth of the hysteresis controller. The circular trajectory of the command flux $\overline{\psi_s}^*$ with hysteresis band rotates in anti- clockwise direction as shown in Fig.3.2.The actual stator flux ψ_s is constrained within the hysteresis band and is tracked by command flux in a zigzag path.

The torque control loop has three levels of digital output which have the following relationships,

$$H_{Te} = 1 \quad for\ E_{Te} > +HB_{Te} \tag{3.23}$$

$$H_{Te} = -1 \quad for\ E_{Te} < -HB_{Te} \tag{3.24}$$

$$H_{Te} = 0 \quad for\ -HB_{Te} < \ E_{Te} < +HB_{Te} \tag{3.25}$$

The output of the torque hysteresis comparator is denoted as $H\psi$, the output of the flux hysteresis comparator as H_{Te} and the flux linkage sector is denoted as θ. The torque hysteresis comparator is a three valued comparator and the flux hysteresis comparator is a two valued comparator. The output of the hysteresis comparators along with the flux sector selector output are applied to the inputs of the voltage source inverter which generates appropriate voltage vectors necessary to minimize the error. If the torque ripple needs to be kept as small as with the original switching table, a higher switching frequency must be used [3].

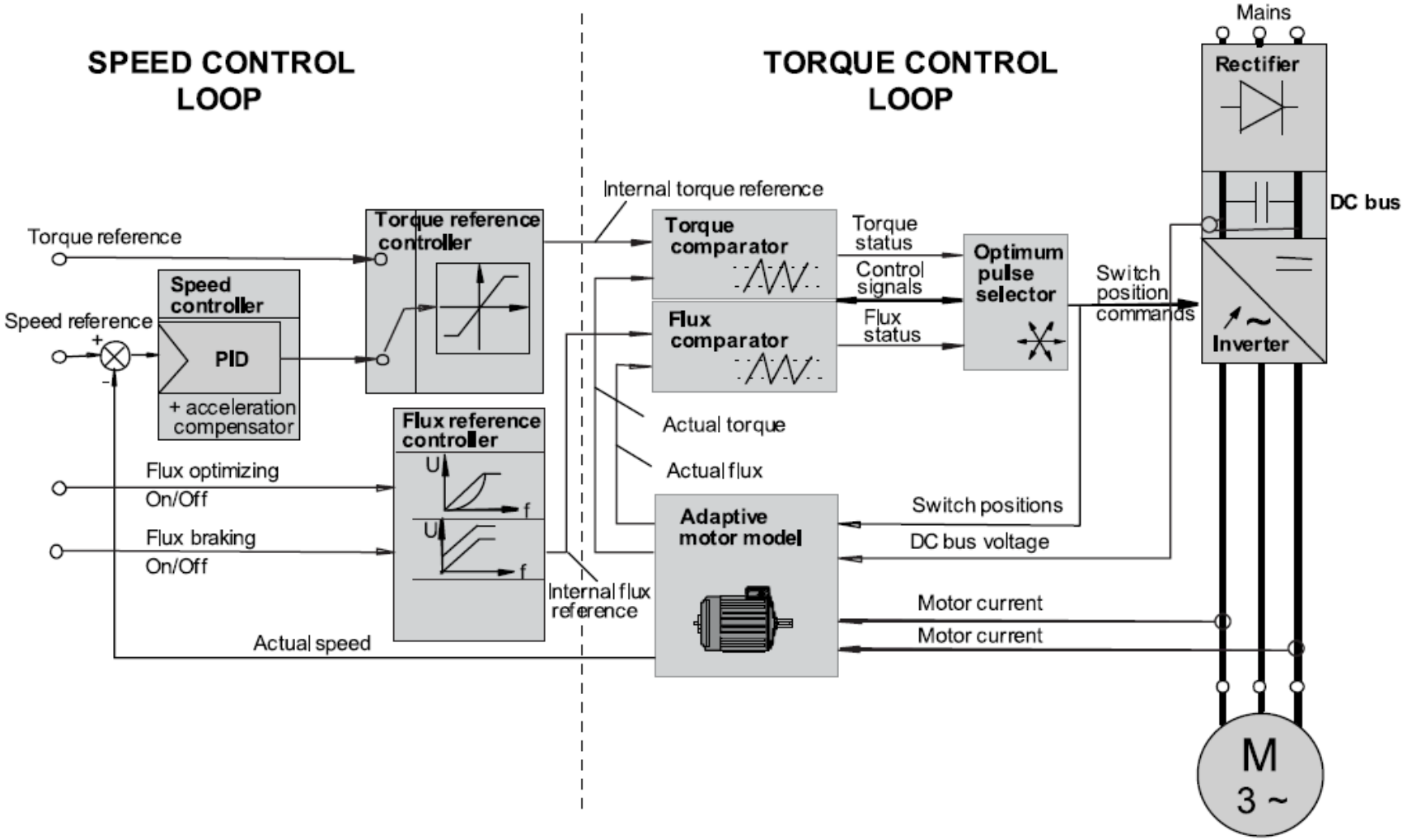

Fig.3.10: Block diagram of Direct Torque Control Scheme for Induction Motor Drive [20]

Chapter 4

Development of Adaptive Neuro-Fuzzy Controller for DTC based Induction Motor Drives

4.1 Introduction:

In classical control systems the accuracy of the control is highly plant mathematical model dependent. Unfortunately, majority of the controllers are parameter dependent and are based on many assumptions for simplicity. These assumptions introduce inaccuracy in the plant model and as a result controller performance deteriorates. Conclusively, the approximated model based classical controllers are inaccurate and parameter sensitive. Classical controllers (like- PI, PID) suffer from the inaccuracies in plant model, variations of system parameter during operations as well as adapting to these variations. The use of artificial intelligence was industrialized since 1960s [63]. The earlier use was limited to only decision making process for monitoring the industrial process. The major advantage of intelligent controllers is that they need only an approximate mathematical model. The ideal behavior of artificial intelligent controller (AIC) is its capability to learn, recall and generalize from training patterns like human brain [64]. The use of advanced electronics has made it possible to implement complex controllers by using powerful microprocessor. There are mainly three kinds of AICs which include fuzzy, neural networks and their hybrid neuro-fuzzy controller. There also exist some other forms of AI like genetic algorithm (GA) assisted neural networks. But these algorithms are not the function approximations rather they are simple and powerful general purpose stochastic optimization methods. The pure fuzzy logic controller is based on the expert knowledge. If high performance is wanted, it needs manual adjustments by trial and error. In most FLCs, the response accuracy is largely dependent on the number of membership functions and the rules used for designing the controller [65, 66]. The expert knowledge is the key for forming the rules. Any deficiency in the rules directly affects the controller performance. Moreover, larger number of rules and

membership functions cause high computational burden, which is the major limitation for their practical industrial applications.

The artificial neural network (ANN) can cope with any system nonlinearities and uncertainties. Optimization of number of hidden layers and their nodes are the main features in the design of such controllers [39]. Generally, a larger ANN requires proportional computation burden and converges slowly. The design of a supervised ANN with error back propagation scheme needs three kinds of data set. The training data algorithm plays extremely important role in the design of neural network and requires a careful selection. Sometimes, it is tough to create a serial of training data for ANN that can handle all the operating modes [67]. The concept of a neuro-fuzzy controller (NFC) combines the advantages and eliminates the drawbacks of both standalone FLC and ANN. The NFC utilizes the transparent and linguistic representation of a fuzzy system with the learning ability of artificial neural networks. NFC (which is also called Adaptive Neuro Fuzzy Inference System) enables the system to be adaptive and requires minimum human intervention for the tuning. Therefore, in this thesis, to improve dynamic performance, a Takagi Sugeno Kang (TSK) type self-tuned NFC is developed. This controller is robust to parameter sensitivity and has a learning/training algorithm to adapt with system uncertainties. There is no need to change the controller during the course of running as in the above cited works. The adaptive-neural network-based fuzzy inference system (ANFIS) is relatively fast convergent due to neural learning and the ability of fuzzy logic to construct reasonably good input membership functions. It has better tracking performance and better adaptability than the other controllers since the training back propagation algorithm trains the networks in such a way as it becomes capable of adapting to any parametric variation during the operation. Finally, the proposed NFC is integrated with the DTC scheme in order to achieve both high dynamic performance and optimum torque ripples. The performance of the developed ANFIS based controller is also compared with the classical PI controller for evaluating their individual dynamic performance for the same plant model.

4.2 Classical Proportional-Integral (PI) Controller for IM Drive

The best known controller used in industry is the proportional-integral (PI) controller because of its simple structure and its robust performance in a wide range of operating conditions. This linear regulator is based on a very simple structure, whose functioning depends only on two

parameters, namely the proportional gain (k_p) and the integral gain (k_i). Mathematically the functionality of a PI controller can be expressed as:

$$u = K_p.e(t) + K_i \int_0^t e(\tau)\, d\tau \tag{4.1}$$

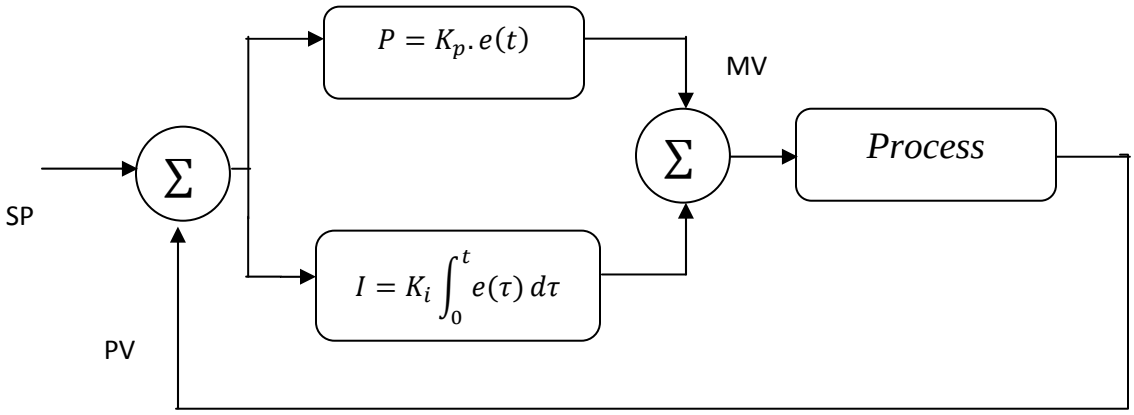

Fig.4.1: Proportional Integral (PI) Controller Structure

The major inconvenience of this type of controllers is the necessity of the a priori knowledge of the various parameters of the system (i.e. induction motor). Any imperfections in the system model can deteriorate the controller performance. Moreover, PI controllers are sensitive to system parameter variations during operation and are required to be tuned externally in order to maintain satisfactory performance during operation where system parameters may vary under various operation conditions.

Several methods of tuning a PI controller have been proposed in the literature; the most used are the poles assignment method and the Ziegler-Nichols method [45, 52]. To surmount this inconvenience, it is possible to use a procedure of optimization to better design this type of controller. Genetic Algorithm methods have been widely used in these control applications. They are stochastic optimization methods based on the principles of natural biological evolution. The GA methods have been employed successfully to solve complex optimization problems. The use of GA methods in the determination of the different controller parameters is practical due to their fast convergence and reasonable accuracy [7]. The parameters of the PI controller are determined by the minimization of an objective function.

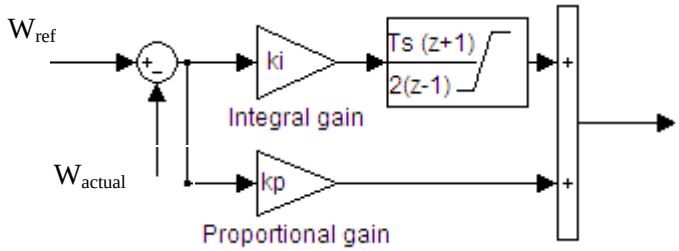

Fig.4.2: Simulink Model of Proportional Integral (PI) Controller for Speed Control of IMs

In this thesis, the performance of a classical PI controller driven DTC based induction motor drive is compared with the performance of the proposed hybrid neuro-fuzzy controller driven DTC based induction motor drive.

4.3. Development of a Neuro-Fuzzy Controller

4.3.1. Design of a TSK-Type Neuro-Fuzzy Controller

After their successful industrial applications by Hitachi and Yaskawa, AICs are gaining practical popularity in the drive realm [67]. These manufacturers applied pure fuzzy and pure neural network based controllers separately. But the general/universal motor drive must have a tunable controller. None of the motor manufacturers have prior knowledge of the load it will run. The manually tuned controller is useless without expert knowledge. Since the AICs are the future of drive schemes, therefore, the motor manufacturer must provide a controller which could be tuned without expert knowledge.

This thesis presents a simple ANFIS based DTC scheme for IM drives. The nonlinear mapping from inputs (normalized speed error and normalized change in speed error) to the output (motor developed torque) is done by using a TSK-type NFC. The general structure of a TSK-type NFC with two inputs, for the control of electrical motors is shown in Fig.4.3 [67, 68].

Each linguistic variable consists of five triangular and two trapezoidal membership functions as shown in Fig.4.7. This combination naturally produces 49 rules for the neuro-fuzzy controller structure shown in Fig.4.3 which are given in Appendix - C.

The excellence of triangular and trapezoidal membership function is their linear and constant slope. As a result of this linear and constant slope, the triangular and trapezoidal membership

functions offer lesser computational burden. Generally, this is one of the speed controller desired property. But this property has to be paid back in the main two costs for the controller.

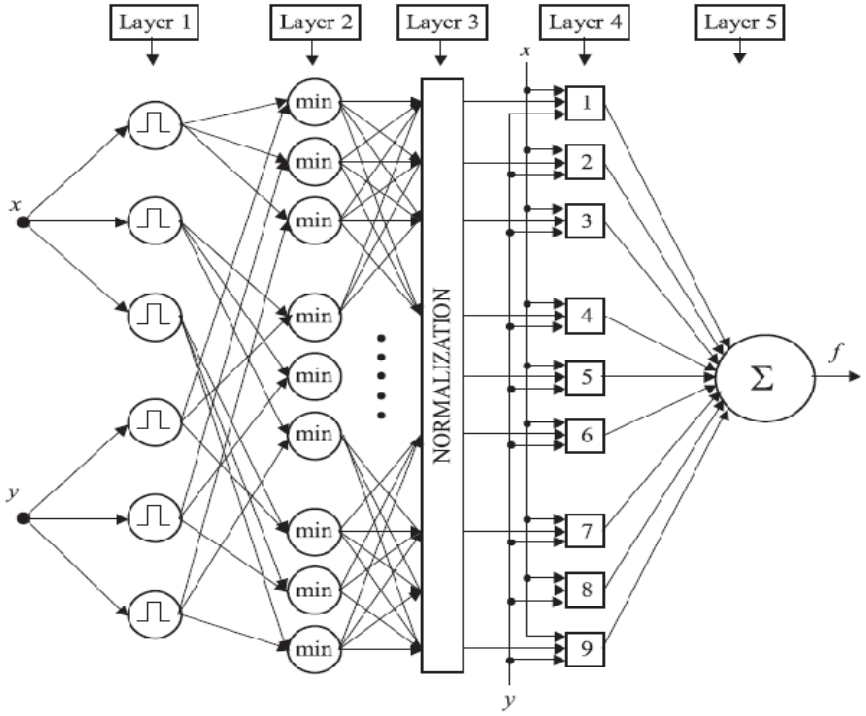

Fig.4.3: Two Input Adaptive NFC Controller Structure [39]

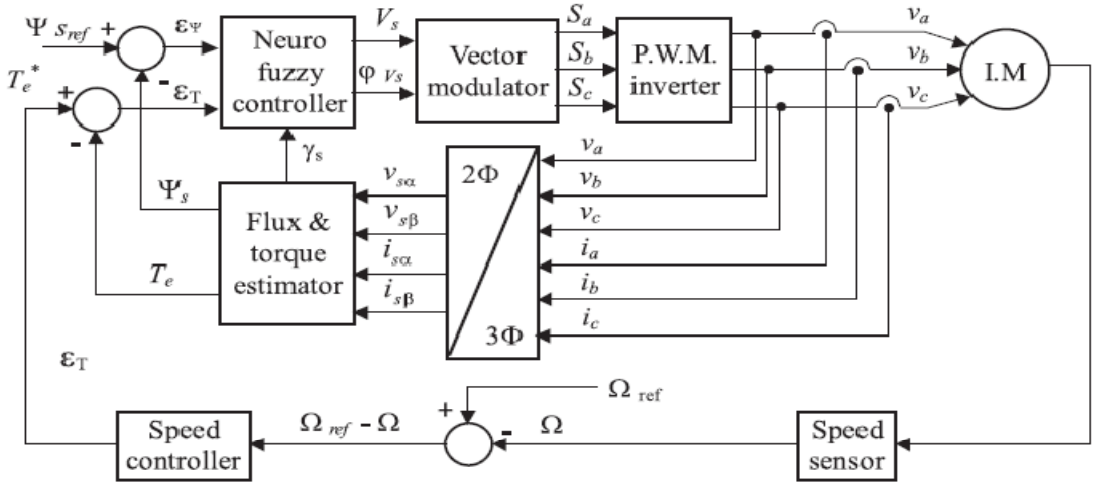

Fig.4.4: Direct Torque Neuro Fuzzy Scheme for Speed Control of Induction Motor Drives [55]

Primarily, the values of triangular functions are calculated by using some computer algorithms based on approximation of some infinite series (like-Taylor series). Secondly, the exponential

function value is nonzero for the whole operating range of the controller input variables. It means that all the rules are non-zero all the time irrespective of their values are of no significance for the controller. Both the factors introduce high volume of computational burden on the processor [69]. This may cause the processor for the real time implementation to over run. Consequently, to run the controller smoothly it may need to increase the sampling time which ruin the whole advantage of these functions.

In the controller shown in Fig 4.3, the first layer is the input layer. This layer just passes the scaled controller input to the next layer. The second layer is the fuzzification layer. Each input is fuzzified by using some suitable membership functions (MFs) like sigmoid, triangular and Gaussian etc. These are not the revealed membership functions and may be customized according to requirement. The number of membership functions used may vary based on the system requirement. The third and fourth layers are the rule layers. The common fuzzy if...then rules may be replaced by product, minimum or some different technique. Each technique has its own relevant advantages and drawbacks.

4.2.2 Detailed Design of the Proposed TSK - Type NFC

Since ANFIS design starts with a pre-structured system, DOF for learning is limited, i.e., the MF of input & output variables contain more information that NN has to drive from sampled data sets. Knowledge regarding the systems under design can be used right from the start. Part of the system can be excluded from the training. Hence, this ANFIS process is more efficient. The rules are in the linguistic forms and so intermediate results can be analyzed and interpreted easily. The modification of rules is possible during the training and optimization can be done manually. Further the ANFIS strategy supports the TSK based systems. To start the ANFIS learning; first, a training data set that contains the desired input / output data pairs of target systems to be modeled is required. The design parameters required for any ANFIS controller are viz., Number of data pairs, Training data set & checking data sets, Fuzzy inference systems for training, Number of epochs to be chosen to start the training, Learning results to be verified after mentioning the step size [7].

In this context, the general ANFIS control structure for the control of any plant is presented here in the Fig.4.5 [25], [43]. This structure contains the same components as the FIS, expect for the

NN block. The structure of the network is composed of a set of units (and connections) arranged into five connected network layers as shown in Fig.4.5.

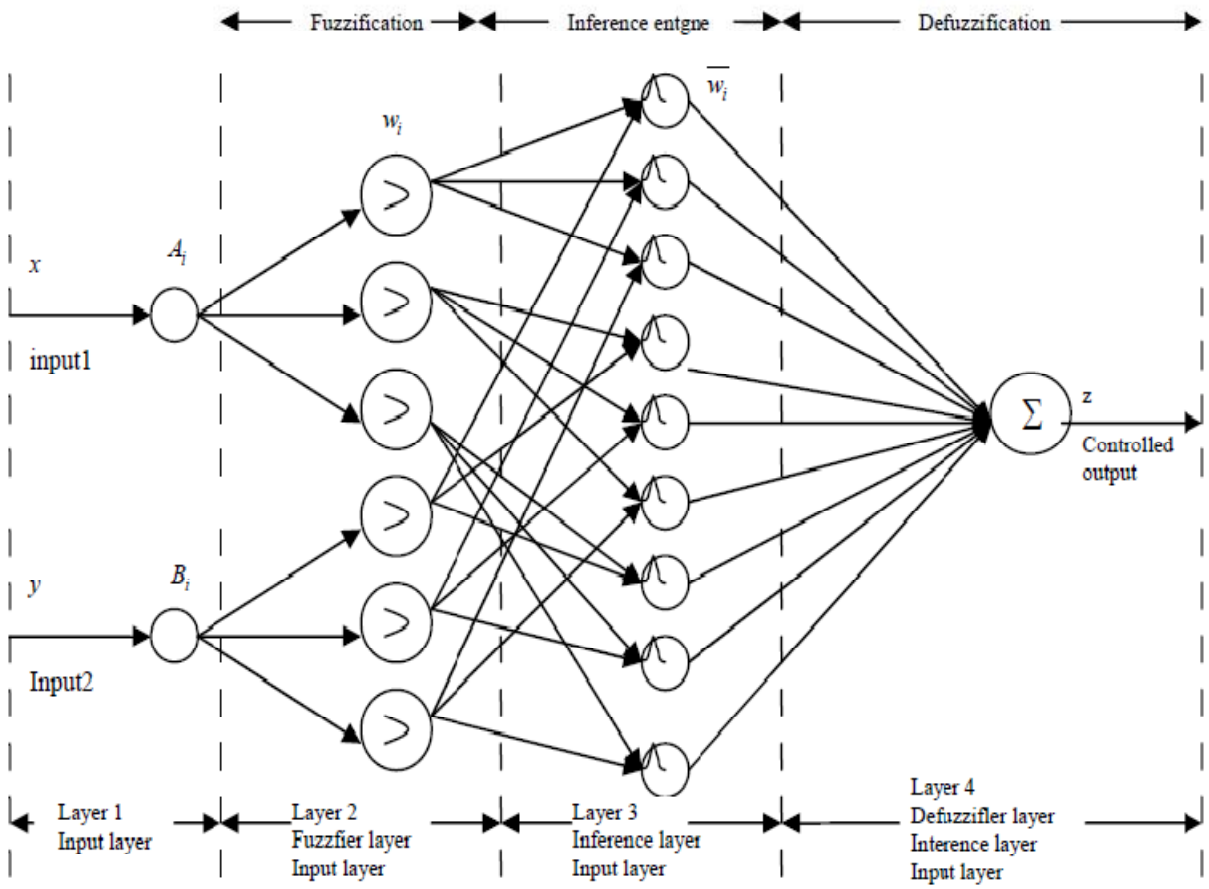

Fig. 4.5: Adaptive Neuro Fuzzy Inference System Structure

The functionalities of each of the five interconnected layers are explained in details below:

Layer-1: This layer consists of input variables (membership functions), i.e. input 1 & input 2. Here, triangular and trapezoidal shaped MFs are used in this work. This layer just supplies the input values o_i^1 to the next layer, where i = 1 to n.

$$o_i^1 = \mu_{A_i}(x), i = 1,2 \tag{4.2a}$$

$$o_i^1 = \mu_{B_i}(y), i = 3,4 \tag{4.2b}$$

Where, μ_{A_i} and μ_{B_i}can adopt to any membership function (MF).

Layer-2: This layer (also called the membership layer) checks for the weights of each of the membership functions. It receives the input values o_i^1 from the 1st layer and acts as MFs to represent the fuzzy sets of the respective input variables. Further, it computes the membership values which specify the degree to which the input value o_i^1 belongs to the fuzzy set, which acts as the inputs to the next layer.

$$o_i^2 = w_i = \mu_{A_i}(x).\mu_{B_i}(y), i = 1,2 \tag{4.3}$$

Layer-3: This layer is called the rule layer. Each node (also called neuron) in this layer performs the pre-condition matching of the fuzzy rules, i.e. they compute the activation level of each rule, the number of layers being equal to the number of fuzzy rules. Each node of these layers calculates the weights which are normalized.

$$o_i^3 = \overline{w_i} = \frac{w_i}{w_1+w_2}, i = 1,2 \tag{4.4}$$

Every node in this layer calculates the normalized weight which is expressed by the above equation. Where, $\overline{w_i}$ is referred as the normalized firing strengths.

Layer-4: This layer is called defuzzification layer & provides the output values, z resulting from the inference of rules. Connections between the layers l_3 & l_4 are weighted by the fuzzy singletons that represent another set of parameters for the neuro-fuzzy network.

$$o_i^4 = \overline{w_i}z_i = \overline{w_i}(p_i x + q_i y + r_i), i = 1,2 \tag{4.5}$$

Where, $\overline{w_i}$ is the output of the layer 3 and $\{p_i,\ q_i,\ r_i\}$ is the parameter set. The parameters in this layer are referred as the consequent parameter.

Layer-5: This layer is called the output layer which sums up all the inputs coming from the layer-4 and transforms the fuzzy classification results into a crisp value.

$$o_i^5 = \sum_{i=1}^{2} \overline{w_i}z_i = \frac{w_i z_i + w_2 z_2}{w_1+w_2} \tag{4.6}$$

The output z in Fig.4.5 can be rewritten as:

$$z = (\overline{w_1}x)p_1 + (\overline{w_1}y)q_1 + (\overline{w_1})r_1 + (\overline{w_2}x)p_2 + (\overline{w_2}y)p_2 + (\overline{w_2})r_2 \tag{4.7}$$

The normalized membership functions of input variables and output variable are shown in Fig.4.7.a, Fig.4.7.b and Fig.4.7.c respectively. The three dimensional plot of the Fuzzy Control

Surface is shown in Fig.4.11 and the internal structure of the developed adaptive neuro fuzzy inference system is shown in Fig.4.10 which is developed using Fuzzy Logic Toolbox in MATLAB.

The ANFIS structure can be tuned automatically by using either least-square estimation or the back propagation algorithm. The back propagation algorithm mentioned above is used in the next section to tune the developed ANFIS controller to control various parameters of induction motor. Because of its flexibility, the ANFIS strategy can be used for a wide range of control applications.

The development of the control strategy for control of various parameters of the induction machine such as the speed, flux, torque, voltage and current is presented using the concepts of ANFIS control scheme, the block diagram of which is shown in the Fig.4.6. To start with, we design the controller using the ANFIS scheme. Fuzzy logic is one of the successful applications of fuzzy set in which the variables are linguistic rather than the numeric variables. Linguistic variables, defined as variables whose values are sentences in a natural language (such as large or small), may be represented by the fuzzy sets. Fuzzy set is an extension of a 'crisp' set where an element can only belong to a set (full membership) or not belong at all (no membership). Fuzzy sets allow partial membership, which means that an element may partially belong to more than one set.

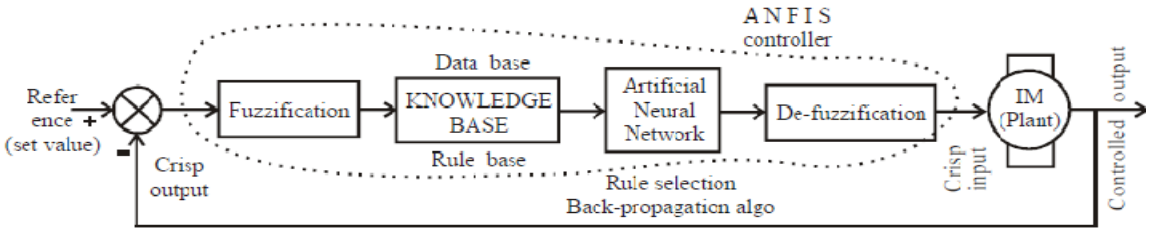

Fig.4.6: Block diagram of the ANFIS control scheme for the speed control of the IM [55]

A fuzzy set, A of a universe of discourse, X is represented by a collection of ordered pairs of generic element and its membership function, μ: X →[0 1], which associates a number μA(x): X → [0 1], to each element x of X. A fuzzy logic controller is based on a set of control rules called as the fuzzy rules among the linguistic variables. These rules are expressed in the form of conditional statements.

Our basic structure of the developed ANFIS controller to control the speed of the IM consists of four important parts, namely- fuzzification, knowledge base, neural network and the de-fuzzification blocks, which are explained in brief in following paragraphs.

The inputs to the ANFIS controller, i.e., the error & the change in error are expressed as:

$$e(k) = \omega_{ref} - \omega_r \tag{4.8}$$

$$\Delta e(k) = e(k) - e(k-1) \tag{4.9}$$

Where, ω_{ref} is the reference speed, ω_r is the actual rotor speed, $e(k)$ is the error and $\Delta e(k)$ is the change in error at the sampling instant k. The fuzzification unit converts the crisp data into linguistic variables, which is given as inputs to the rule based block. The set of 49 rules are written on the basis of previous knowledge / experiences in the rule based block. The rule base block is connected to the neural network block. Back propagation algorithm is used to train the neural network to select the proper set of rule base. For developing the control signal, the training is a very important step in the selection of the proper rule base. Once the proper rules are selected & fired, the control signal required to obtain the optimal outputs is generated.

The output of the NN unit is given as input to the de-fuzzification unit and the linguistic variables are converted back into the numeric form of data in the crisp form. In the fuzzification process, i.e., in the first stage, the crisp variables, the speed error & the change in error are converted into fuzzy variables or the linguistics variables. The fuzzification maps the two input variables to linguistic labels of the fuzzy sets. Each fuzzy label has an associated membership function. The membership functions of triangular and trapezoidal types are used in this work and are shown in the Fig.4.7.

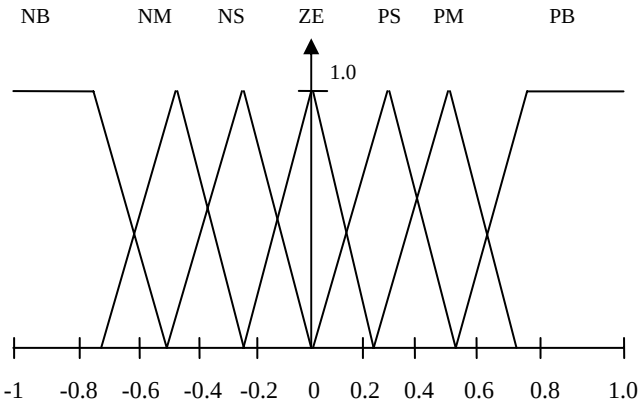

Fig 4.7.a: Membership Function for Input Variable Error, ‘e’.

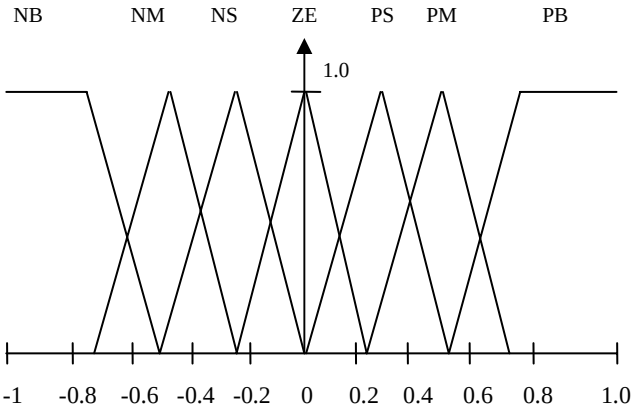

Fig 4.7.b: Membership Function for Input Variable Error, 'ce'.

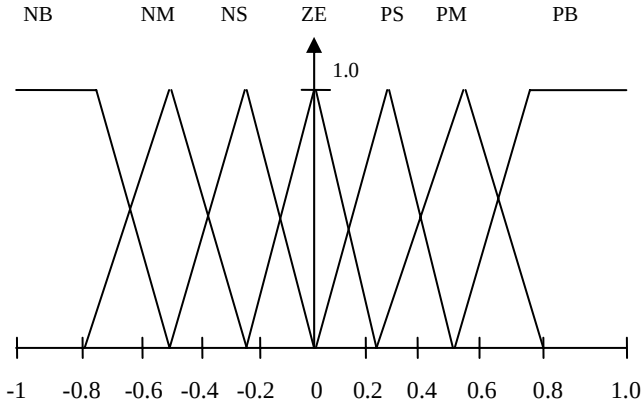

Fig 4.7.c: Membership Function for Output Variable Controlled Output, 'z'.

Table II: Rule Base for Fuzzy Logic Controller for IM Drive

'e' / 'ce'	**NB**	**NM**	**NS**	**ZE**	**PS**	**PM**	**PB**
NB	NB	NB	NB	NB	NM	NS	ZE
NM	NB	NB	NB	NM	NS	ZE	PS
NS	NB	NB	NM	NS	ZE	PS	PM
ZE	NB	NM	NS	ZE	PS	PM	PB
PS	NM	NS	ZE	PS	PM	PB	PB
PM	NS	ZE	PS	PM	PB	PB	PB
PB	ZE	PS	PM	PB	PB	PB	PB

The inputs are fuzzified using the fuzzy sets and are given as input to ANFIS controller. The rule base for selection of proper rules using the back propagation algorithm is written as shown in the Table II. The developed 49 (7x7) fuzzy rules included in the ANFIS controller are given in the Appendix - C.

The control decisions are made based on the fuzzified variables in the Table II. The inference involves a set of rules for determining the output decisions. As there are 2 input variables with each having 7 membership functions each and the controller has a set of 49 rules. Out of these 49 rules, the proper rules are selected by training the neural network with the help of back propagation algorithm & these selected rules are fired. Further, it has to be converted into numerical output, i.e., they have to be de-fuzzified. This process is what is called as defuzzification, which is the process of producing a quantifiable result in fuzzy logic.

The defuzzification transforms fuzzy set information into numeric data information. There are so many methods to perform the defuzzification, i.e. centre of gravity method, centre of singleton method, maximum methods, and marginal properties of the centroid methods and so on. In our work, we use the centre of gravity method. The output of the defuzzification unit will generate the control commands which in turn is given as input (called as the crisp input) to the plant. If there is any deviation in the controlled output (crisp output), this is fed back and compared with the set value and the error signal is generated which is given as input to the ANFIS controller which in turn brings back the output to the normal value, thus maintaining stability in the system.

This controlled output ‘z’ is nothing but the final output of the controller and is the weighted average of the proper rule based outputs, which are selected by the back propagation algorithm.

4.3.3 Development of Simulink Model

The proposed ANFIS controller is developed in the Matlab/ Simulink platform using the Simulink Power System Toolbox and Fuzzy Logic Toolbox. The Simulink model for the proposed ANFIS controller is shown in Fig.4.8 and the speed controller that employs the proposed neuro-fuzzy controller is shown in the Fig.4.9.

The adaptive neuro fuzzy inference system was developed using the ANFIS editor platform provided with the Fuzzy Logic Toolbox in Matlab. The internal structure of the ANFIS is shown

in the Fig.4.10. From the internal structure it is evident that the system has five layers in it including three hidden layers, two input variables and one output variable in the input and output layers respectively. The values of the neurons (nodes) and their corresponding synapses (connections) are adjusted using training of the Neural Network (NN) using the back-propagation algorithm. For training the network, three training epochs have been used which represents the system (induction motor) behavior under different operating conditions. The training data sets have been generated by simulating the same direct torque control scheme based speed control of induction motor drive using PI speed controller under various and wide range of speed references and speed changes. The training of the network converged to within a training error of 0.002 and a testing error of 0.004. The three dimensional plot of the control surface of the developed ANFIS is given in Fig.4.11.

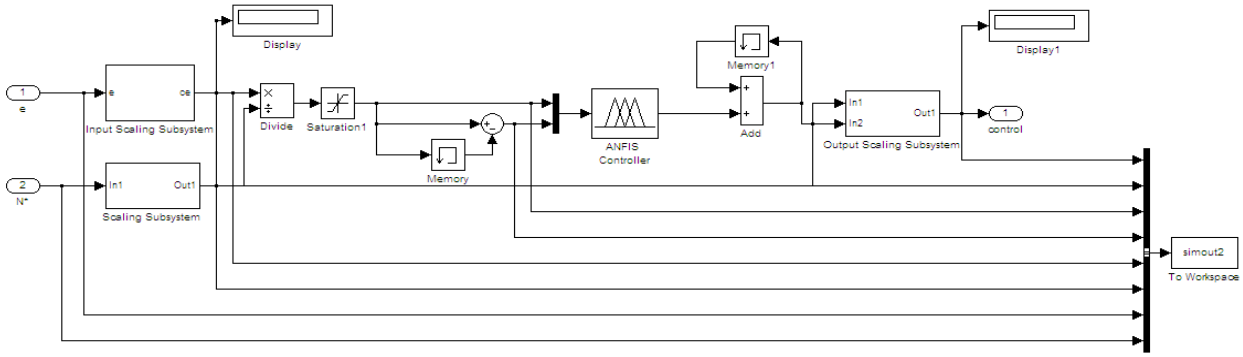

Fig.4.8: Proposed Adaptive Neuro Fuzzy Inference System based Controller for IM Drive

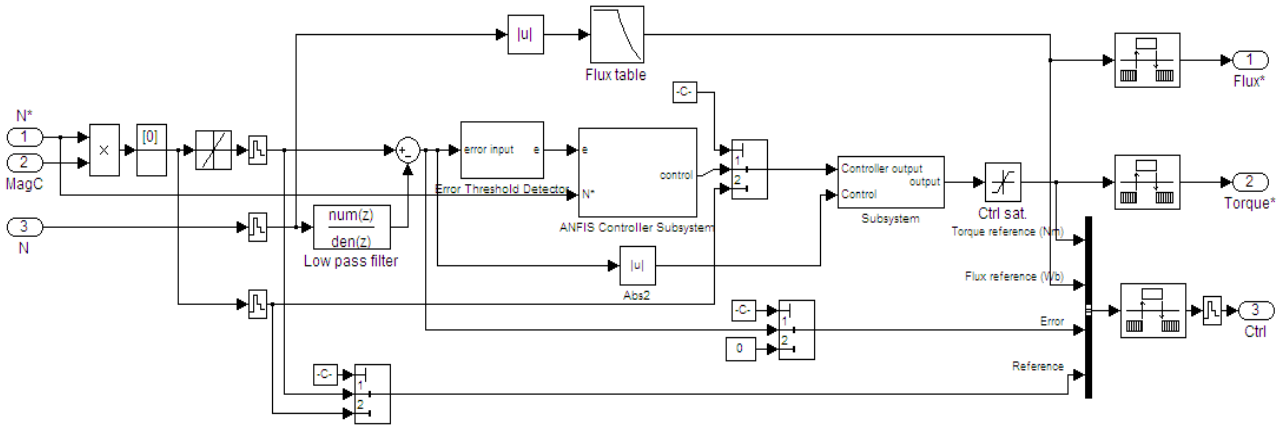

Fig.4.9: Complete Simulink Model of the Proposed ANFIS based Speed Controller for the Induction Motor Drive

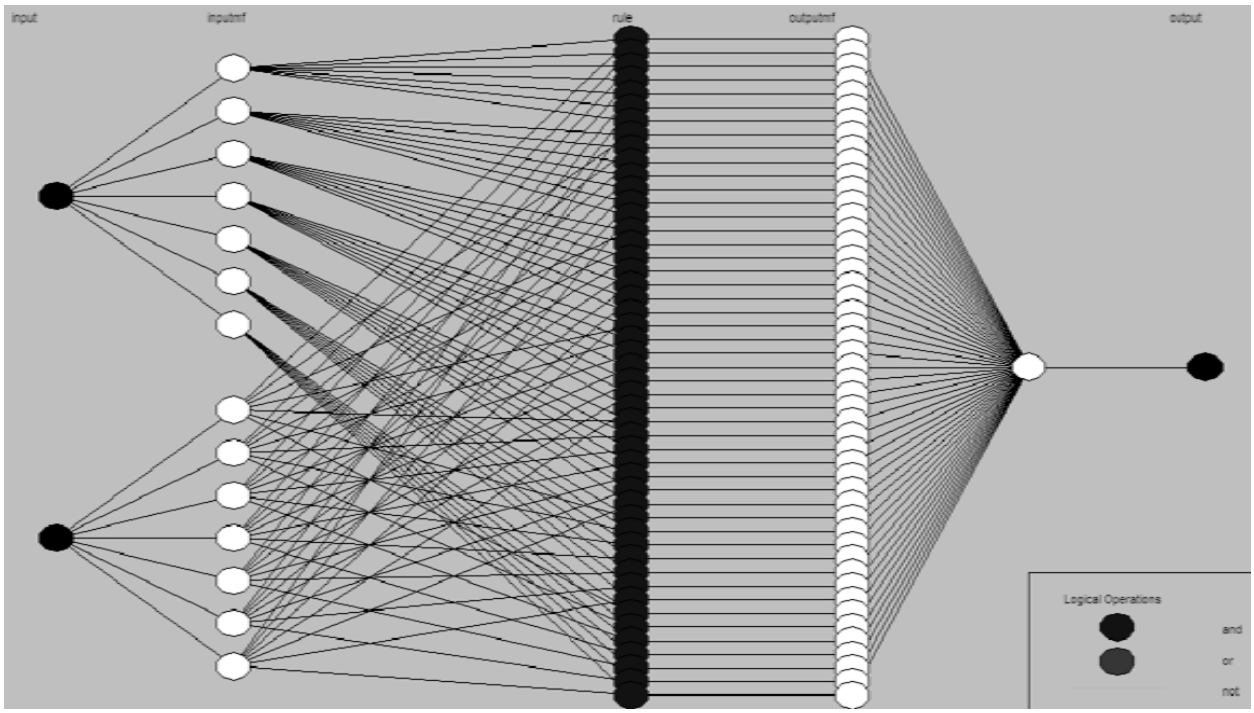

Fig.4.10: The Proposed Adaptive Neuro Fuzzy Inference System Structure

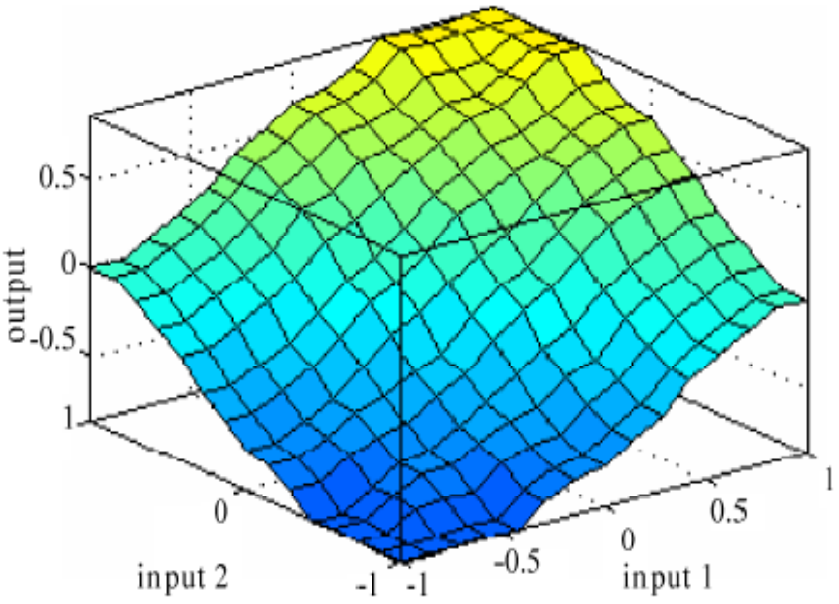

Fig.4.11: Three Dimensional Control Surface Plot of the Proposed ANFIS Structure

Chapter 5

Simulation Results

The effectiveness of the proposed ANFIS based Speed Controller for IM drive is investigated thoroughly by the help of simulation. The simulation model was developed by using MATLAB/Simulink software. The complete Simulink model of the drive system is shown in Fig.5.1. The complete model using PI controller for the same purpose of speed control of the IM drive is shown in Fig.5.2, where TSK type NFC has been replaced by the classical PI controller. The NFC Simulink model is shown in Fig.5.3.

The parameters of the motors used for simulation are listed in Appendix-A. The detailed Simulink subsystems of the ANFIS based IM drive is attached in Appendix-B. From here onward to avoid the repetition of phrase "Proposed ANFIS based DTC scheme for Speed Control of Induction Motor Drive" will be replaced by "proposed controller". In order to test the effectiveness of the proposed controller based DTC scheme for IM drive, numerous simulations have been carried out. The performance of the proposed controller is also compared with the conventional DTC scheme with PI controller to prove its superiority. Sample simulation results are presented in the following paragraphs.

The developed model of the proposed adaptive neuro fuzzy inference system based induction motor drive has been simulated for various speed references using the Simulink platform and for each of the reference speed the simulation results for the rotor speed in radians per second (rad/sec), developed torque (N-m), stator current (Amps) and the plot of the stator flux linkage (ψ_s) components in α-β plane ($\psi_{s\alpha} and\ \psi_{s\beta}$) against each other are compiled. Each of these results for the proposed controller has been compared with the same from the simulation results of the conventional PI controller based DTC induction motor drive. From each of these simulation results the performances of the individual controllers (i.e. ANFIS and PI controller) are compared on the basis of comparing steady state speed error, percent overshoot, rising time, settling time, ripples in the developed torque, stator current ripples and percentage of the stator flux ripple. At the end the results are compiled in the Table III.

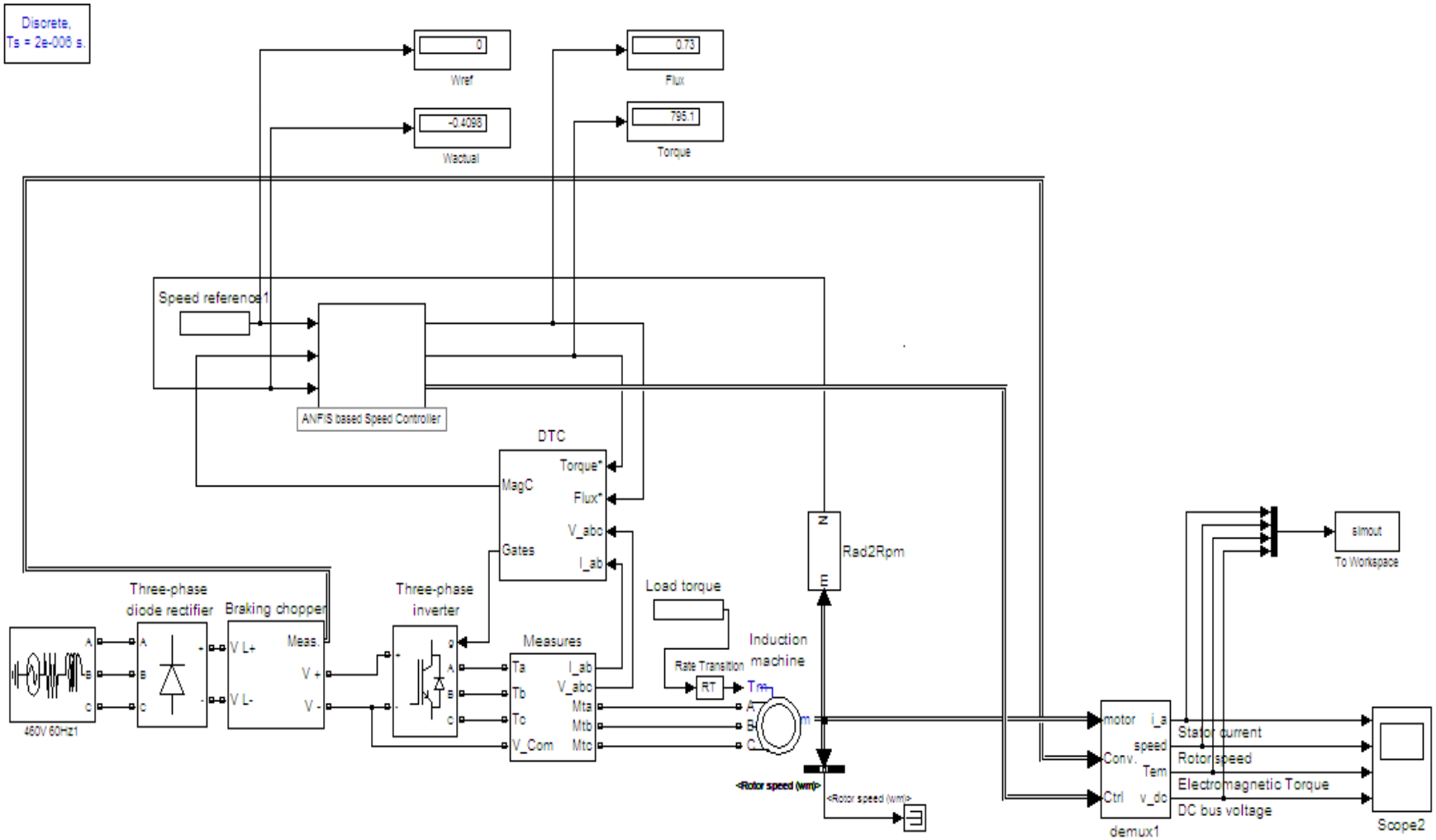

Fig.5.1: Simulink model for the ANFIS based Direct Torque Control Scheme based Induction Motor Drive

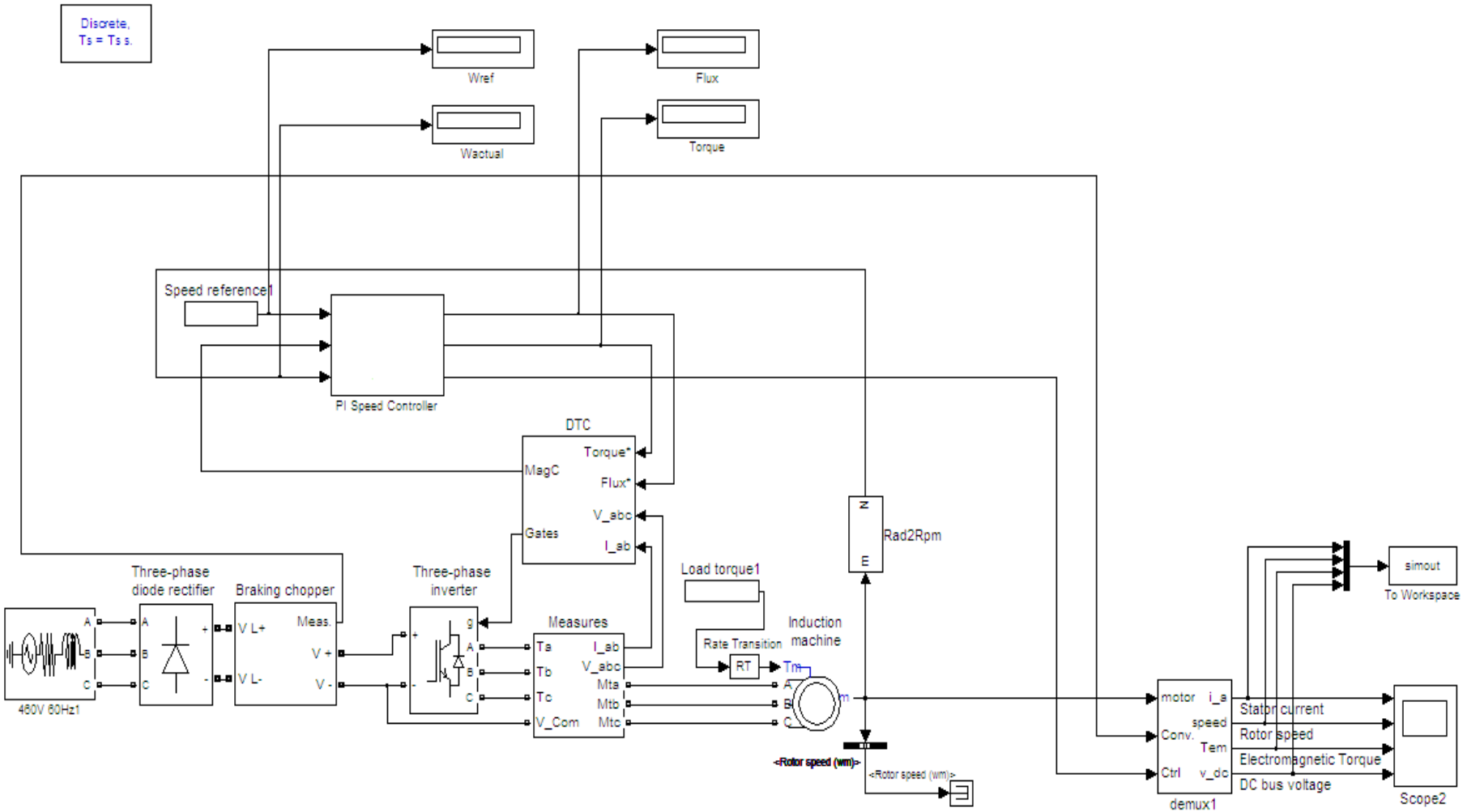

Fig.5.2: Simulink model for the PI controller based Direct Torque Control Scheme based Induction Motor Drive

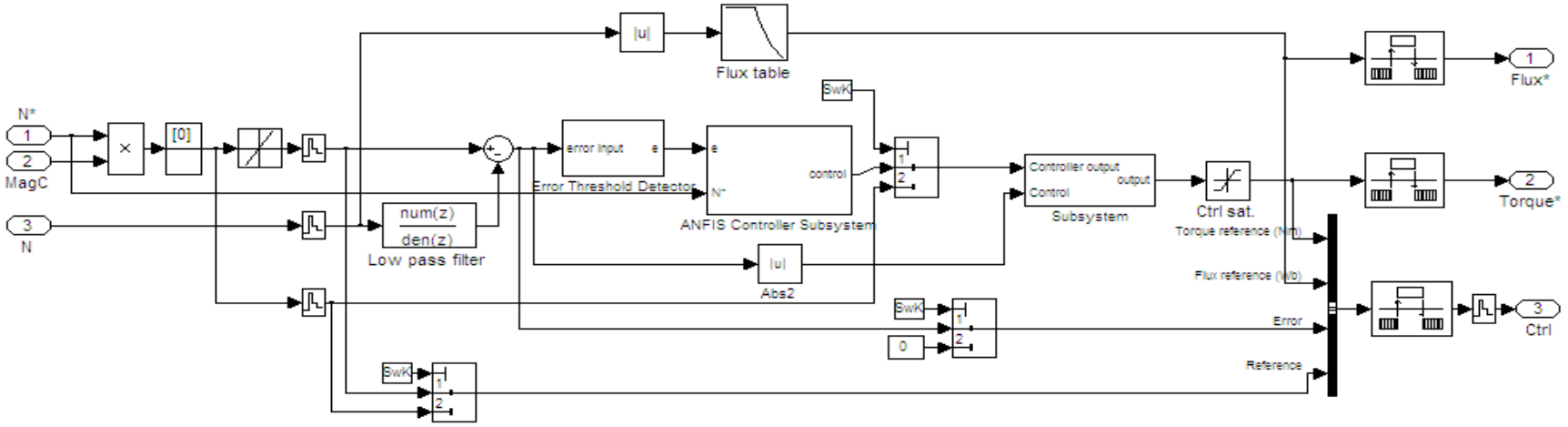

(a)

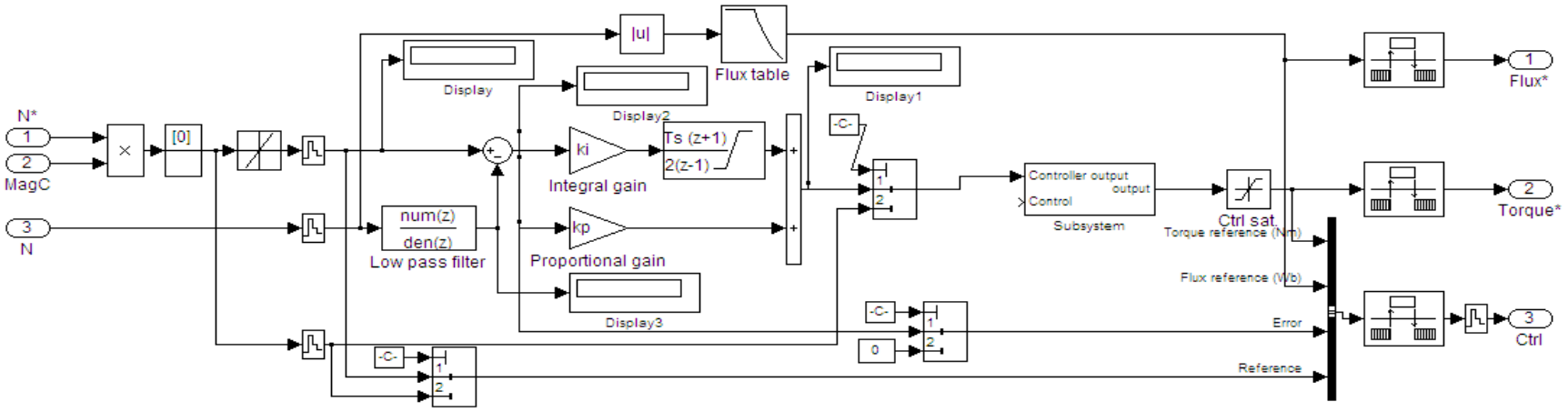

(b)

Fig.5.3: Simulink model for (a) Proposed ANFIS Controller, (b) Classical Proportional Integral Controller

5.1. Simulation Results

Case – I: Motor running at no load and reference speed is set to be equal to the rated speed of the motor.

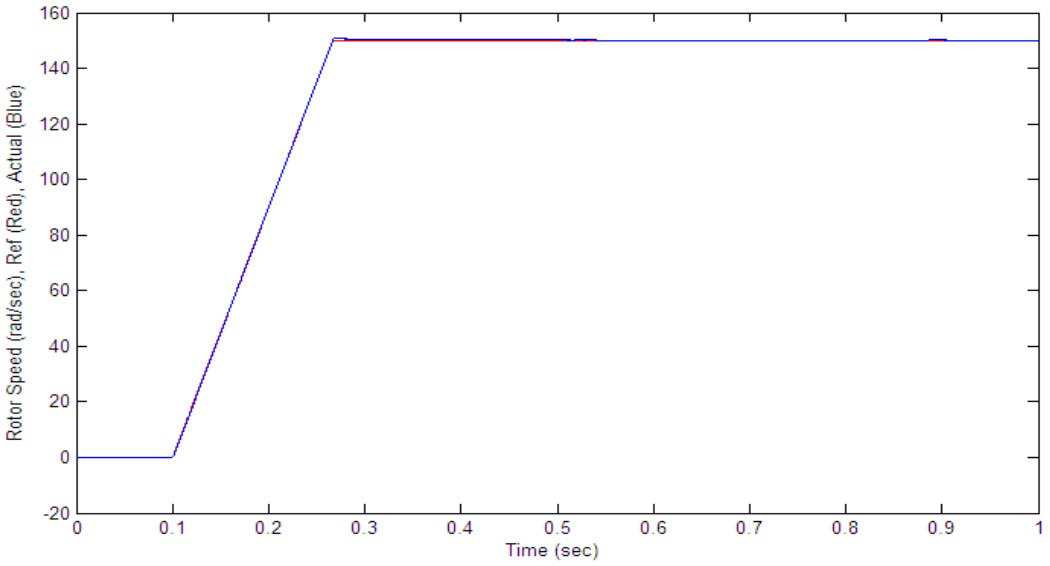

(a)

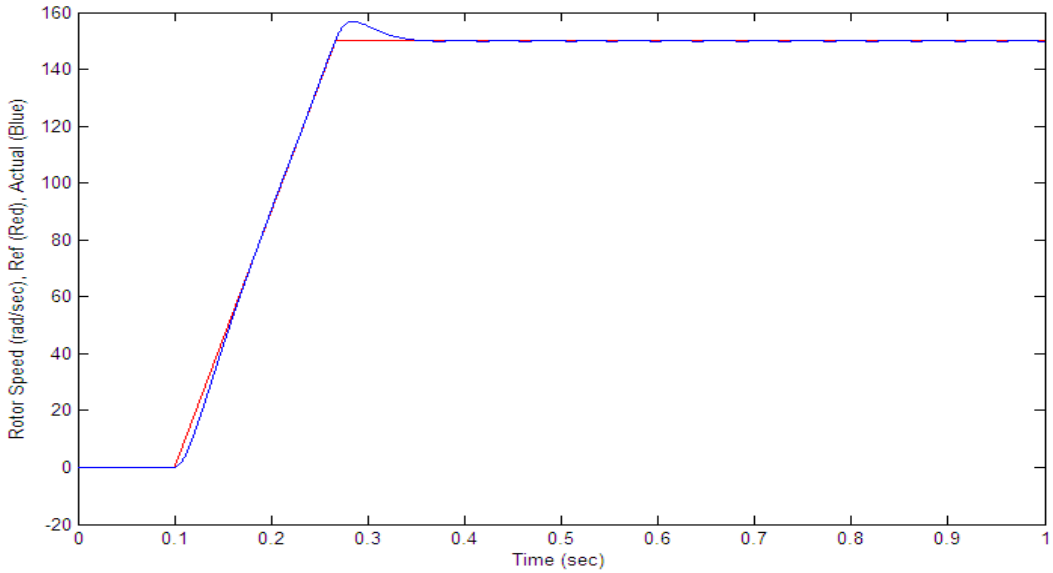

(b)

Fig.5.4: Speed response of the IM drive at no-load and rated speed of 150 rad/sec; (a) proposed ANFIS based speed controller response, (b) classical PI controller response

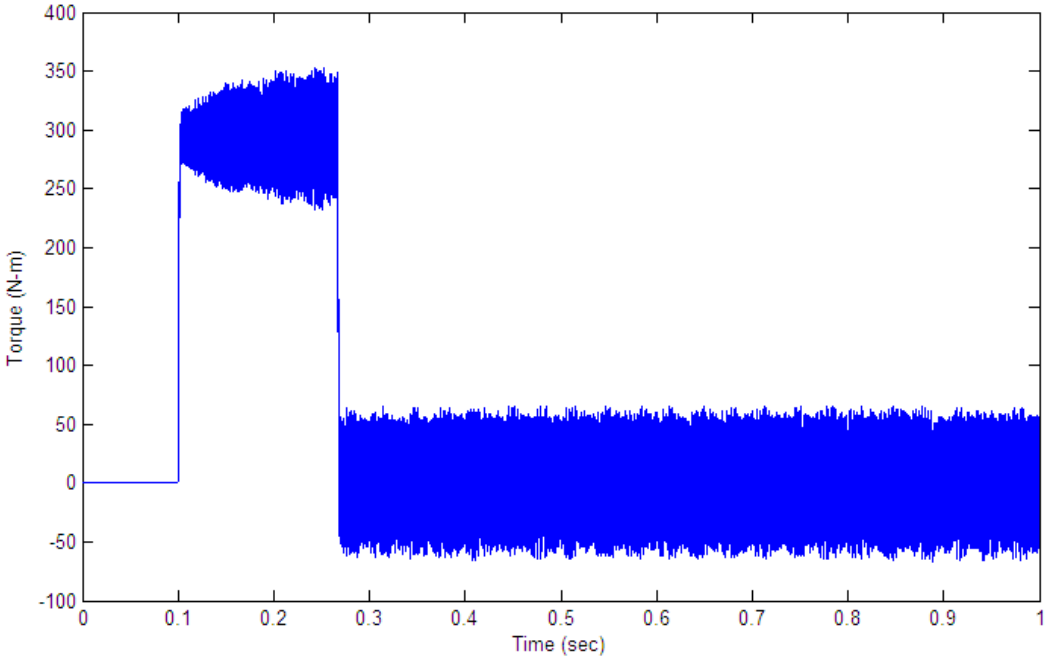

(a)

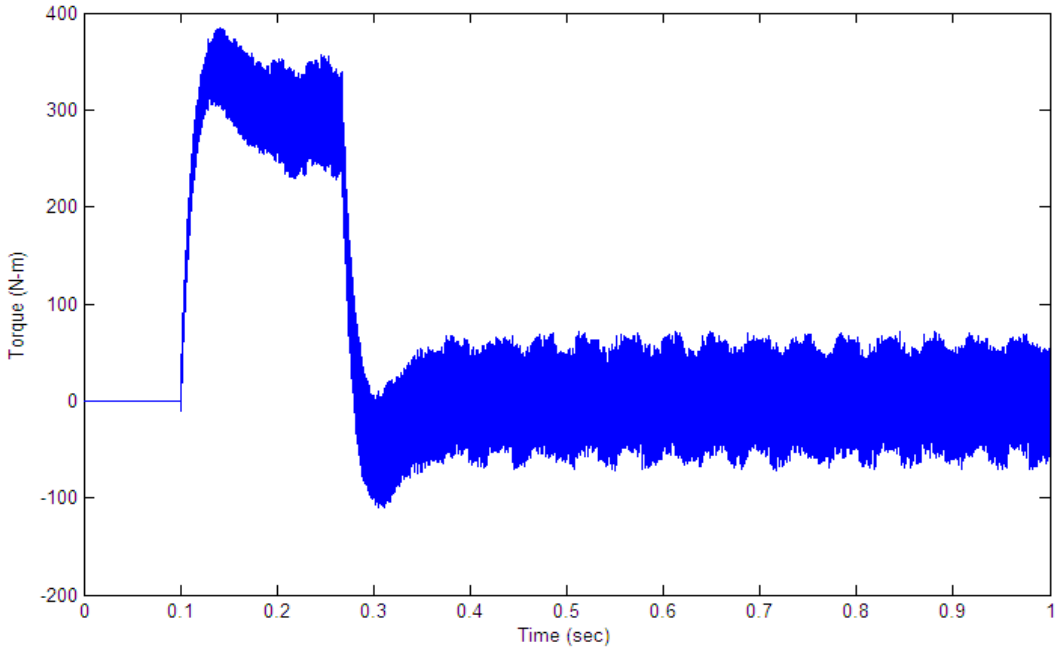

(b)

Fig.5.5: Torque Response of the IM drive at no-load and rated speed of 150 rad/sec (a) proposed ANFIS controller based DTC, (b) classical PI controller based DTC

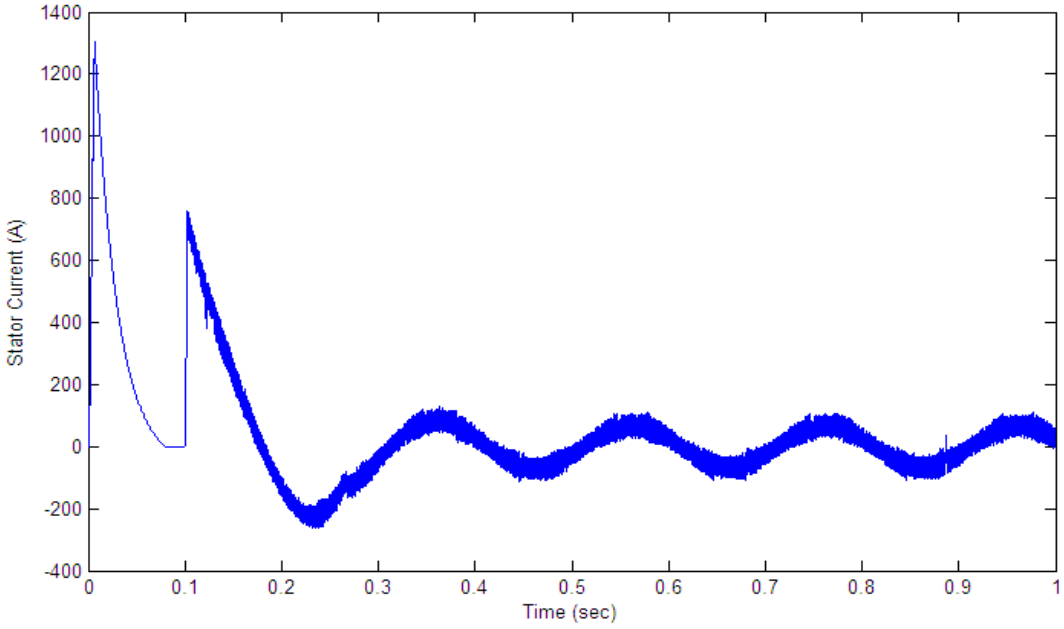

(a)

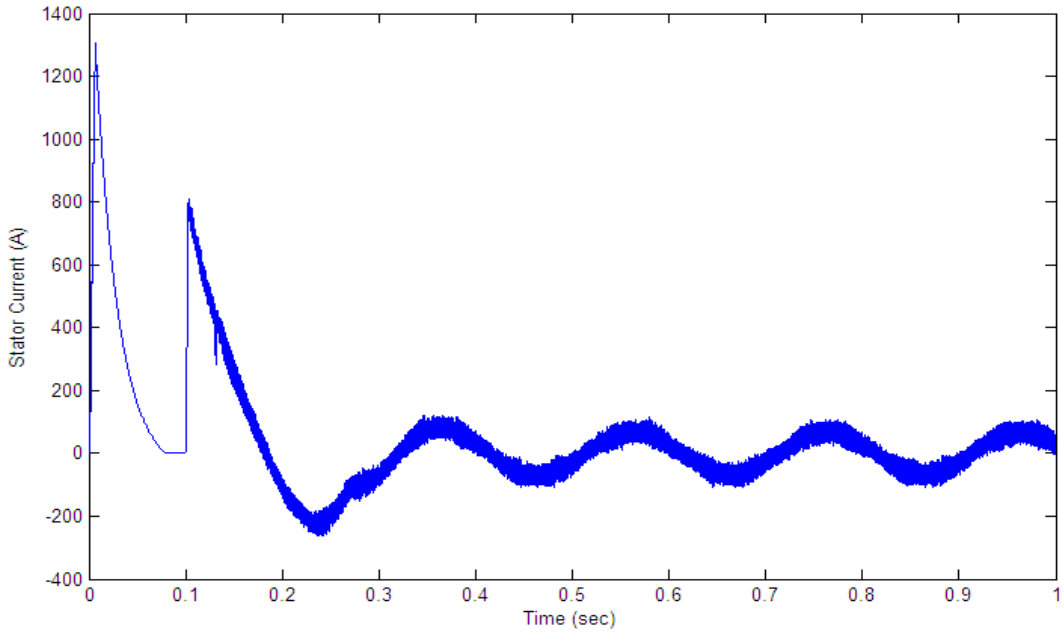

(b)

Fig.5.6: Stator current of response of the IM drive running at no-load and rated speed of 150 rad/sec, (a) proposed ANFIS based DTC, (b) classical PI controller based DTC

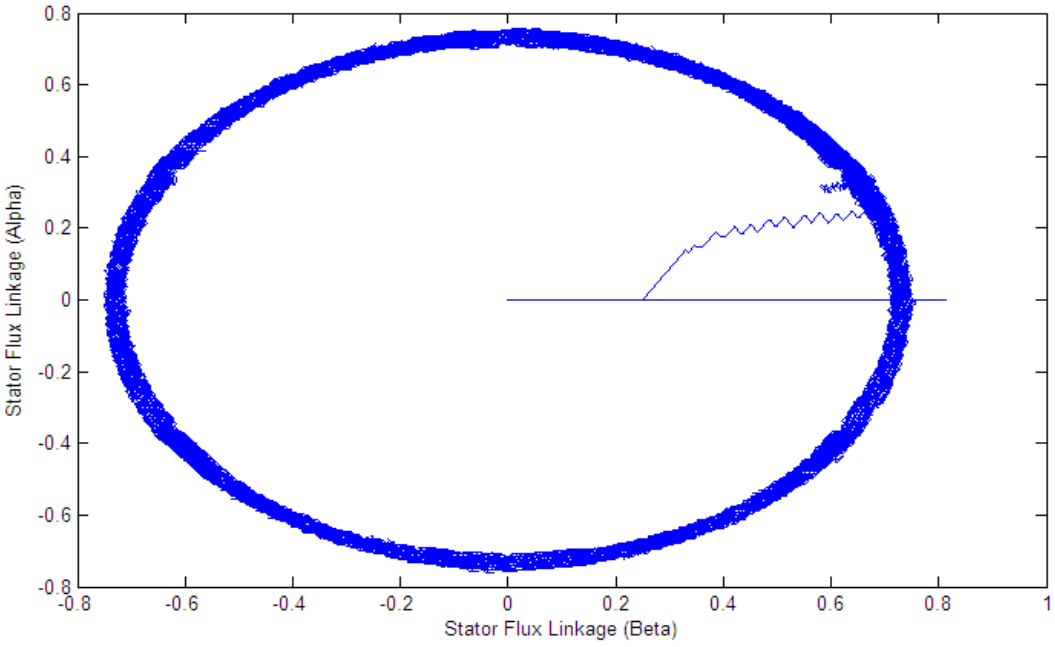

(a)

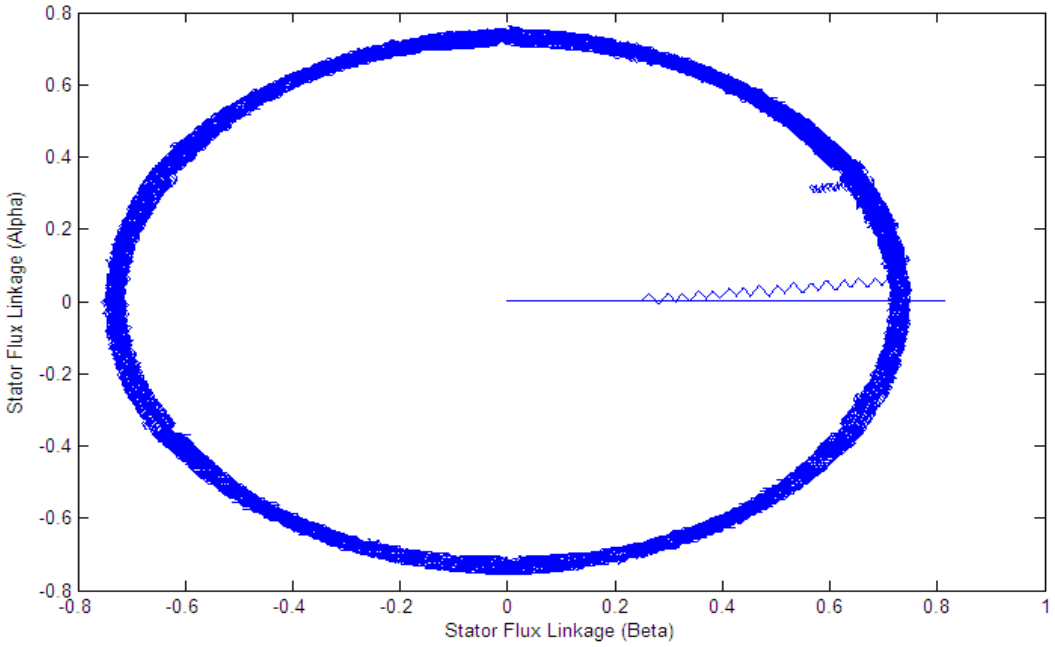

(b)

Fig.5.7: Stator Flux Linkage of the IM drive running at no-load and rated speed of 150 rad/sec, (a) proposed ANFIS based DTC, (b) classical PI controller based DTC

Case – II: Motor running at a reference speed equal to the rated speed of the motor with an abrupt change in the load.

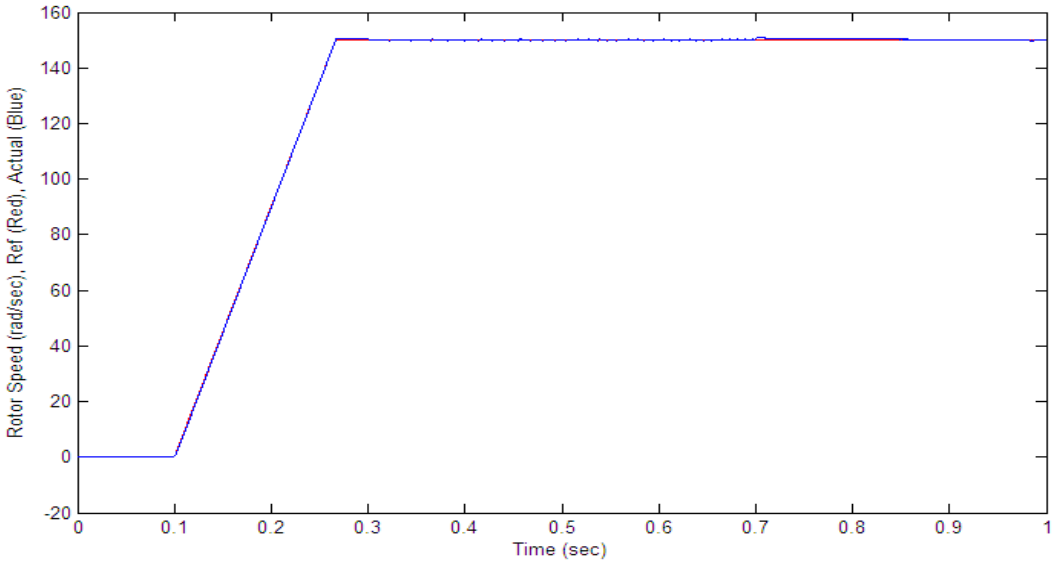

(a)

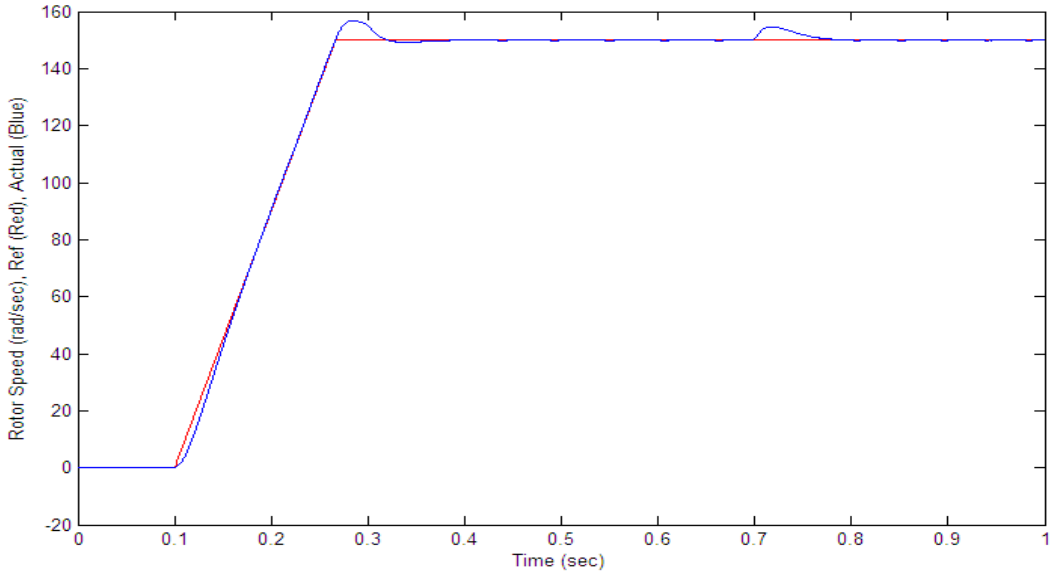

(b)

Fig.5.8: Speed response of the IM drive at rated speed of 150 rad/sec and with an abrupt load change from +100 N-m to -100 N-m; (a) proposed ANFIS based speed controller response, (b) classical PI controller response

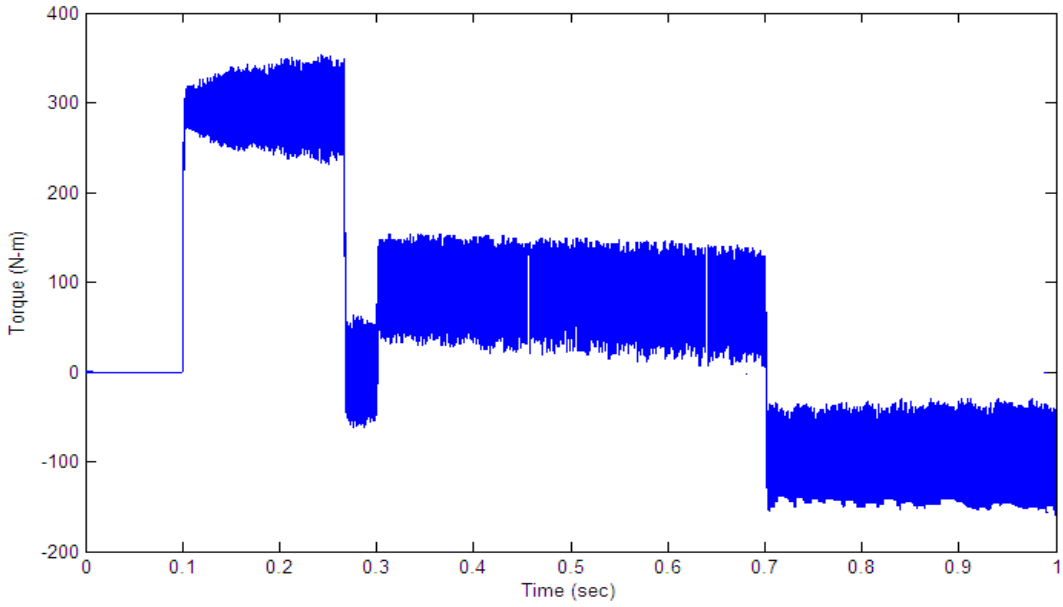

(a)

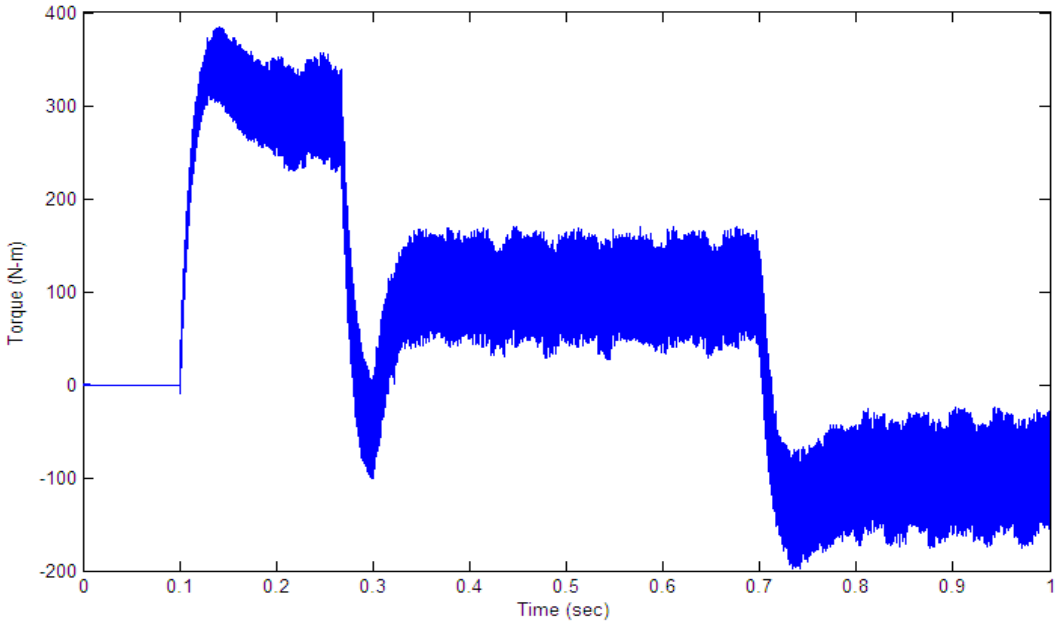

(b)

Fig.5.9: Torque response of the IM drive at rated speed of 150 rad/sec and with an abrupt load change from +100 N-m to -100 N-m; (a) proposed ANFIS based speed controller response, (b) classical PI controller response

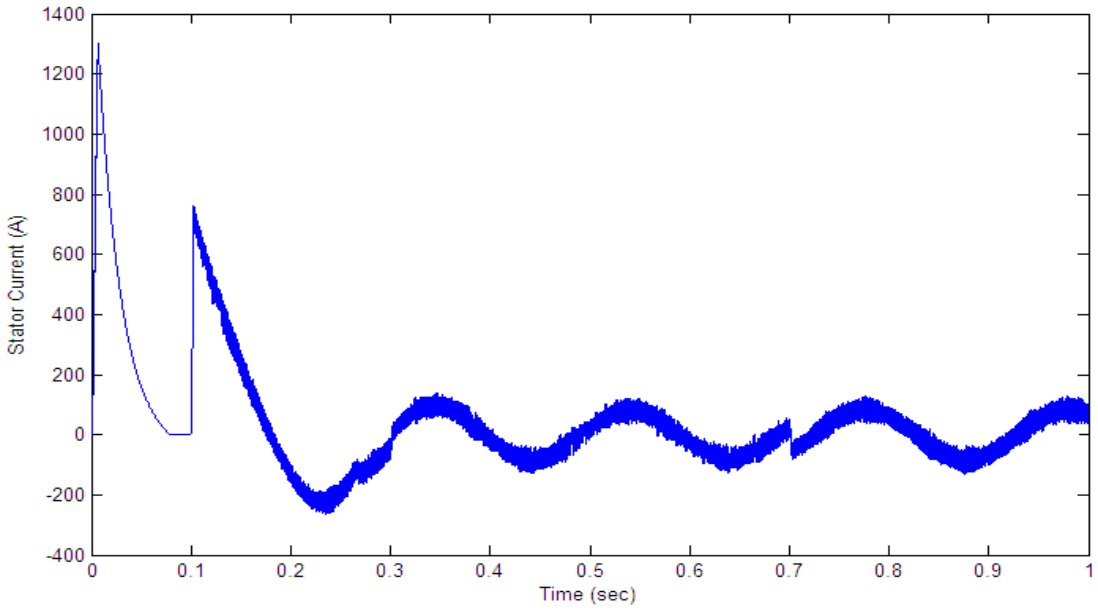

(a)

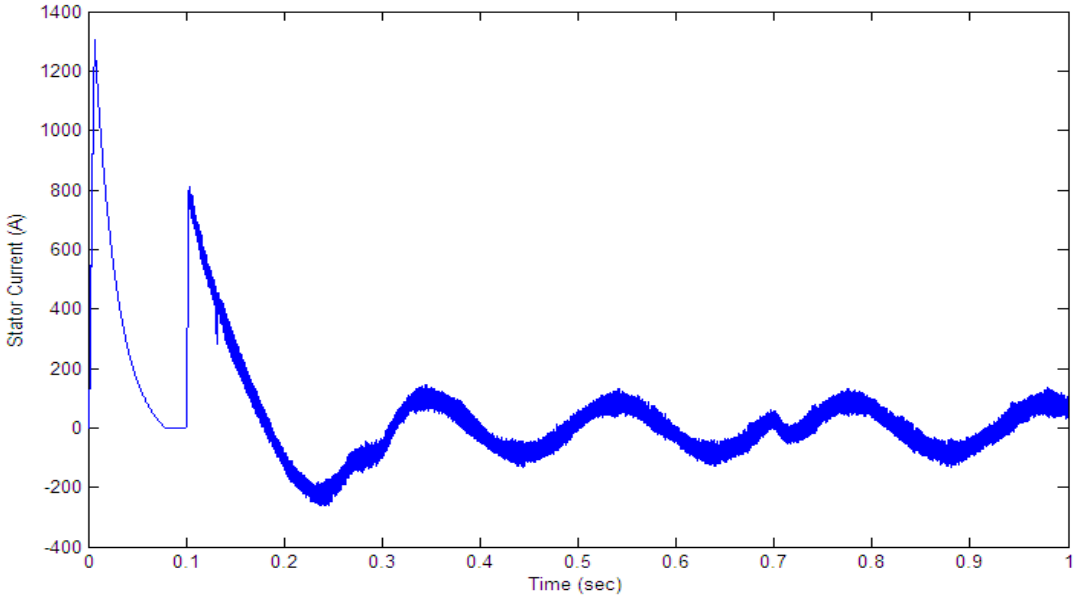

(b)

Fig.5.10: Stator Current of the IM drive at rated speed of 150 rad/sec and with an abrupt load change from +100 N-m to -100 N-m; (a) proposed ANFIS based speed controller response, (b) classical PI controller response

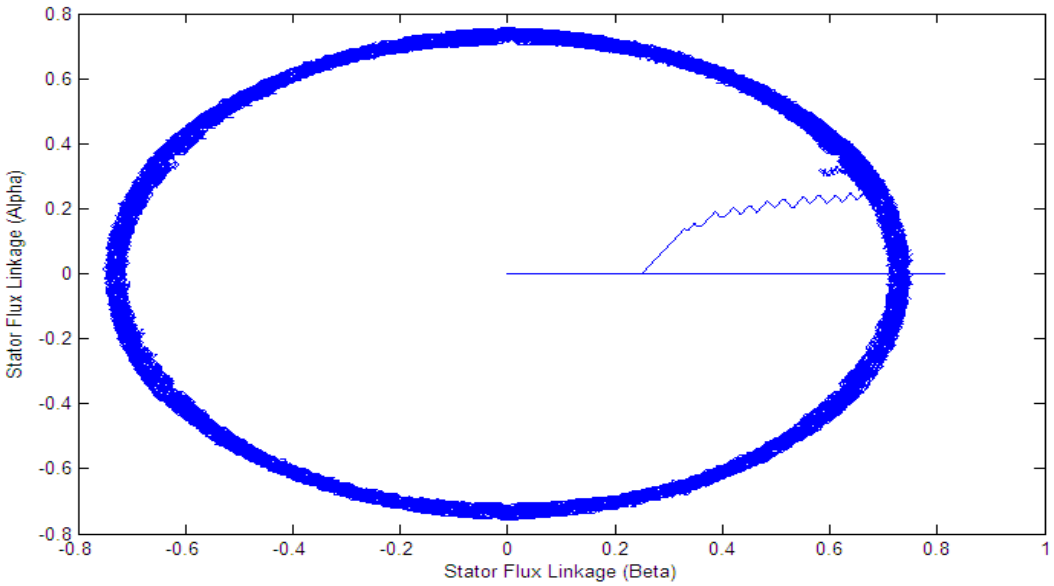

(a)

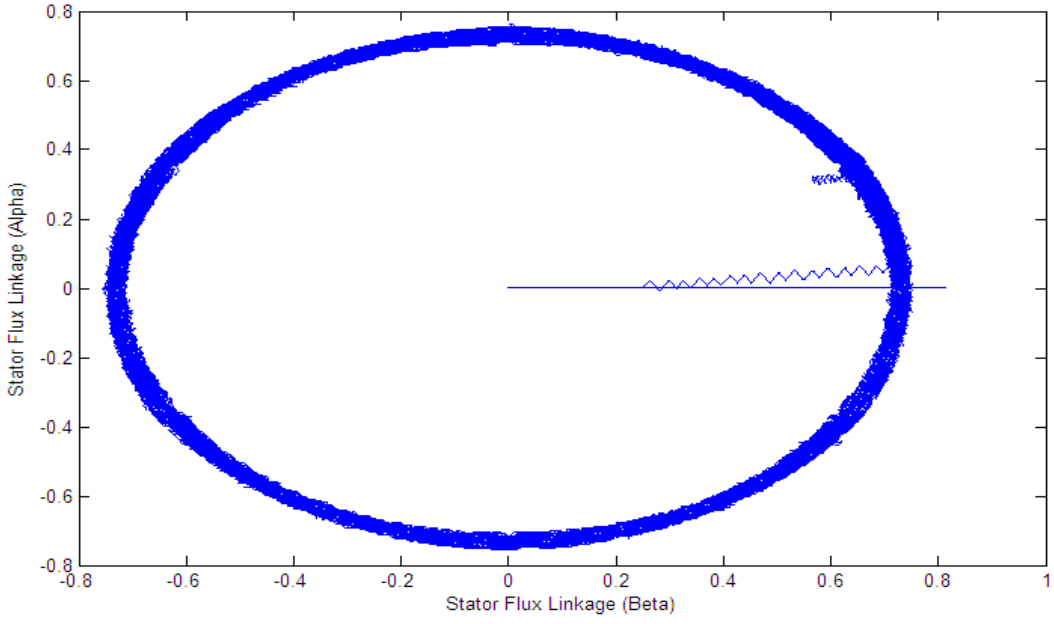

(b)

Fig.5.11: Stator Flux Linkage of the IM drive at rated speed of 150 rad/sec and with an abrupt load change from +100 N-m to -100 N-m; (a) proposed ANFIS based speed controller response, (b) classical PI controller response

Case – III: Motor running at no load with a step change in the reference speed of the motor.

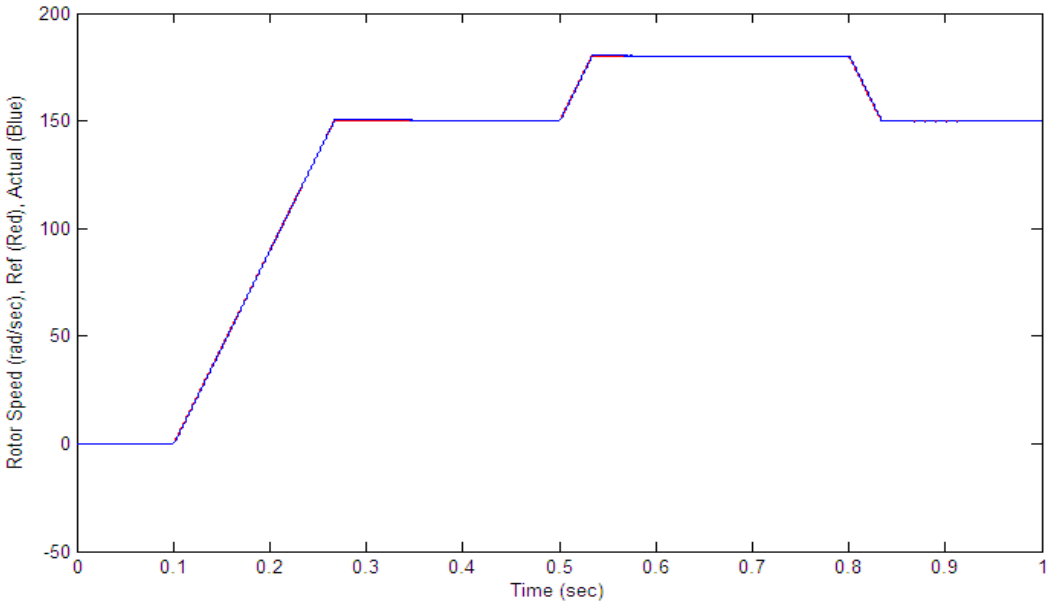

(a)

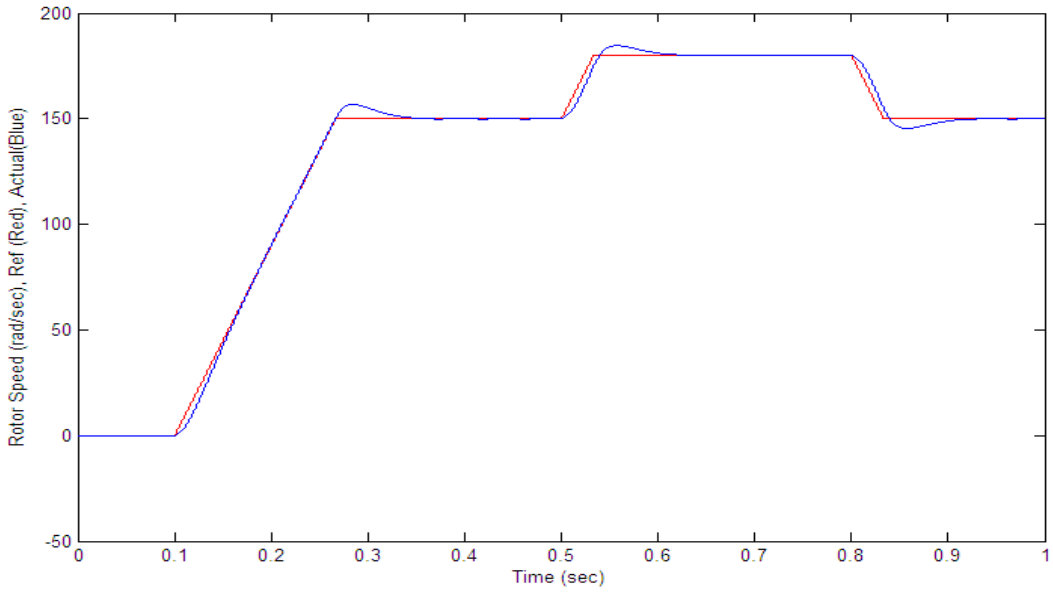

(b)

Fig.5.12: Speed response of the IM drive running at no load and at a reference speed of 150 rad/sec and a step change to 180 rad/sec; (a) proposed ANFIS based speed controller response, (b) classical PI controller response

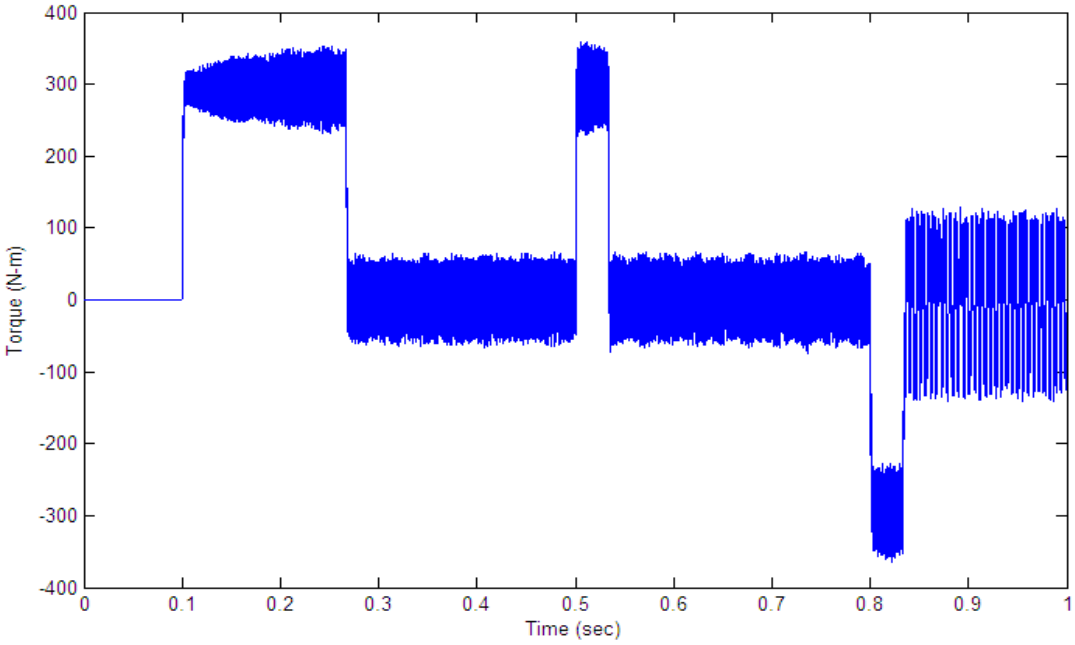

(a)

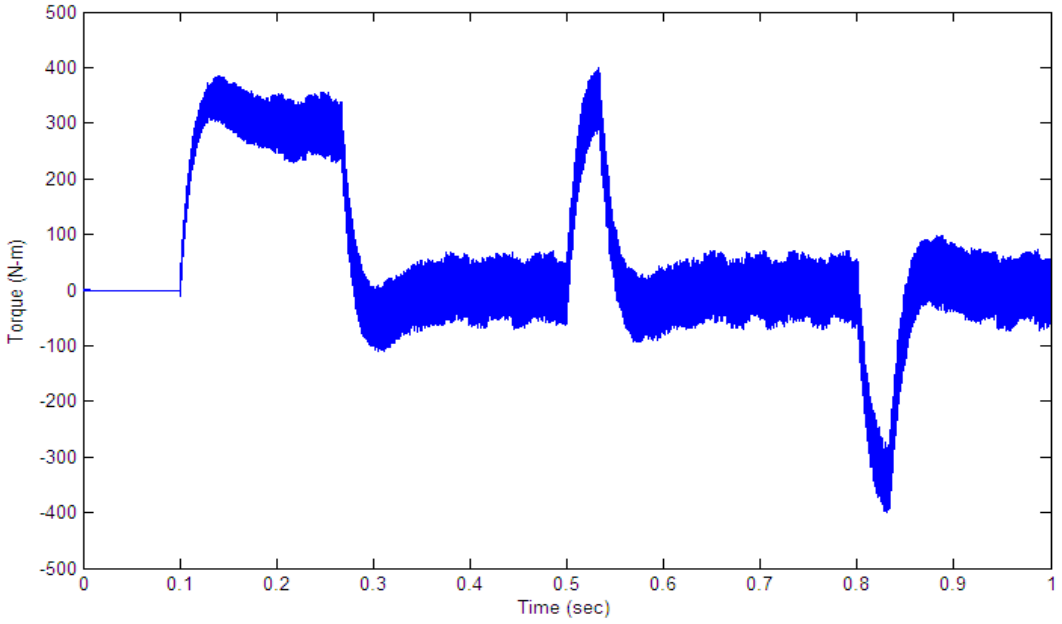

(b)

Fig.5.13: Torque response of the IM drive running at no load and at a reference speed of 150 rad/sec and a step change to 180 rad/sec; (a) proposed ANFIS based speed controller response, (b) classical PI controller response

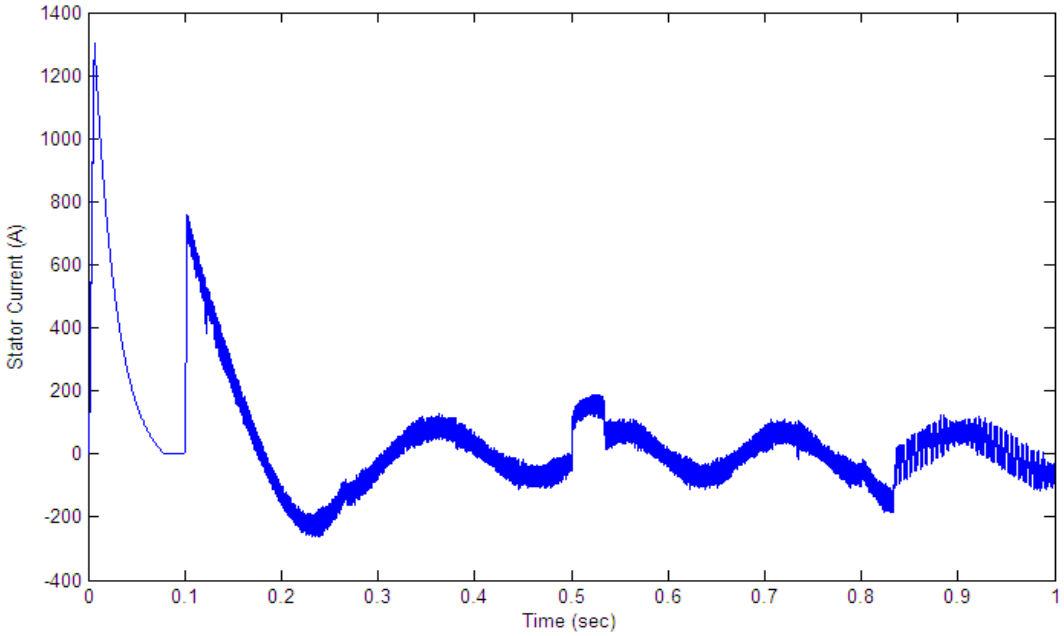

(a)

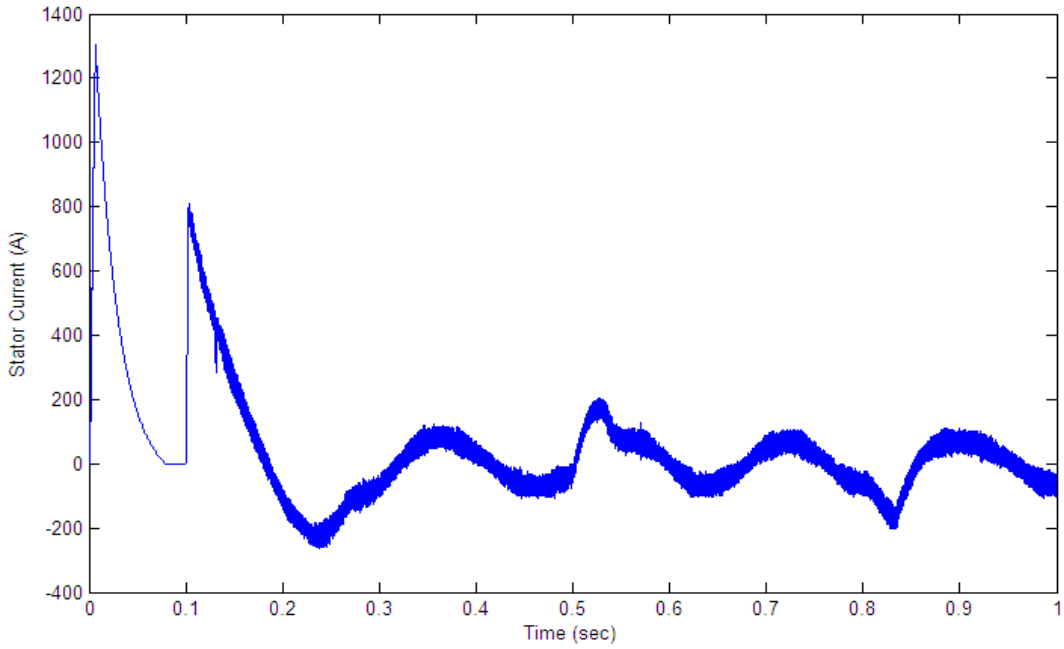

(b)

Fig.5.14: Stator current response of the IM drive running at no load and at a reference speed of 150 rad/sec and a step change to 180 rad/sec; (a) proposed ANFIS based speed controller response, (b) classical PI controller response

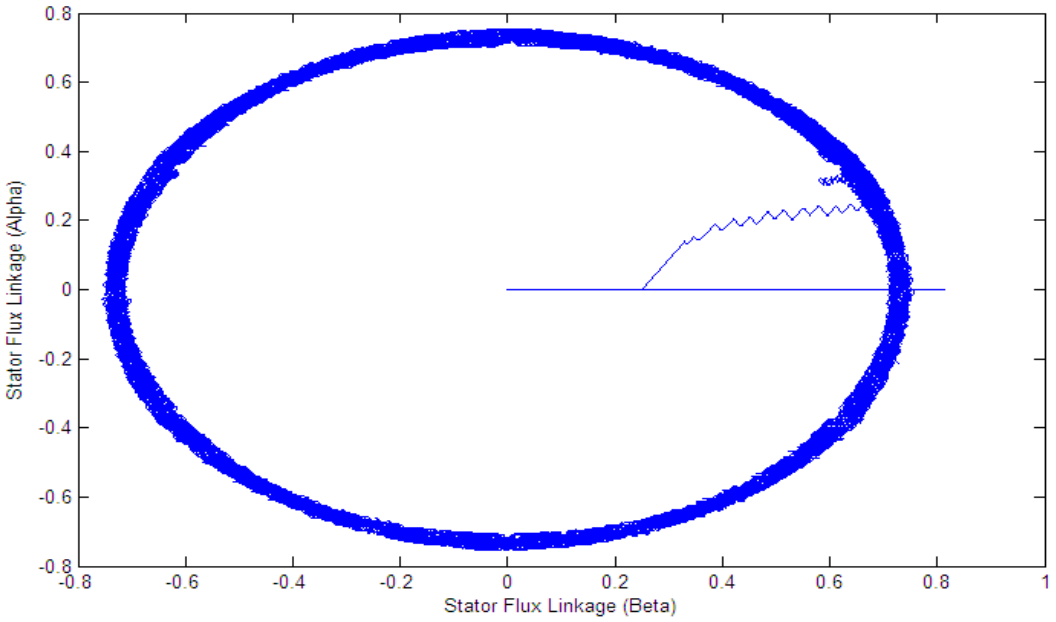

(a)

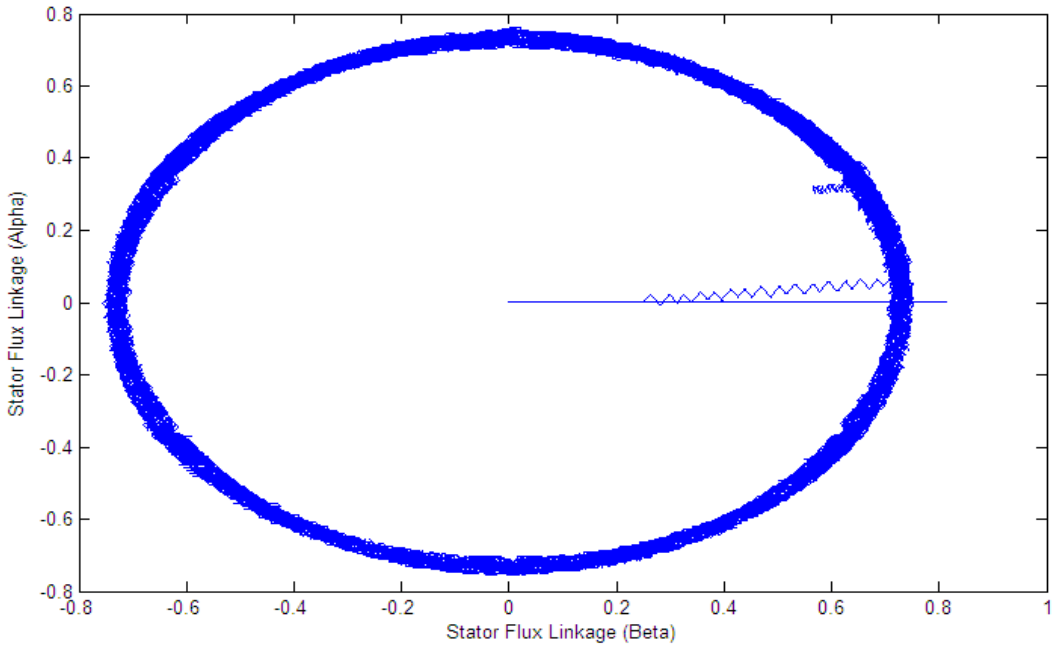

(b)

Fig.5.15: Stator Flux Linkage of the IM drive running at no load and at a reference speed of 150 rad/sec and a step change to 180 rad/sec; (a) proposed ANFIS based speed controller response, (b) classical PI controller response

Case – IV: Motor running at half the rated load with a step change in the reference speed of the motor.

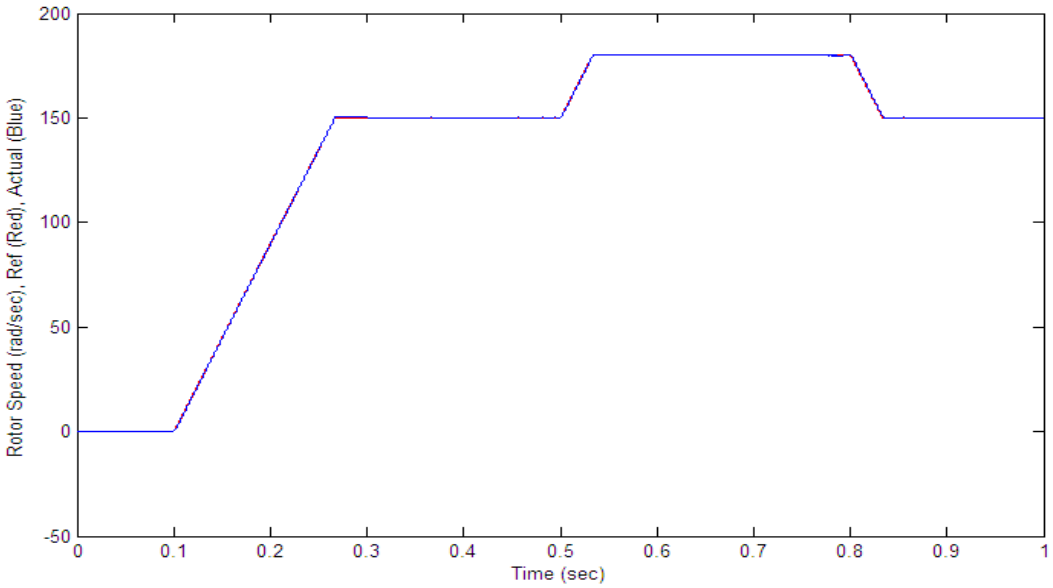

(a)

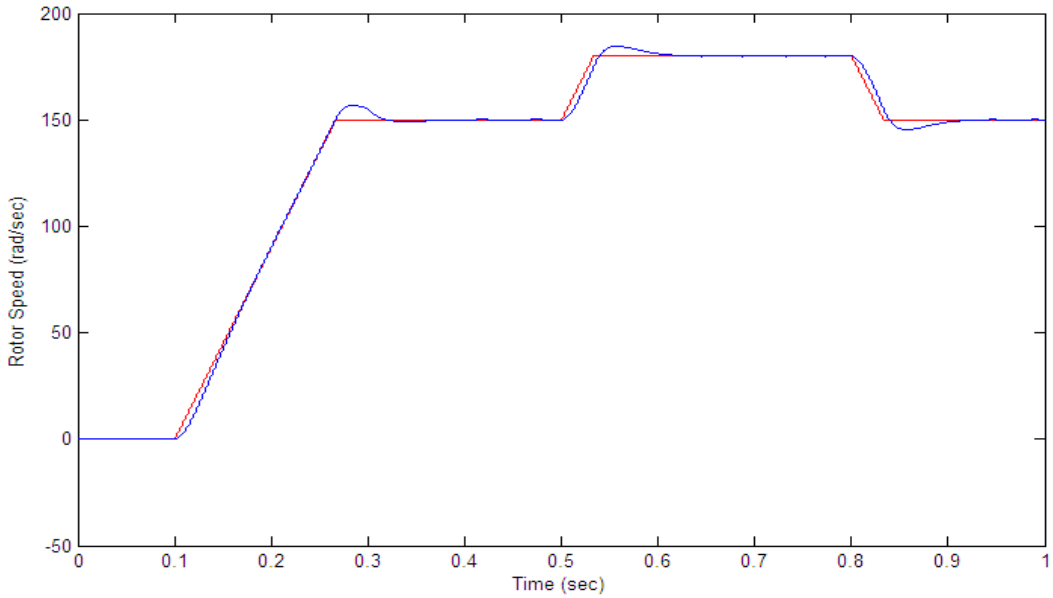

(b)

Fig.5.16: Speed response of the IM drive running at half the rated load and at a reference speed of 150 rad/sec and a step change to 180 rad/sec; (a) proposed ANFIS based speed controller response, (b) classical PI controller response

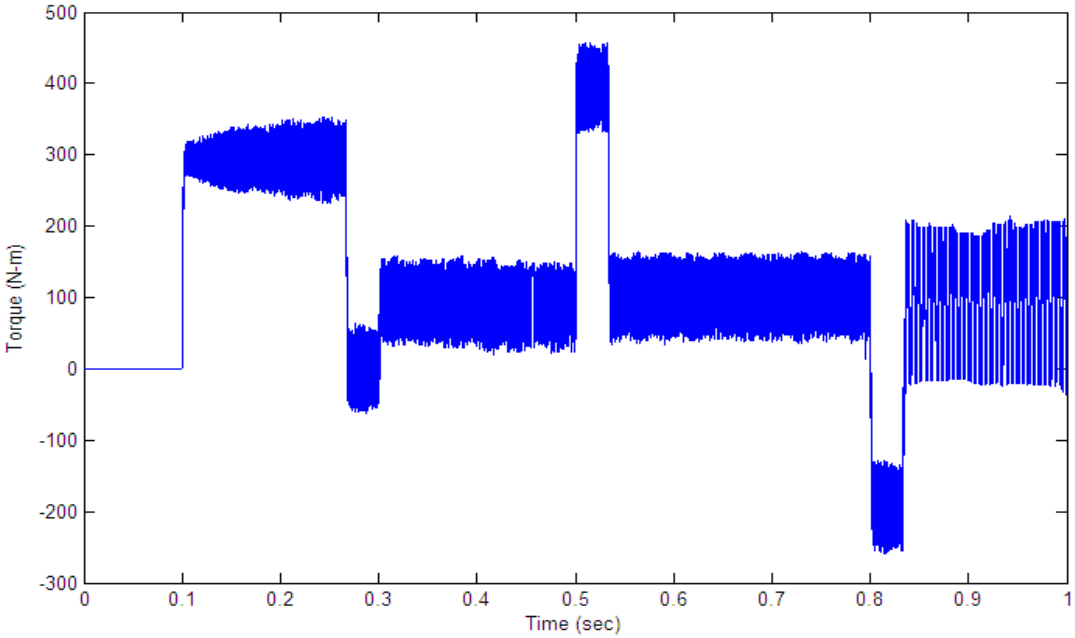

(a)

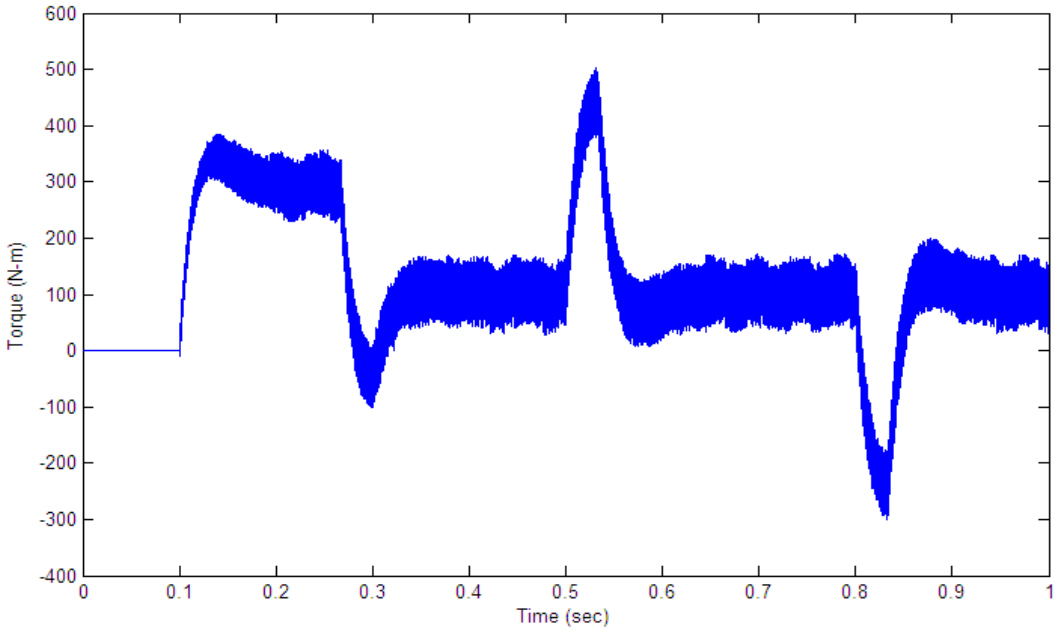

(b)

Fig.5.17: Torque response of the IM drive running at half the rated load and at a reference speed of 150 rad/sec and a step change to 180 rad/sec; (a) proposed ANFIS based speed controller response, (b) classical PI controller response

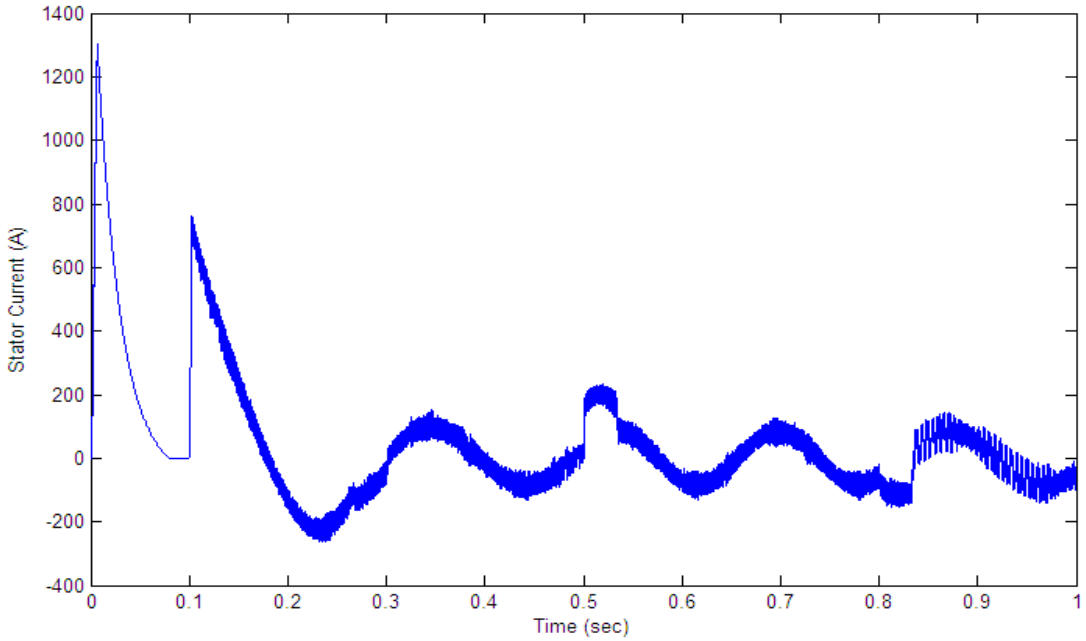

(a)

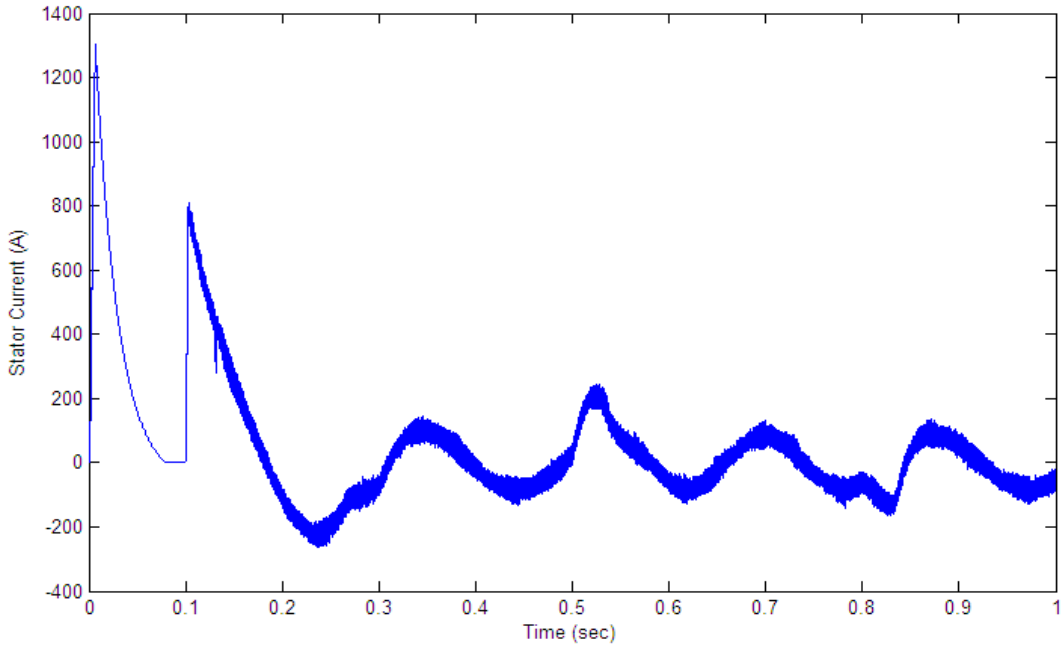

(b)

Fig.5.18: Stator Current of the IM drive running at half the rated load and at a reference speed of 150 rad/sec and a step change to 180 rad/sec; (a) proposed ANFIS based speed controller response, (b) classical PI controller response

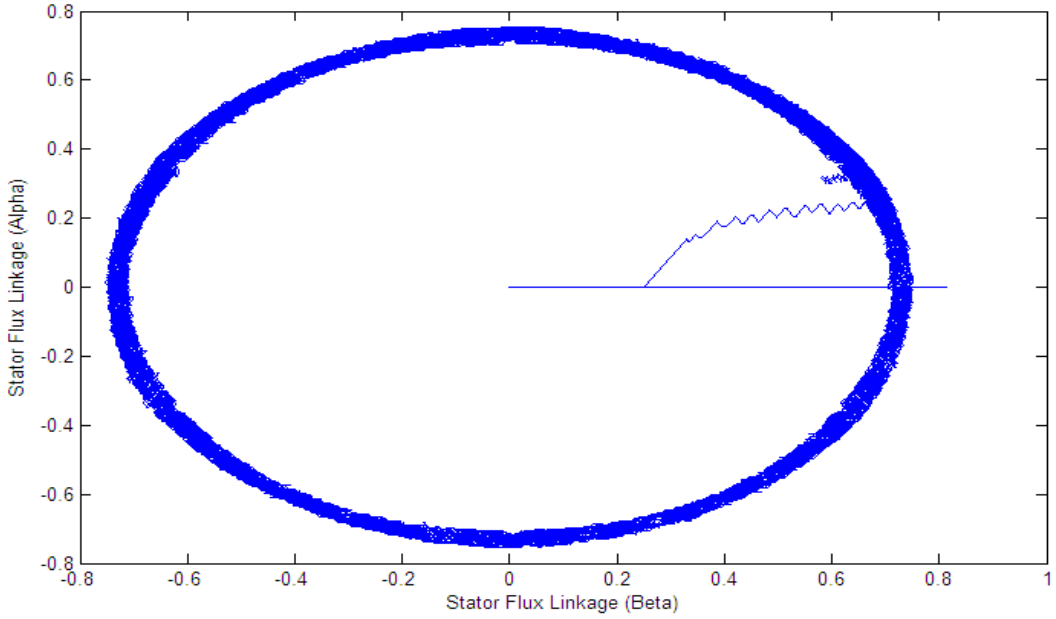

(a)

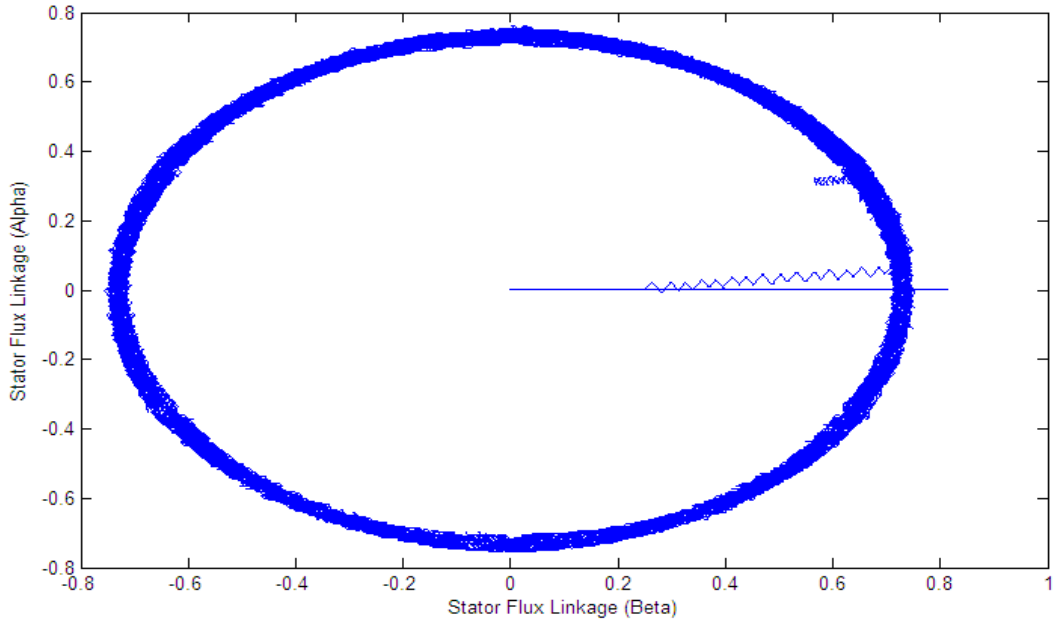

(b)

Fig.5.19: Stator Flux Linkage of the IM drive running at half the rated load and at a reference speed of 150 rad/sec and a step change to 180 rad/sec; (a) proposed ANFIS based speed controller response, (b) classical PI controller response

Case – V: Motor running at step change in the load as well as with a step change in the reference speed of the motor.

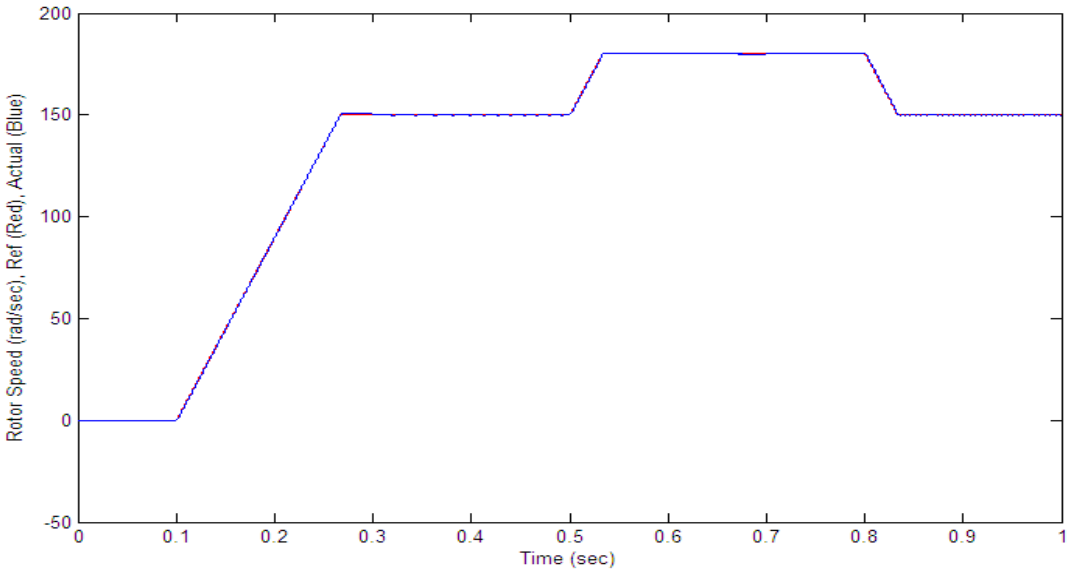

(a)

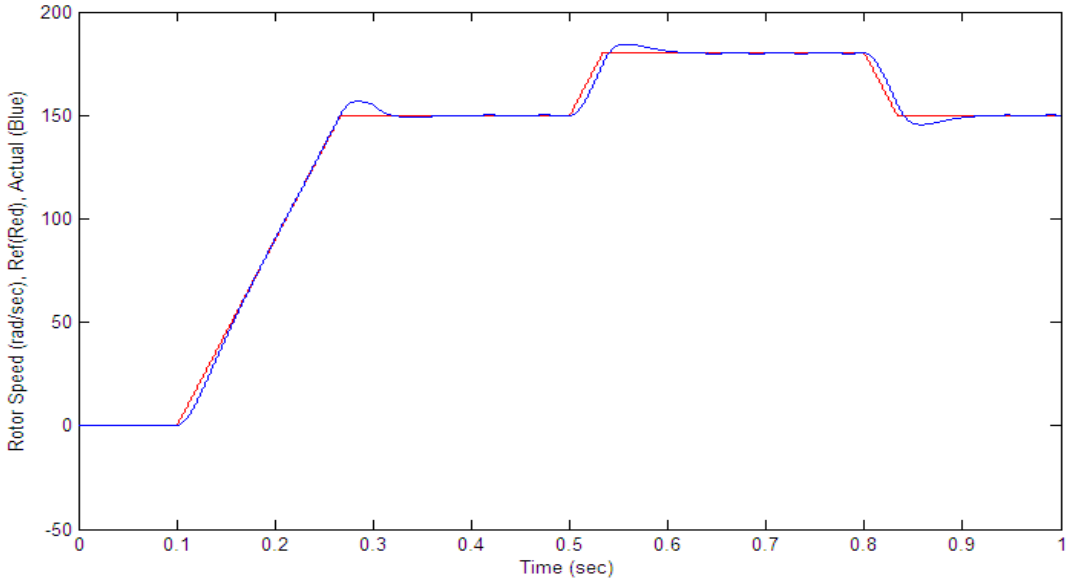

(b)

Fig.5.20: Speed response of the IM drive running with a step change in load from 100 N-m to 120 N-m and at a reference speed of 150 rad/sec and a step change to 180 rad/sec; (a) proposed ANFIS based speed controller response, (b) classical PI controller response

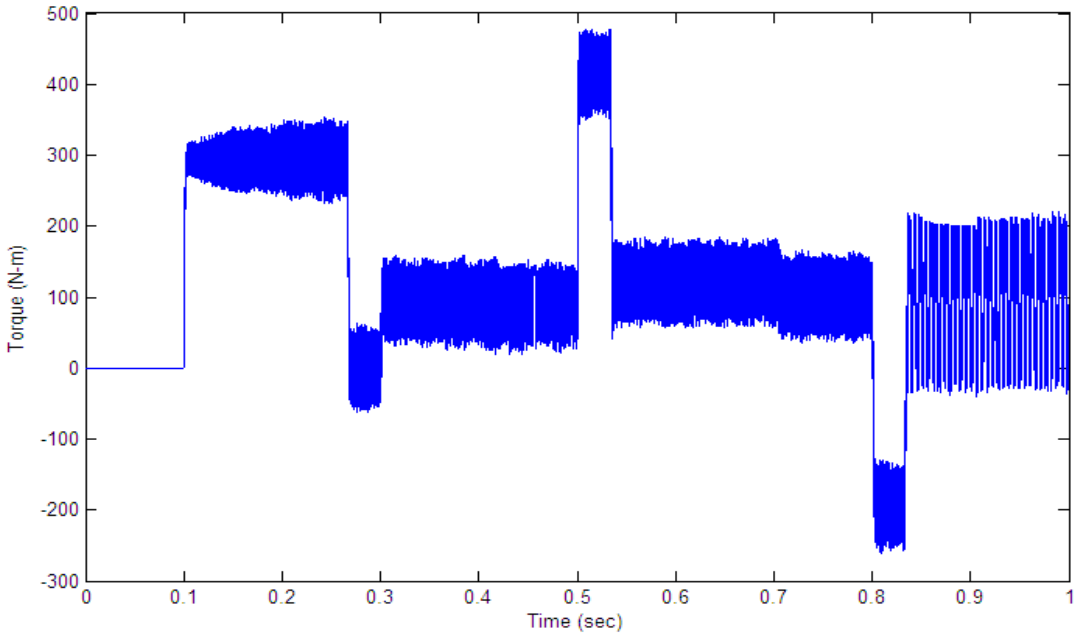

(a)

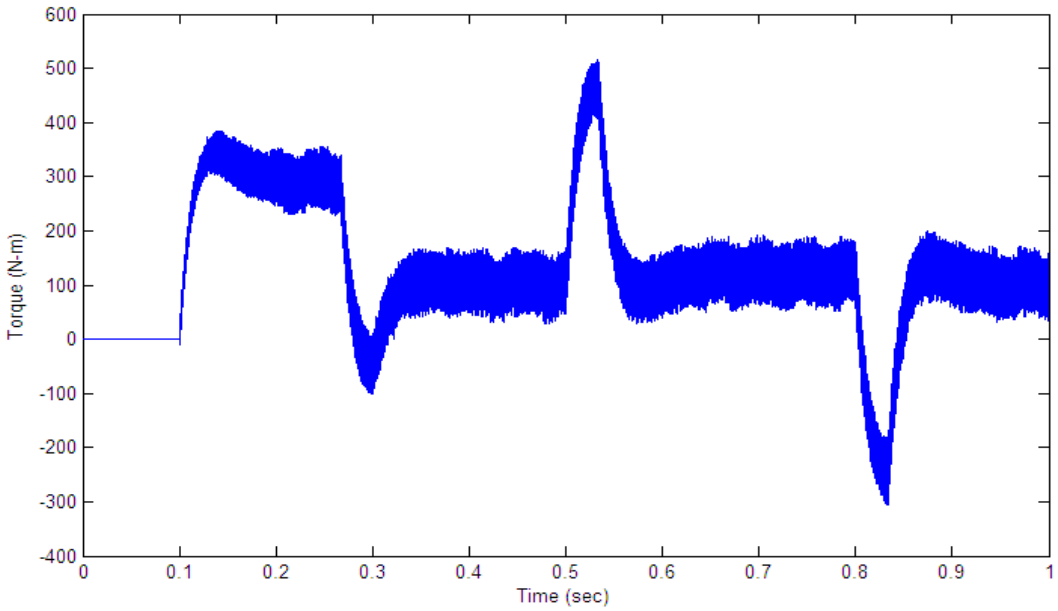

(b)

Fig.5.21: Torque response of the IM drive running with a step change in load from 100 N-m to 120 N-m and at a reference speed of 150 rad/sec and a step change to 180 rad/sec; (a) proposed ANFIS based speed controller response, (b) classical PI controller response

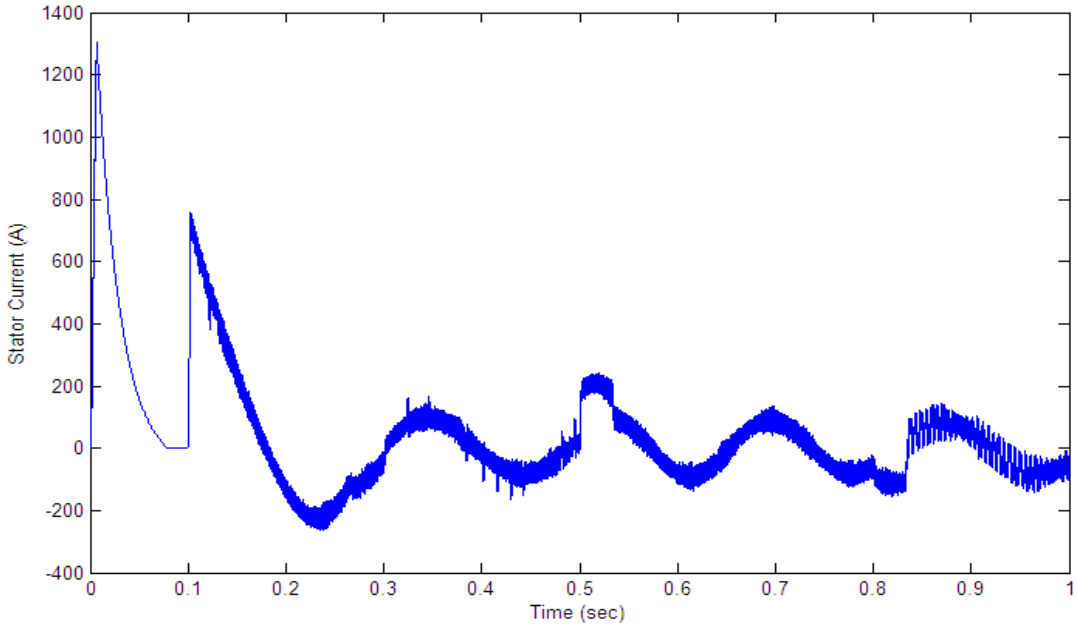

(a)

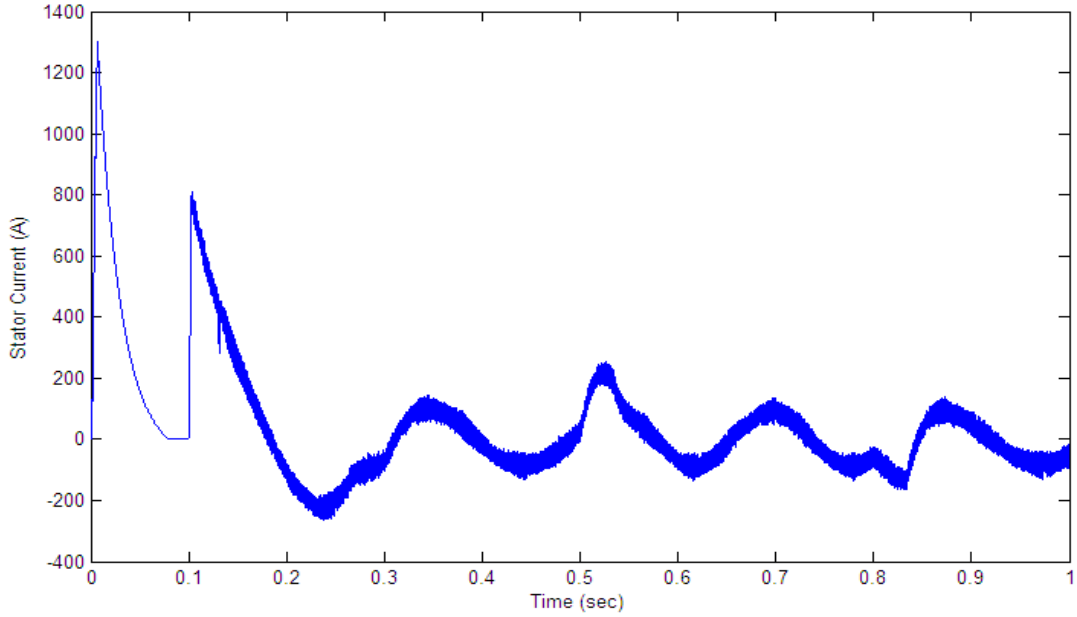

(b)

Fig.5.22: Stator current response of the IM drive running with a step change in load from 100 N-m to 120 N-m and at a reference speed of 150 rad/sec and a step change to 180 rad/sec; (a) proposed ANFIS based speed controller response, (b) classical PI controller response

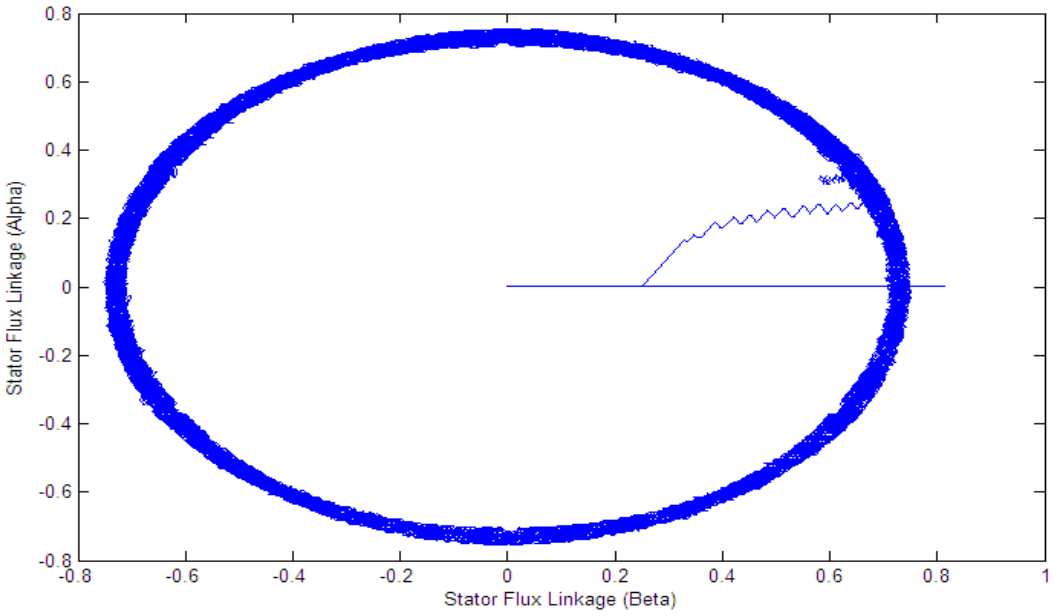

(a)

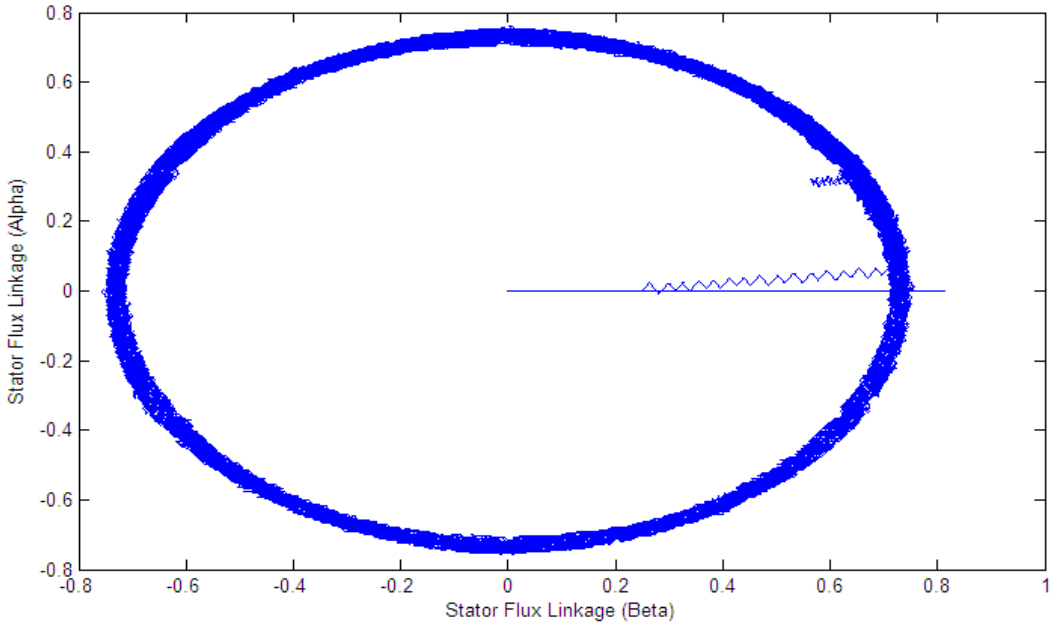

(b)

Fig.5.23: Stator Flux Linkage of the IM drive running with a step change in load from 100 N-m to 120 N-m and at a reference speed of 150 rad/sec and a step change to 180 rad/sec; (a) proposed ANFIS based speed controller response, (b) classical PI controller response

Case – VI: Motor running at rated load and rated speed.

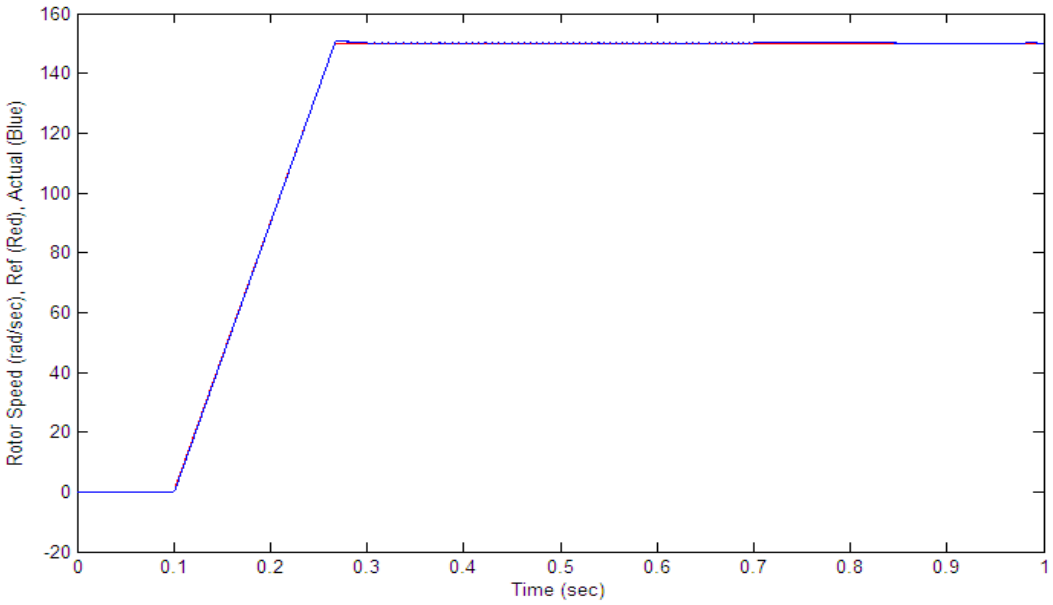

(a)

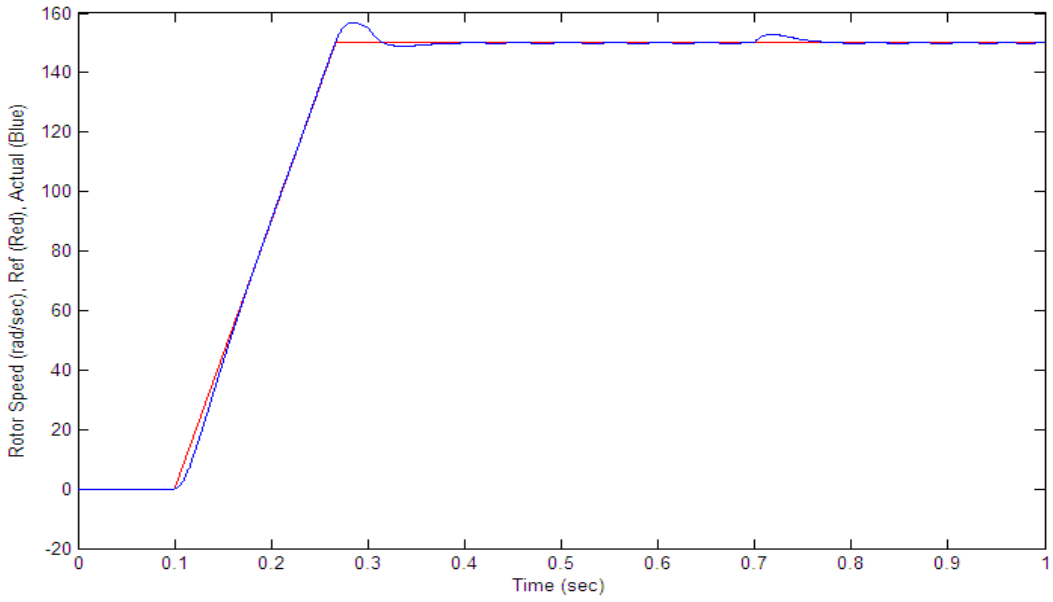

(b)

Fig.5.24: Speed response of the IM drive running with a rated load of 120 N-m and at a reference speed of 150 rad/sec; (a) proposed ANFIS based speed controller response, (b) classical PI controller response

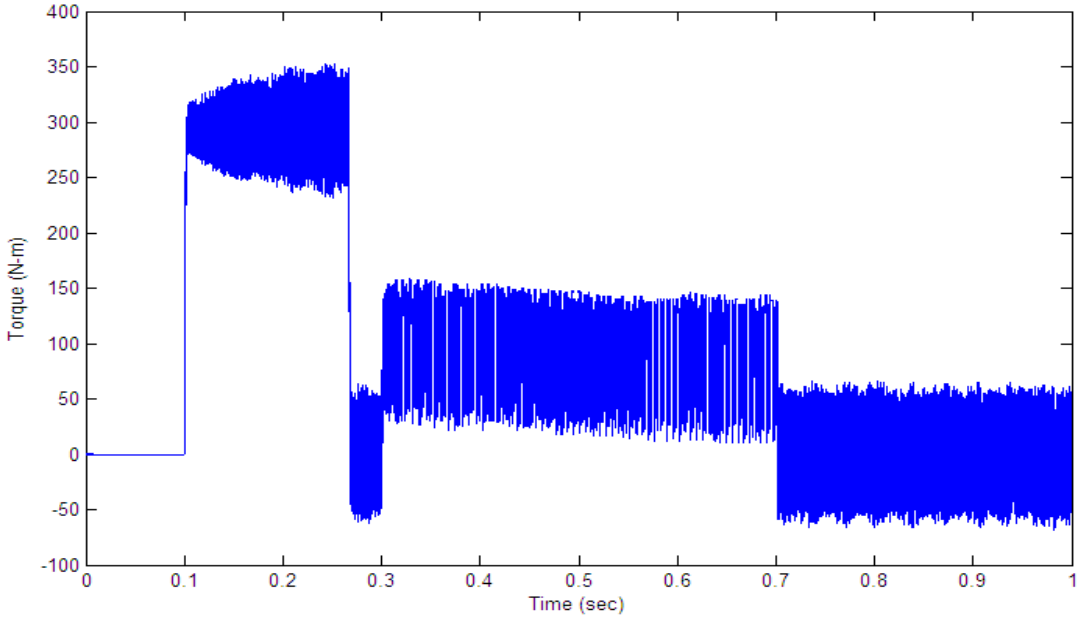

(a)

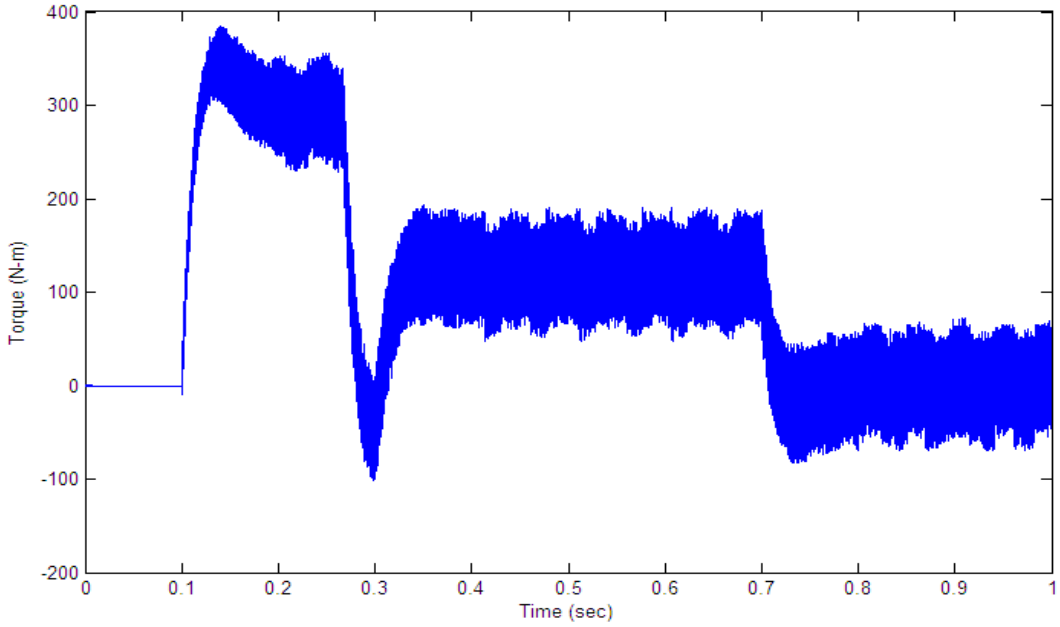

(b)

Fig.5.25: Torque response of the IM drive running with a rated load of 120 N-m and at a reference speed of 150 rad/sec; (a) proposed ANFIS based speed controller response, (b) classical PI controller response

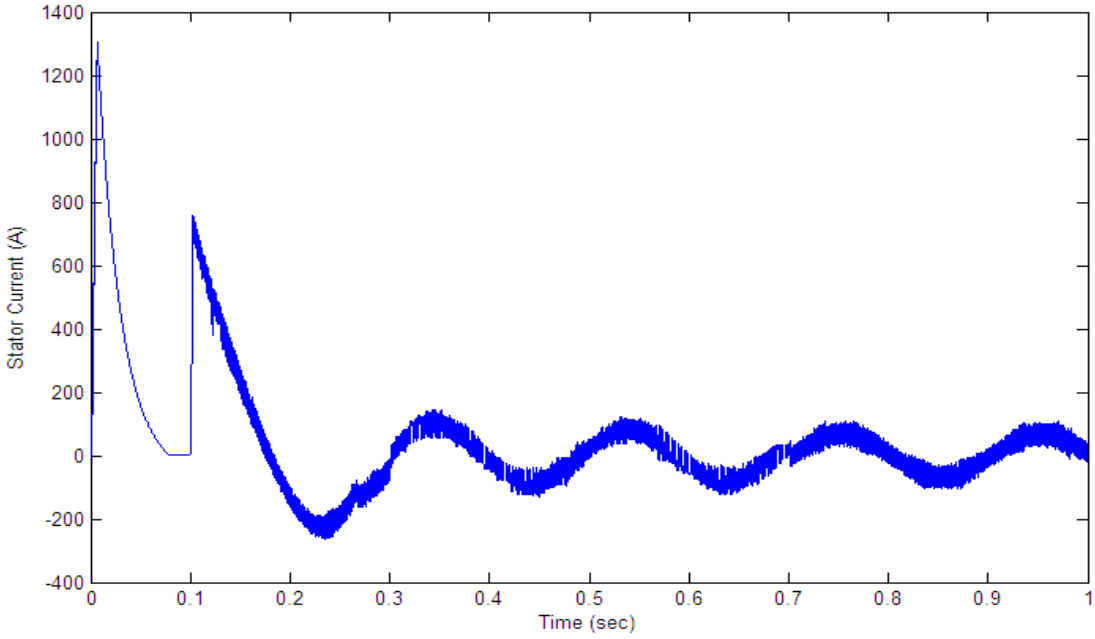

(a)

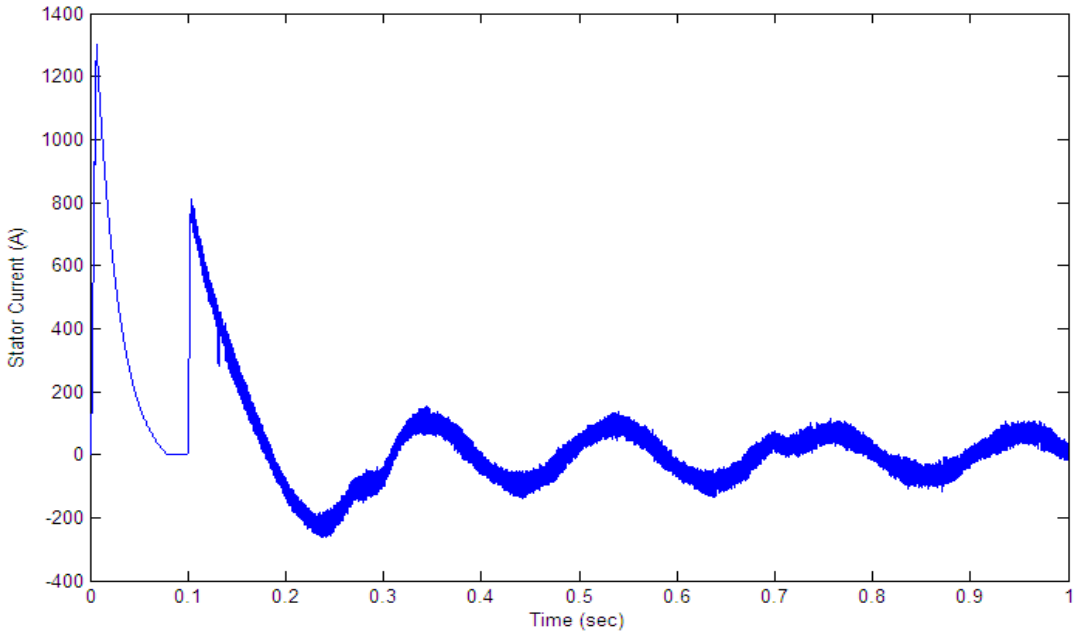

(b)

Fig.5.26: Stator current response of the IM drive running with a rated load of 120 N-m and at a reference speed of 150 rad/sec; (a) proposed ANFIS based speed controller response, (b) classical PI controller response

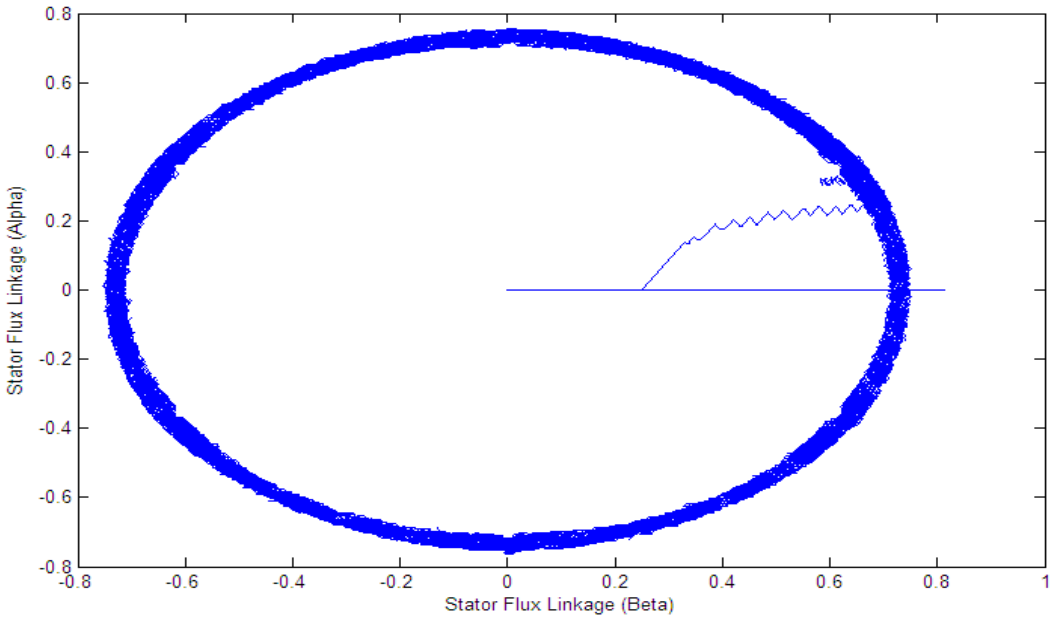

(a)

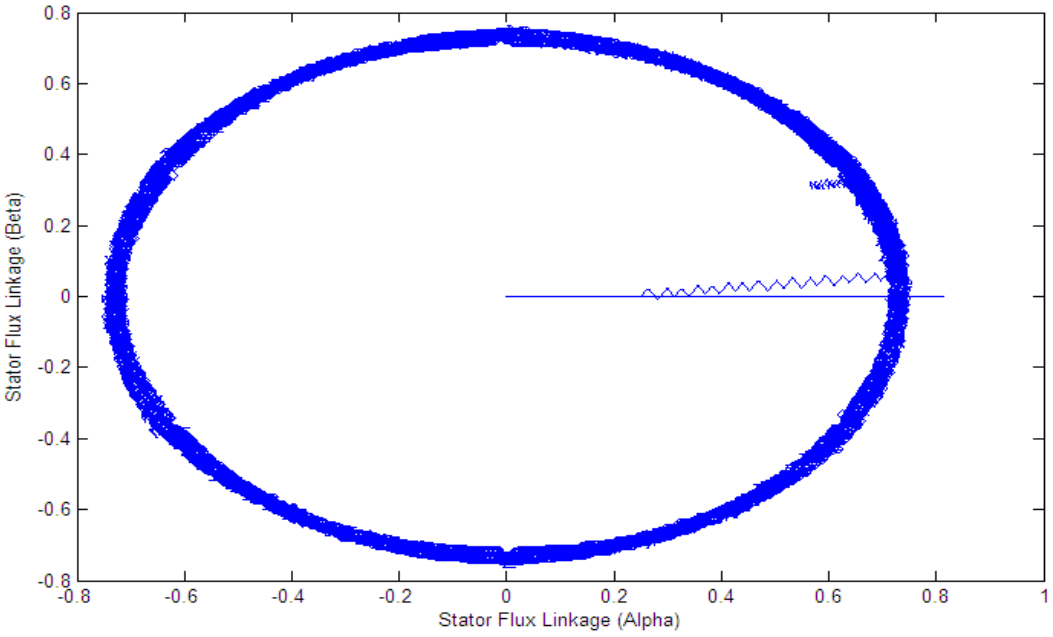

(b)

Fig.5.27: Stator Flux Linkage of the IM drive running with a rated load of 120 N-m and at a reference speed of 150 rad/sec; (a) proposed ANFIS based speed controller response, (b) classical PI controller response

5.2. Discussion

In the above section, Fig.5.4 to Fig.5.7 show the various simulation results of the IM drive at no load and command rated speed of 150 rad/sec. The responses of the proposed ANFIS controller and the conventional PI controller are compared for the above mentioned operating conditions. Fig.5.4 represents the speed responses, which clearly indicates the improvement in the transient response of the system. Both the overshoot and settling time have been reduced significantly by the use of the proposed ANFIS controller. Fig.5.5 represents the torque responses for both of the controllers. From the torque responses it is evident that the torque ripples have been reduced in steady state. From the plot it can be measured that the steady state peak to peak torque ripples have been measured in the range of 4 N-m to 20 N-m for the proposed controller where as for the conventional PI controller they have been detected to be in the range of 12 N-m to 45 N-m. So the proposed controller significantly contributes to the minimization of the steady state torque ripples. Fig.5.6 shows the stator current for the stator phase-A. The proposed scheme has improved both the transient and steady state current responses. The peak to peak ripples in stator currents have been measured as 24A in transient state and 8A in steady state where as the same have been measured as 32A for transient state and 14A in steady state for the conventional PI controller. Fig.5.7 compares the stator flux linkage responses from the proposed controller and the conventional PI controller. The propose ANFIS based DTC scheme for IM drive exhibits smoother response and lesser ripple in flux as compared to the classical PI controller based DTC scheme for IM drive.

From Fig.5.8 to Fig.5.11 various simulation results of the IM drive for command rated speed of 150 rad/sec and an abrupt change in load from 100 N-m to -100 N-m can be observed. The responses of the proposed ANFIS controller and the conventional PI controller are compared for the above mentioned operating conditions. Fig.5.8 represents the speed responses, which clearly indicates the improvement in the transient response of the system. Both the overshoot and settling time have been reduced significantly by the use of the proposed ANFIS controller. Fig.5.9 represents the torque responses for both of the controllers. From the torque responses it is evident that the torque ripples are reduced in steady state. From the plot it can be measured that the steady state peak to peak torque ripples have been measured in the range of 6 N-m to 23 N-m for the proposed controller where as for the conventional PI controller they have been detected to be in the range of 14 N-m to 43 N-m. It can also be seen from the plot that during the changes in

the applied load the torque ripples for the conventional PI controller is much higher than that of the proposed ANFIS controller not only in the steady state but also in the transient states. This is an important improvement since it not only improves the steady state torque responses but also the transient torque responses. Fig.5.10 shows the stator current for the stator phase-A. The proposed scheme has improved both the transient and steady state current responses. The peak to peak ripples in stator currents have been measured as 18A in transient state and 4A in steady state where as the same have been measured as 34A for transient state and 16A in steady state for the conventional PI controller. Moreover the convention PI controller driven DTC based IM drive draws a much higher current than the proposed controller driven DTC IM drive during the load reversal. Fig.5.11 compares the stator flux linkage responses from the proposed controller and the conventional PI controller. The propose ANFIS based DTC scheme for IM drive exhibits smoother response and lesser ripple in flux as compared to the classical PI controller based DTC scheme for IM drive.

Fig.5.12 to Fig.5.23 represents the simulation results for step changes in the rated speed as well as in the applied load torque. The responses of the proposed ANFIS controller and the conventional PI controller are compared for operating conditions mentioned in the previous paragraphs. From the plots of the speed responses, it can be identified clearly that the proposed controller introduces significant improvement in the transient response of the system under various operation conditions involving sudden changes in load or in the reference speed. The overshoot and settling time have been reduced significantly and the improvement in the rise time has only been slight by the use of the proposed ANFIS controller. The comparisons of torque responses for both of the controllers depicts that the torque ripples are reduced in steady state for the proposed ANFIS controller as compared to the conventional PI controller. From the plot it can be measured that the steady state peak to peak torque ripples have been measured in the range of 3N-m to 19 N-m for the proposed controller where as for the conventional PI controller they have been detected to be in the range of 9 N-m to 33 N-m under various operating conditions. It can also be seen from the plot that during the changes in the applied load the torque ripples for the conventional PI controller is much higher than that of the proposed ANFIS controller not only in the steady state but also in the transient states. This is an important improvement since it not only improves the steady state torque responses but also the transient torque responses. From the plots of stator current for stator phase-A, it is evident that the

proposed scheme has improved both the transient and steady state current responses. The peak to peak ripples in stator currents have been measured as 15A in transient state and 3.5A in steady state where as the same have been measured as 21A for transient state and 11.4A in steady state for the conventional PI controller. Moreover the convention PI controller driven DTC based IM drive draws a much higher current than the proposed controller driven DTC IM drive during the load reversal. By comparing the stator flux linkage responses of the proposed controller and the conventional PI controller, it is found that, the propose ANFIS based DTC scheme for IM drive exhibits smoother response and lesser ripple in stator flux as compared to the classical PI controller based DTC scheme for IM drive.

The overall comparison of the proposed ANFIS controller and the PI is shown in Table III. The comparison clearly shows how effective the proposed controller based DTC scheme for IM drives is for all dynamic respect.

Table III: Comparison of classical PI and proposed ANFIS controller

Operating Condition	Rated Speed at No Load		Rated Speed at Load Reversal (+100 to -100 N-m)		Rated Speed with Step Load Change (100-120 N-m)		Step Change in Speed (150-180 rad/sec) at 50% of Rated Load		Step change in speed (150-180 rad/sec) with step change in load (100 – 120 N-m)		Rated speed at rated load	
Parameter	ANFIS	PI	ANFIS	PI	ANFIS	PI	ANFIS	PI	ANFIS	PI	ANFIS	PI
% Overshoot	0.01	1.22	0.17	2.13	0.14	1.34	0.04	0.93	0.21	2.21	0.02	0.78
Rise Time	0.07	0.08	0.10	0.126	0.78	0.11	0.082	0.096	0.12	0.143	0.09	0.092
Settling Time	0.076	0.084	0.12	0.132	0.81	0.124	0.097	0.104	0.146	0.174	0.098	0.102
%Speed Ripple	0.02	0.11	0.026	0.173	0.021	0.132	0.02	0.106	0.028	0.241	0.018	0.103
%Torque Ripple	13.3	35.4	19.6	43.2	16.3	36.6	14.3	23.04	18.45	38.65	13.58	33.45
%Flux Ripple	2.67	3.56	5.33	9.21	3.1	5.33	4.2	6.05	5.02	7.95	2.89	3.78
%Current Ripple	17.08	25.04	12.54	19.43	8.33	12.5	8.45	12.5	9.13	13.04	7.87	13.94

Chapter 6

Development of Fuzzy Logic Controlled Dynamic Voltage Restorer for Induction Motor Drives

6.1.Introduction

Power quality and reliability in distribution systems have been attracting an increasing interest in modern times and have become an area of concern for modern industrial and commercial applications. Introduction of sophisticated manufacturing systems, industrial drives, precision electronic equipments in modern times demand greater quality and reliability of power supply in distribution networks than ever before. Power quality problems encompass a wide range of phenomena. Voltage sag/swell, flicker, harmonics distortion, impulse transients and interruptions are a prominent few. These disturbances are responsible for problems ranging from malfunctions or errors to plant shut down and loss of manufacturing capability. Voltage sags/swells can occur more frequently than any other power quality phenomenon. These sags/swells are the most important power quality problems in the power distribution system [70].

Voltage Sag or Voltage Dip (IEC term) is defined by the IEEE 1159 as the decrease in the RMS voltage level to 10% - 90% of nominal, at the power frequency for durations of ½ cycle to one minute [71]. The IEC terminology for voltage sag is dip. The IEC defines voltage dip as a sudden reduction of the voltage at a point in the electrical system, followed by voltage recovery after a short period, from half a cycle to a few seconds [72]. According to IEEE 1159-1995 voltage sag amplitude of voltage sag is the value of the remaining voltage during the sag. Sag (dip) threshold magnitude specified for the purpose of detecting the start and the end of voltage sag (dip) which is defined to be 0.9 pu as defined by IEC 1000-4-30. Generally the sag magnitude ranges from 0.1 to 0.9 pu [71, 72]. Voltage sags are usually associated with system faults but they can also be generated by energization of heavy loads or starting of large motors which can draw 6 to 10 times its full load current during starting. Sag durations are subdivided

into three categories, instantaneous, momentary, and temporary-all of which coincide with utility device operation times [73, 74].

Voltage Swell is defined by IEEE 1159 as the increase in the RMS voltage level to 110% - 180% of nominal, at the power frequency for durations of ½ cycles to one minute [71]. It is classified as a short duration voltage variation phenomena, which is one of the general categories of power quality problems. The term "momentary overvoltage" is used as a synonym for the term swell. According to IEEE 1159-1995, voltage swell magnitude is to be described by its remaining voltage, which is always greater than 1.0 pu. Voltage magnitude specified for the purpose of detecting the start and the end of a swell is known as swell threshold which is defined to be 1.1 pu as defined by IEC 1000-4-30.Generally the swell magnitude ranges from 1.1 to 1.8 pu [71, 72]. Like sags, swells are associated with system fault conditions but are not as common as sags. Swells can occur from the temporary voltage rise on the healthy phases during a single-line-to-ground (SLG) fault. Swells can also be caused by switching off a large load or energizing a large capacitor bank and are characterized by their magnitude (rms value) and duration. The severity of a voltage swell is a function of the fault location, system impedance and grounding [73, 74].

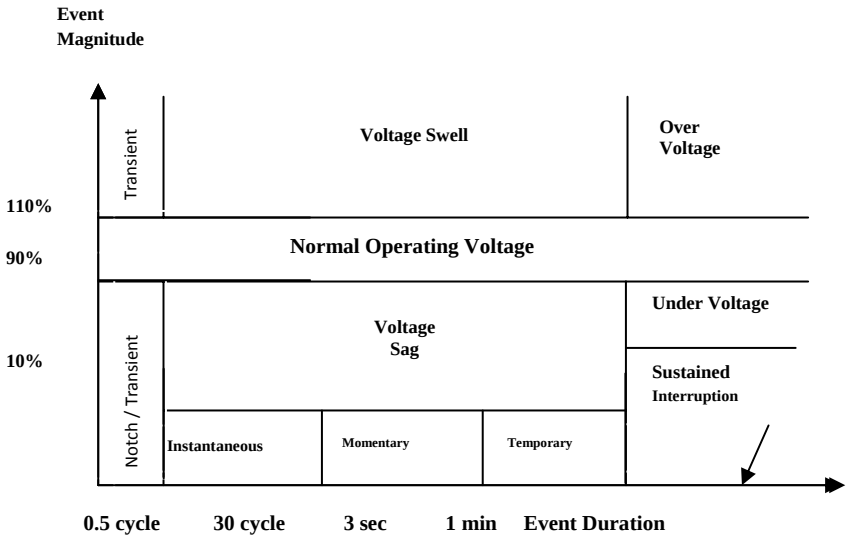

Fig.6.1: Voltage Reduction Standard of IEEE Std. 1159-1995

To calculate the voltage sag/swell magnitude at the Point of Common Coupling (PCC) in radial systems (which is the most prevailing one in industrial distribution networks), it is common to use the voltage divider model, shown in Fig.6.2, where the voltage magnitude at the PCC is given by:

$$U_{sag/swell} = \frac{Z_f}{Z_S + Z_f} \quad (6.1)$$

Where:

Z_s = the source impedance including the transformer impedance

Z_f = the impedance between the PCC and the fault including fault and line impedances [75]

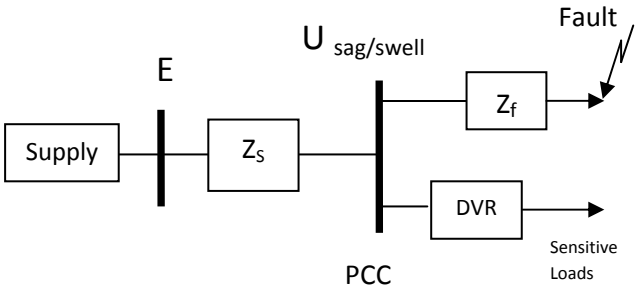

Fig.6.2: Faults on Parallel Feeders Causing Voltage Sag/Swell

As the quality of power is strictly related to the economic consequences associated with the equipment and should therefore be evaluated considering the customers point of view. So the need for solutions dedicated to single customers with highly sensitive loads is great since a fast response of voltage regulation is required. Further it needs to synthesize the characteristics of voltage sags/swells both in domestic and industrial distributions [76, 77]. Alongside the variation in magnitudes, voltage sags/swells can also be accompanied by a change in phase angle. This phenomenon is known as phase angle jump (i.e. the variation of phase angle before the onset and during the voltage sag/swell events and is calculated as an argument of the complex voltage) [78]. Phase angle jumps can also be detrimental for the cases of sensitive devices. In order to meet these challenges, it needs a device capable of injecting minimum energy so as to regulate load voltage at its predetermined value.

Dynamic Voltage Restorer (DVR) is one of the prominent methods for compensating the power quality problems associated with voltage sags/swells. Dynamic voltage restorer (DVR) can provide an effective solution to mitigate voltage sag/swell by establishing the appropriate predetermined voltage level required by the loads. It is recently being used as the active solution for voltage sag/swell mitigation in modern industrial applications. Induction Motors are the most

widely used motors in modern industrial applications because of their relatively inexpensive rudimentary design, reliable operation and low maintenance costs. Induction motors are generally robust, but they can be susceptible to inadequate of improper operating voltages causing problems ranging from loss of quality to complete plant shutdowns. Voltage sags/swells have been identified as the pivotal cause for tripping of large induction motors in industrial systems. Studies on the effects of voltage sags/swells on Induction Motors demonstrated that IMs are insensitive to very short duration sags (and interruptions) or swells. IMs were also unaffected by phase angle jumps associated with most of the voltage sags/swells [79].

This study proposes a new configuration of Dynamic Voltage Restorer (DVR) with fuzzy logic based feedback controller capable of compensating for power quality problems associated with voltage sags/swells and maintaining a prescribed level of supply voltage at the induction motor drive load terminals. The simulation of the proposed DVR is accomplished using MATLAB/SIMULINK simpower systems toolbox. The performance of the proposed DVR for different supply disturbances is tested under various operating conditions. The simulation results have shown that the proposed DVR is capable of mitigating both balanced and unbalanced voltage sags/swells with acceptable efficiency and reliability.

6.2.DYNAMIC VOLTAGE RESTORER

Dynamic Voltage Restorer (DVR) is a series connected device capable of regulating the load side voltage in a distribution network. The DVR provides a three phase independently controlled voltage source utilizing power electronic components, whose voltage vector (magnitude and angle) is added to the source voltage to restore the load voltage to a prescribed level [80]. The main function of DVR is the protection of sensitive loads from voltage sags/swells arising from the distribution network. Thus it is generally installed in a distribution system between the supply and the sensitive load feeders [81]. In addition to voltage sags and swells compensation, DVR can also be used for line voltage harmonics compensation, voltage transients reductions and fault current limitations. Various circuit topologies and control schemes are available that can be used to implement a DVR.

6.2.1. Configuration of DVR

The general configuration of the DVR consists of an Injection transformer, a Harmonic filter, a Voltage Source Converter (VSC), Energy Storage Unit and a Control and Protection unit as shown in Fig.6.3.

Energy Storage Unit in DVR can be external batteries or capacitors charged from the supply line feeder through a rectifier. Generally the energy storage unit of a DVR can be divided into two parts (i.e. Storage devices and DC Charging Circuit). The purpose of energy storage devices is to supply the necessary energy to the VSC via a dc link for the generation of injected voltages.

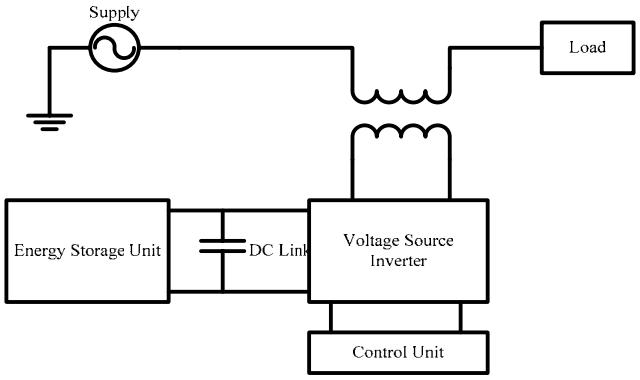

Fig.6.3: Schematic Diagram of DVR Configuration

The different kinds of energy storage devices are superconductive magnetic energy storage (SMES) [82], batteries, and capacitors [83, 84]. In fact, the capacity of the stored energy directly determines the duration of the sag which can be mitigating by the DVR. Batteries are the common choice and can be highly effective if a high voltage battery configuration is used [85]. However, batteries in general have a short lifetime and often require some type of battery management system, which can be quite costly [86]. An interesting alternative to batteries is the use of supercapacitors, which have a wider voltage range than batteries and can be directly paralleled across the input bus. Supercapacitors have a specific energy density less than that of a battery, but a specific power greater than a battery, making them ideal for short (up to several seconds) pulses of power. Certain supercapacitors can hold charge over extended periods of time, so as to act like a battery. However, unlike batteries, these supercapacitors have a short charging time and much longer lifetime [73, 74]. The purpose of the DC Charging Circuit is to charge the energy storage devices after the compensation of a voltage sag/swell event as well as

maintain a nominal dc link voltage. The charging circuit can be an external power supply or a rectifier fed from the supply mains of the distribution network.

A Voltage Source Converter is a power electronic system capable of generating a sinusoidal voltage at any required frequency, magnitude, and phase angle. DVR configurations use the VSC to generate the voltage required to compensate for the voltage sag/swell events [87, 88]. Since the majority of the voltage sags/swells observed on distribution systems are unbalanced, the VSC will often be required to operate with unbalanced switching functions for the three phases and must therefore be able to treat each phase independently. Moreover, sag on one phase may result in swell on another phase, so the VSC must be capable of handling both sags and swells simultaneously. The output voltage of the inverter is varied by using different PWM schemes available.

Given to the nonlinear nature of the semiconductor devices Voltage waveform distortion associated with the high frequency harmonics at the output of the inverter circuit is a common phenomenon. A harmonic filter unit is generally used at the output of the inverter circuit to keep the harmonic distortions at a permissible level. Although the filter unit keeps the harmonic distortion minimum and improves the quality of the generated voltage, it can also introduce voltage drop and phase shift in the fundamental component of the inverter output and needs to be accounted for in the generated compensation voltage [89].

Injection transformers are responsible for connecting the DVR to the sensitive loads in the distribution network via the high tension windings and transforming and coupling of the injected compensating voltages generated by the voltage source converters to the incoming supply voltage. In addition, the Injection transformer also serves the purpose of isolating the load from the system (VSC and control mechanism). Generally three single-phase transformers are used as injection transformers for injecting the compensating voltages to the system at the load bus. Proper integration of the injection transformer into the DVR, the MVA rating, the primary winding voltage and current ratings, the turn-ratio and the short-circuit impedance values of transformers are required. The existence of the transformers allow for the design of the DVR in a lower voltage level, depending upon the stepping up ratio. In such case, the limiting factor will be the ability of the inverter switches to withstand higher currents [90]. The control unit of DVR is solely responsible for controlling the compensating voltage generation by controlling the

PWM pulses to the gates of semiconductor switches of the VSC. To maximize dynamic performance of DVR, efficient control architecture capable of achieving fast compensation is necessary [91, 92]. The protection unit of DVR generally consists of By-pass switches, breakers, measuring and protection relays etc. Depending upon the operating conditions, the control and protection unit maximizes the system performance and minimizes the losses associated with the operation of DVR.

6.2.2. Compensation Methods

Compensation of voltage sags/swells is dependent upon a number of factors including DVR power rating, different load conditions and different types of voltage sags/swells. Some loads are very sensitive to phase angle jump while others are tolerant to it. Therefore, the compensation strategy depends upon the type and characteristics of the load connected to DVR. There are three different methods for DVR voltage injection which are presented below.

6.2.2.1.Pre-Fault Compensation

The DVR injects the difference voltage between during fault and pre-fault voltages to the system. In this method the DVR compensates for both magnitude and Phase angle. The main drawback of this technique is it requires a higher capacity energy storage device [92]. Fig.6.4a shows the vector diagram for the pre-fault control strategy for a voltage sag event. This method is best suited to loads sensitive to phase angle jumps as it compensates for both the magnitude and phase angle.

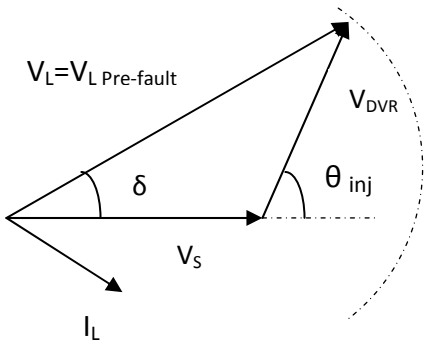

Fig 6.4a: Compensation to pre-fault conditions for a voltage sag event (magnitude and phase)

In this diagram, $V_{pre\text{-}fault}$ and V_{Sag} are voltage at the point of common coupling (PCC), respectively before and during the sag. In this case V_{DVR} is the voltage injected by the DVR, which can be obtained as:

$$V_{DVR} = \sqrt{{V_L}^2 + {V_S}^2 - 2V_L V_S cos\delta} \quad (6.2)$$

and the required angle of injection θ_{inj} is calculated as:

$$\theta_{inj} = \tan^{-1} \frac{V_S sin\delta}{V_S cos\delta - V_L} \quad (6.3)$$

A closer look at Fig.6.4a shows that, in normal conditions (pre-fault), the system or supply voltage is equal to the load voltage V_L, both are equal to 1 p.u. with zero angle. During sag, the system voltage decreases to a value V_s less than 1 p.u., this reduction in voltage is associated with a phase angle jump δ. The DVR reacts to the sag event and injects a compensating voltage V_{DVR} to restore the voltage at the load to pre-fault conditions of both magnitude and angle. The method gives nearly undisturbed load voltage [90, 92].

6.2.2.2.In Phase Compensation

In Phase compensation technique is designed to compensate for the voltage magnitude only. In this method jumps in the phase angle is not compensated [92, 93].

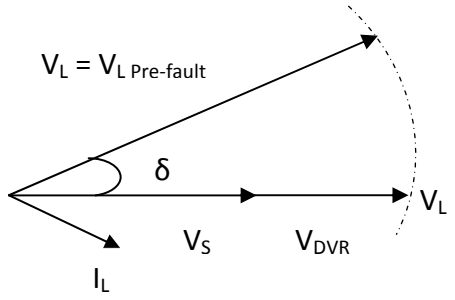

Fig 6.4b: In Phase Compensation to pre-fault conditions for voltage sag event (magnitude only)

The vector diagram corresponding to In Phase Compensation method is shown in Fig.6.4b. Here, the pre-fault voltage is 1 p.u. with zero angle and during sag, the system voltage decreases to V_S with a phase angle δ. The DVR injects a compensating voltage V_{DVR} in phase with the system voltage V_S, to boost the voltage magnitude up to the pre-fault voltage magnitude V_L, with no attention to the angle δ. This method is suitable for loads that can withstand phase angle jumps, which is a typical case for induction motor loads which comprise a large portion of the industrial power system, with no sensitive equipment such as adjustable speed drives or any equipment depending in its operation on phase triggered switches. This method is very simple in

implementation, very fast especially in calculating the DVR compensation voltage, which is obviously calculated as:

$$|V_{DVR}| = |V_L| - |V_S| \tag{6.4}$$

6.2.2.3.In Phase Advanced Compensation

Pre-fault compensation and in-phase compensation must inject active power to loads almost all the time. Due to the limit of energy storage capacity of DC link, the DVR restoration time and performance are confined in these methods.

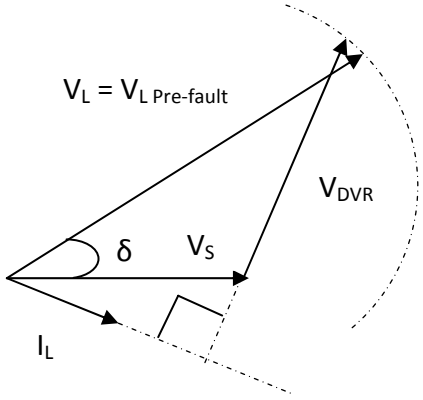

Fig 6.4.c: In Phase Advanced Compensation to pre-fault conditions for voltage sag event.

The fundamental idea of in phase advanced compensation method is to make injection of active power zero. In order to minimize the use of real power the voltages are injected at 90° phase angle to the supply current. Fig.6.4c shows the vector diagram to describe the In Phase Advanced Compensation method [94].

6.2.3. Operation Modes of DVR

The operation of Dynamic Voltage Restorer (DVR) can be categorized into three modes namely protection mode, standby mode and injection mode. In protection mode of operation DVR is protected from the over current in the load side due to short circuit on the load or large inrush currents. Bypass switches are used to separate the DVR from the system in protection mode. Generally DVR operates in standby mode in normal steady state conditions. In this mode of operation, the DVR may either be bypassed or inject small voltage to compensate the voltage

drop on transformer reactance or losses. DVR is generally bypassed because the small voltage drops do not disturb the load requirements if the distribution circuit is not too weak. DVR enters the injection mode of operation as soon as an abnormality is detected in load side voltage. DVR injects a three phase compensating voltage with each of the three phases having independently controlled magnitude and phase to meet the requirements on that particular phase. The DVR should ensure the unchanged load voltage with minimum energy dissipation for injection due to the high cost of capacitors [95].

6.2.4. Control Methods for DVR

DVR Control strategies fall mainly in one of the two categories namely linear control methods and Non-linear control methods. Linear control methods can be employed with the feedback, the feed-foreword and the combined feed controllers. Non-Linear control methods comprising the Artificial Neural Networks (ANN), the Fuzzy Logic (FL) and the Space Vector (SV) controllers Although feedback controllers are popular, they require load and source tracking, whereas feed-foreword controllers are much simpler yet open-looped, there is no feedback from the load voltage or current [91-93].

The proposed DVR utilizes capacitors as the energy storage units fed through the supply mains via the rectifier. The compensation strategy is chosen to be the pre-fault compensation method due to its simplicity of implementation and induction motor adjustable speed drive being sensitive to phase angle jumps. And the control of the proposed DVR is based on a fuzzy logic based feedback controller.

6.3.MATERIALS AND METHODS

This study proposes a fuzzy logic controlled DVR with pre-fault compensation strategy for voltage sag/swell compensation for industrial induction motor drives. Since the pre-fault compensation strategy is simpler and efficient and compensates for the phase angle jumps which are crucial for adjustable speed drives, the operation of the proposed DVR is simpler and its response time is also faster. Fig.6.5 shows the block diagram of the proposed controller for the DVR.

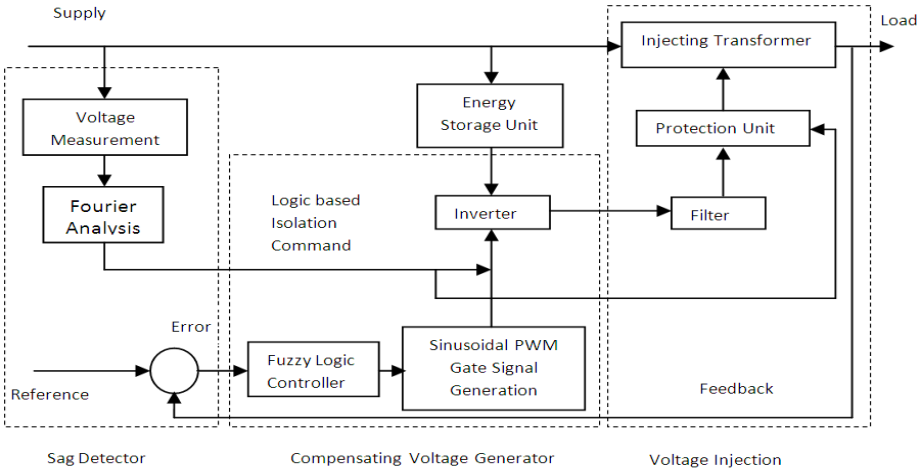

Fig 6.5: Block diagram of the proposed DVR.

The controller of the proposed DVR consists of the following blocks:

6.3.1. Detection of Sag and Swell Events

Sag/Swell detection includes determination of the instants when a sag/swell event starts and ends magnitude of the variation and the phase angle jumps. Several approaches for detection of sag/swell events available are Classical Fourier Transform method, Wavelet analysis, use of RMS values, use of peak values, the transformation of the three phase voltages to a two dimensional frame (d-q frame) and therefore to one phasor etc.[90, 96].

In this study, the proposed DVR uses the traditional Fourier Transform method to detect the voltage sag/swell events. The Fourier transform based sag/swell detector associated with the proposed DVR can track the magnitude and the phase angle of the fundamental frequency component of the supply voltage simultaneously in order to make sure that the injected sine wave will be in-phase with the remaining sine wave during the sag/swell events, to have a constructive vector addition of the DVR and the supply voltages. Since the compensation strategy used in the proposed DVR is in-phase method, computation of the compensating voltage magnitude is done using a comparator with one input as the variable load voltage and the other being the reference voltage for each of the three phases independently. The output of the comparator determines the magnitude of the voltage required to be injected by the DVR and is called the error signal which is the input to the fuzzy logic based feedback controller used for controlling the output voltage of the inverter through the control of the modulation index for each of the three phases of the inverter independently.

6.3.2. Compensating Voltage Generation

The inverter circuit in DVR is responsible for generation of the compensating voltage. Hence the control of the inverter will directly affect the performance of the DVR. The inverter used in the proposed DVR is a three phase six pulse inverter. The thyristors used in the inverter circuit are chosen to be Insulated Gate Bipolar Transistors (IGBT) for their fast response and robust operation. The inverter uses Sinusoidal Pulse Width Modulation (SPWM) for controlling the modulation index hence controlling the output voltage of the inverter.

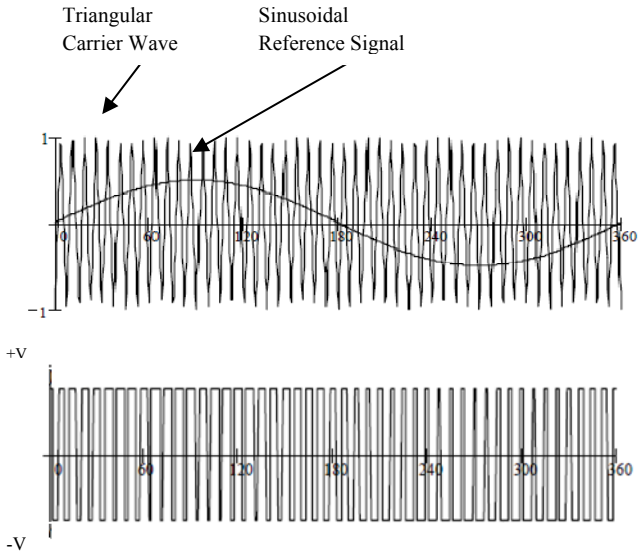

Fig.6.6: Sinusoidal Pulse Width Modulation Scheme.

In SPWM, a sinusoidal reference signal of supply frequency (i.e. 50 Hz) is compared with a high frequency triangular carrier waveform (i.e. 1080 Hz for this study). When the sinusoidal reference signal is greater than the triangular carrier wave, a batch of three IGBT switches out of the six are turned on and the counter switches are turned off and when the reference sinusoidal signal is smaller than the triangular carrier waveform in magnitude then the second batch of three IGBT switches are turned on and the first batch of switches are turned off. The magnitude of the sinusoidal reference signal determines the modulation index of the PWM signal generator which is dependent upon the error signal. The magnitude of the sinusoidal reference signal is controlled by the fuzzy logic based feedback controller which adjusts the magnitude according to the error magnitude and hence control the modulation index. The proposed DVR utilizes large capacitor banks for storing dc energy. Supply line voltage is rectified and used to charge the capacitor

banks. DC voltage from alternative supply sources can also be utilized with the proposed configuration of DVR.

6.3.3. Fuzzy Logic Controller

Fuzzy logic theory is considered as a mathematical approach combining multi-valued logic, probability theory, and artificial intelligence to replicate the human approach in reaching the solution of a specific problem by using approximate reasoning to relate different data sets and to make decisions. The performance of Fuzzy Logic Controllers is well documented in the field of control theory since it provides robustness to dynamic system parameter variations as well as improved transient and steady state performances.

In this study, a fuzzy logic based feedback controller is employed for controlling the voltage injection of the proposed Dynamic Voltage Restorer (DVR). Fuzzy logic controller is preferred over the conventional PI and PID controller because of its robustness to system parameter variations during operation and its simplicity of implementation. Since the proposed DVR uses energy storage system consisting of capacitors charged directly from the supply lines through rectifier and the output of the inverter depends upon the energy stored in the dc link capacitors. But as the amount of energy stored varies with the voltage sag/swell events, the conventional PI and PID controllers are susceptible to these parameter variations of the energy storage system; hence the control of voltage injection becomes difficult. The proposed FLC scheme exploits the simplicity of the Mamdani type fuzzy systems that are used in the design of the controller and adaptation mechanism.

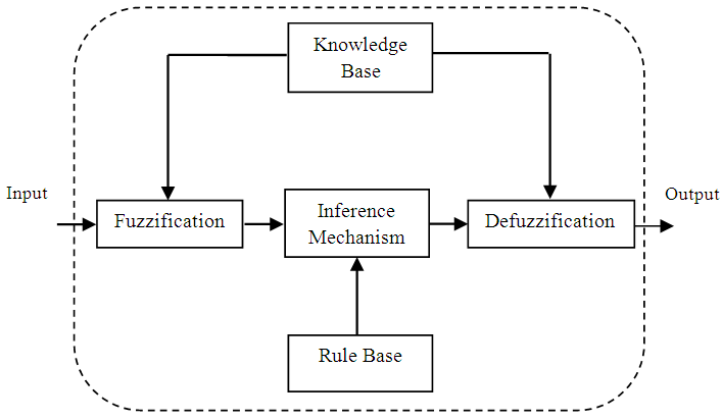

Fig.6.7: Schematic representation of Fuzzy Logic Controller for DVR.

The fuzzy logic based control scheme (Fig.6.7) can be divided into four main functional blocks namely Knowledge base, Fuzzification, Inference mechanism and Defuzzification. The knowledge base is composed of data base and rule base. Data base consists of input and output membership functions and provides information for appropriate fuzzification and defuzzification operations. The rule-base consists of a set of linguistic rules relating the fuzzified input variables to the desired control actions. Fuzzification converts a crisp input signals, error (e), and change in error (ce) into fuzzified signals that can be identified by level of memberships in the fuzzy sets. The inference mechanism uses the collection of linguistic rules to convert the input conditions to fuzzified output. Finally, the defuzzification converts the fuzzified outputs to crisp control signals using the output membership function, which in the system acts as the changes in the control input (u).

The typical input membership functions for error and change in error are shown in Fig.6.8a and Fig.6.8b respectively, whereas the output membership function for change in control input is shown in Fig.6.8c. The output generated by fuzzy logic controller must be crisp which is used to control the PWM generation unit and thus accomplished by the defuzzification block. Many defuzzification strategies are available, such as, the weighted average criterion, the mean-max membership, and center-of-area (centroid) method. The defuzzification technique used here is based upon centroid method.

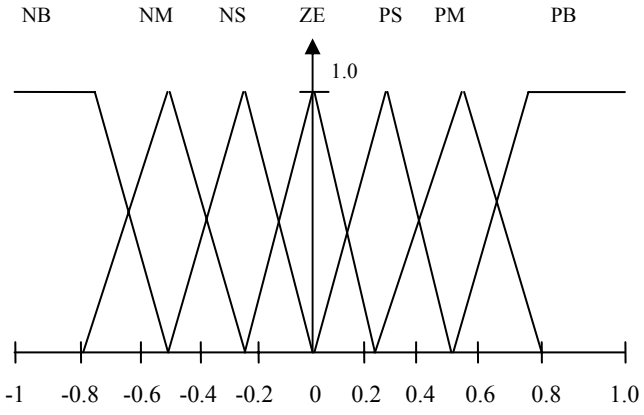

Fig 6.8a: Membership Function for Input Variable Error, ‘e’.

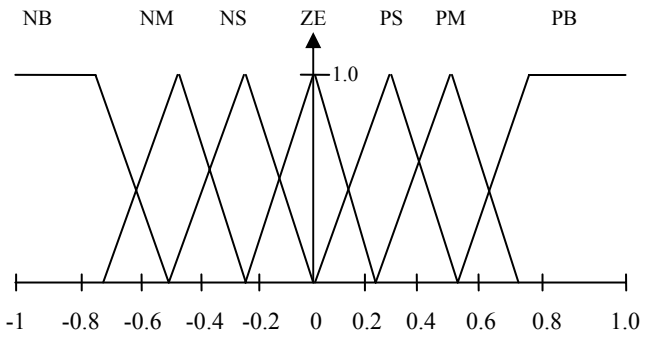

Fig 6.8b: Membership Function for Input Variable Change in Error, 'ce'.

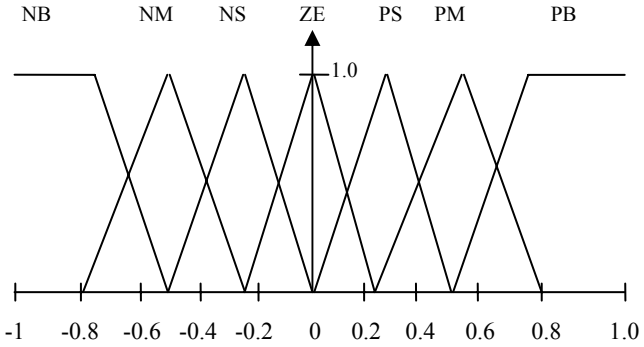

Fig 6.8c: Membership Function for Output Variable Change in Control Signal, 'u'.

The set of fuzzy control linguistic rules is given in Table-IV. The inference mechanism of fuzzy logic controller utilizes these rules to generate the required output.

Table IV: Rule Base for Fuzzy Logic Controller for DVR

'e' 'ce'	**NB**	**NM**	**NS**	**ZE**	**PS**	**PM**	**PB**
NB	NB	NB	NB	NB	NM	NS	ZE
NM	NB	NB	NB	NM	NS	ZE	PS
NS	NB	NB	NM	NS	ZE	PS	PM
ZE	NB	NM	NS	ZE	PS	PM	PB
PS	NM	NS	ZE	PS	PM	PB	PB
PM	NS	ZE	PS	PM	PB	PB	PB
PB	ZE	PS	PM	PB	PB	PB	PB

6.4.MODELING AND SIMULATION

The performance of the proposed fuzzy logic based DVR is evaluated by using MATLAB/SIMULINK program as a simulation platform. The DVR is connected in series between a three phase programmable (controllable) voltage source with 400V line to line RMS voltage, 50 Hz and a load of active power p = 10 KW and reactive power Q = 1 KVAR (with installation of power factor correction capacitors). The Simulink model of the proposed DVR is shown in Fig.6.15.

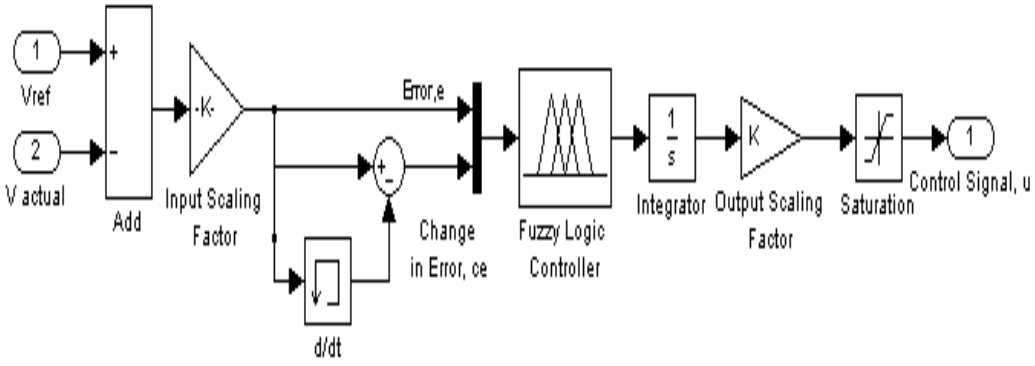

Fig.6.9: SIMULINK model of proposed FLC for DVR.

6.5 Simulation Results

6.5.1. Three Phase Balanced Sag

A three phase balanced voltage sag is simulated by reducing the line to line voltage on each phase to 60% of the normal value for a duration of 0.3 seconds from t=0.4 sec till t=0.7 sec as shown in Fig.6.10. The simulation duration was 1 second.

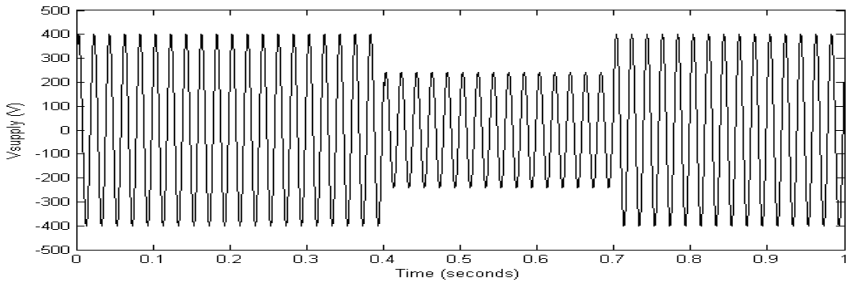

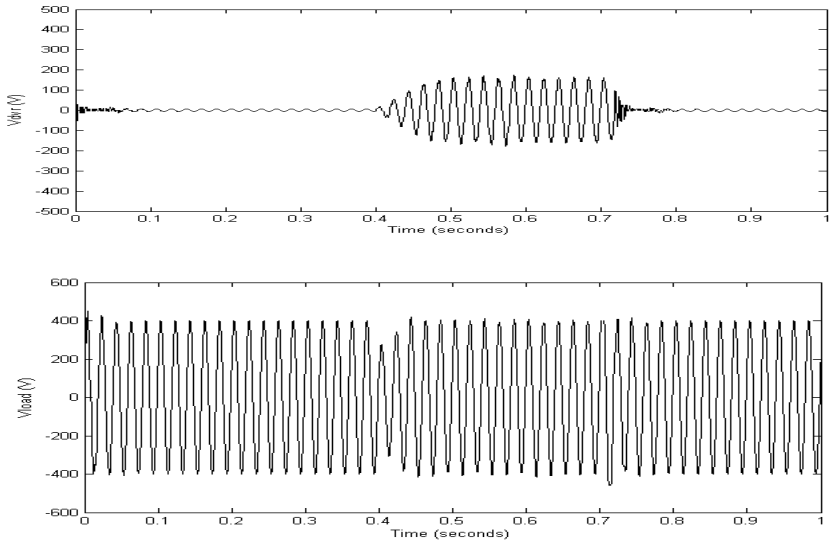

Fig.6.10: Three Phase Balanced Voltage Sag.

6.5.2. Three Phase Balanced Swell

A three phase balanced voltage swell is simulated by increasing the line to line voltage on each phase to 140% of the normal value for a duration of 0.3 seconds from t=0.4 sec till t=0.7 sec as shown in Fig.6.11. The simulation time was 1 second.

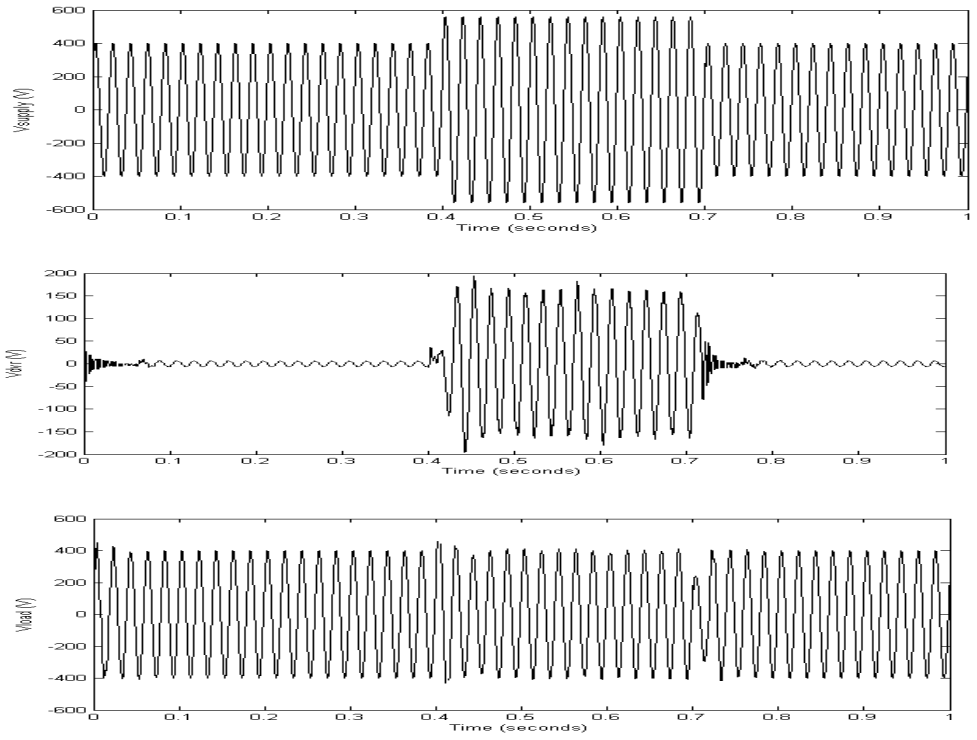

Fig.6.11: Three Phase Balanced Voltage Swell.

6.5.3. Consecutive Sag and Swell

Voltage sag on the three phases of 60% of the normal value is simulated on all of the three phases for 0.4 sec starting from t=0.4 sec and ending at t=0.8 sec which is followed by a balanced three phase voltage swell of 140% of the normal voltage value for t=0.4 sec starting from t=1.0 sec to t=1.4 sec. The duration of the simulation was 2 seconds and the results are shown in Fig.6.12.

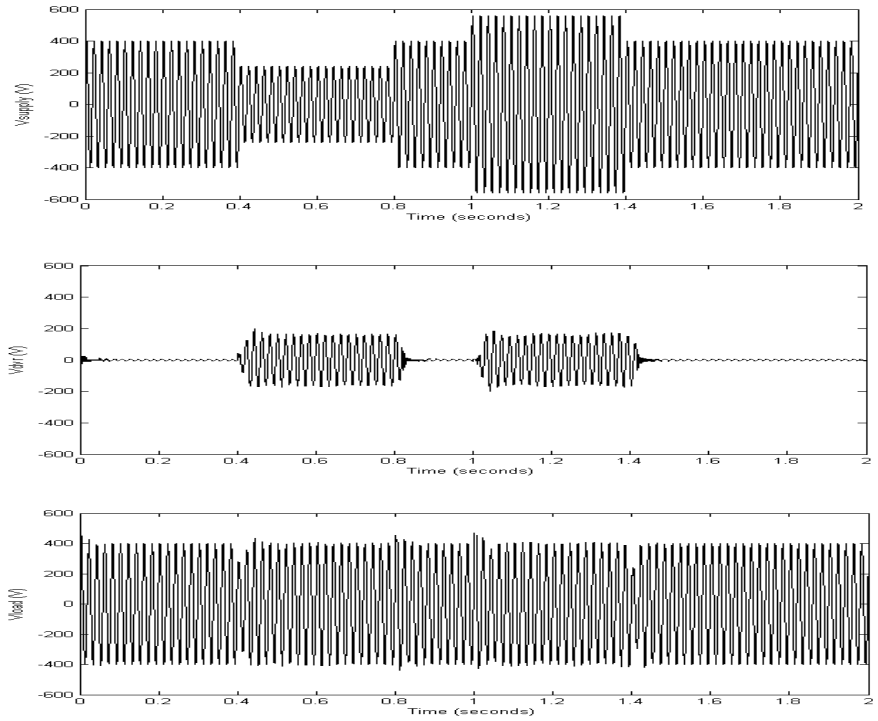

Fig.6.12: Consecutive Voltage Sag and Swell.

6.5.4. Multi-stage Sag

Voltage sags on the three phases at 50% of the normal value is simulated for 0.3 sec from t = 0.3 sec till t = 0.6 sec, after that, the sag prolonged on another stage at 60% of the normal voltage magnitude for 0.2 sec from t = 0.6 to t = 0.8 as shown in Fig.6.13. The duration of the simulation in this case was 1 second.

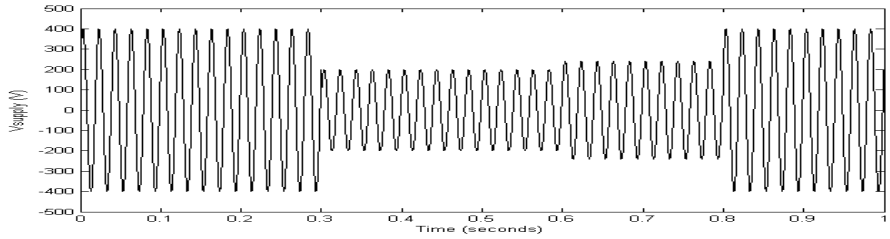

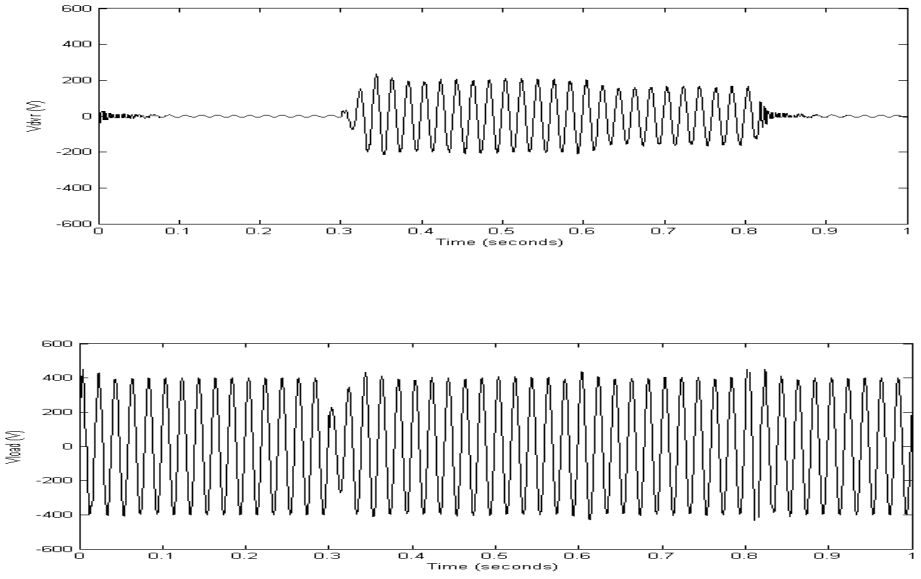

Fig.6.13: Multi-stage Voltage Sag.

6.5.5. Three phase unbalanced sag

Single-Line-To-Ground (SLG) faults are the most prevalent type of three phase unbalanced sags. For the purpose of the simulation, Phase A voltage magnitude is sagged to 50% for 0.5 sec from t = 0.3 sec till t = 0.7. The line to line voltage magnitudes V_{AB} and V_{CA} will be affected but the magnitude of V_{BC} will remain unchanged. The simulation time used was 1 second and the results are shown in Fig.6.14.

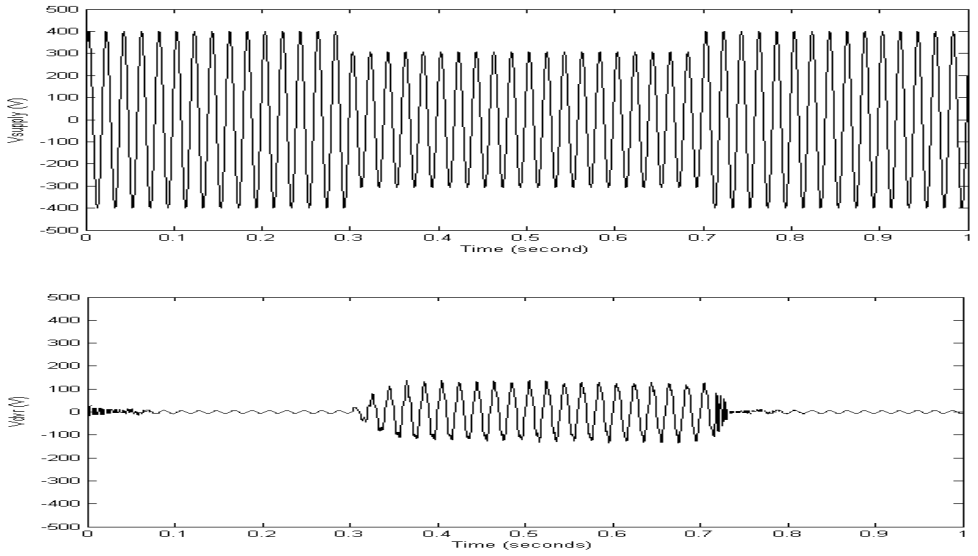

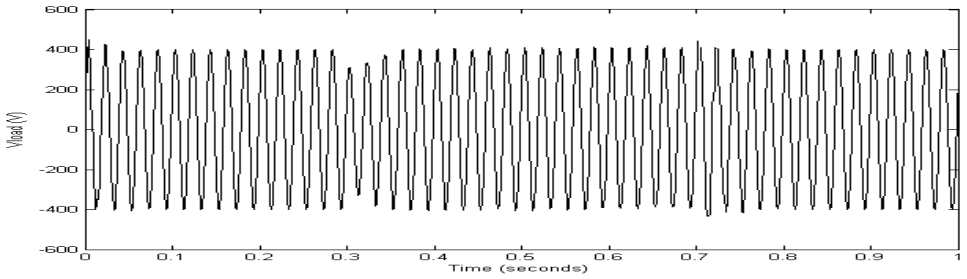

Fig.6.14: Three Phase Unbalanced Voltage Sag.

6.6. Performance Analysis of Proposed DVR in DTC based IM Drive System

The performance of the proposed dynamic voltage restorer developed for the DTC based induction motor drive has been tested through simulations in MATLAB/ Simulink platform under various system fault scenarios. The implemented Simulink model of the proposed DVR along with the DTC based IM drive is shown in Fig.6.20 and the complete Simulink model of the proposed DVR is shown in Fig.6.21.

The performance of the complete system has been tested under various system fault conditions including both symmetric and asymmetric system faults which include three phase balanced sags, three phase balance swells, consecutive sags and swells, multi-stage sags and unbalanced sags. The results are analyzed and compiled in terms of the three phase supply voltages, three phase load voltages and the speed responses of the drive system.

Fig.6.15 shows the performance of the proposed DVR and the IM drive under three phase balanced sag conditions. A three phase balanced voltage sag is simulated by reducing the line to line voltage on each phase to 50% of the normal value for a duration of 0.3 seconds from t=0.4 sec till t=0.7 sec as shown in Fig.6.15. The simulation duration was 1 second.

In Fig.6.16, the performance of the proposed DVR and IM drive has been shown under balanced three phase voltage swell conditions. A three phase balanced voltage swell is simulated by increasing the line to line voltage on each phase to 150% of the normal value for a duration of 0.3 seconds from t=0.4 sec till t=0.7 sec as shown in Fig.6.16. The simulation time was 1 second.

In Fig.6.17, voltage sag on the three phases of 50% of the normal value is simulated on all of the three phases for 0.25 sec starting from t=0.25 sec and ending at t=0.5 sec which is followed by a

balanced three phase voltage swell of 150% of the normal voltage value for 0.3 sec starting from t=0.6 sec to t=0.9 sec. The duration of the simulation was 1 seconds also.

Voltage sags on the three phases at 50% of the normal value is simulated for 0.25 sec from t = 0.25 sec till t = 0.5 sec, after that, the sag prolonged on another stage at 60% of the normal voltage magnitude for 0.3 sec from t = 0.6 to t = 0.9 as shown in Fig.6.18. The duration of the simulation in this case was 1 second.

In order to simulate the unbalanced sag, phase A voltage magnitude is sagged to 50% for 0.3 sec from t = 0.4 sec till t = 0.7. The line to line voltage magnitudes V_{AB} and V_{CA} will be affected but the magnitude of V_{BC} will remain unchanged. The simulation time used was 1 second and the results are shown in Fig.6.19.

In all of the cases the results are analyzed with respect to three phase supply voltages under normal and fault conditions, three phase load voltages and the speed responses of the induction motor drive under sudden step changes in the reference speed from 150 rad/sec to 180 rad/sec. The proposed DVR system compensates for the all of the above mentioned fault conditions and the speed response of the induction motor drive traces the reference speed trajectory with minimum deviations under the simulated voltage sags and swell conditions.

The simulation results strongly showcases the capacity of the proposed dynamic voltage restorer system developed for helping the direct torque control scheme based induction motor drive to maintain its performance under various power quality problems associated with voltage sags and swells.

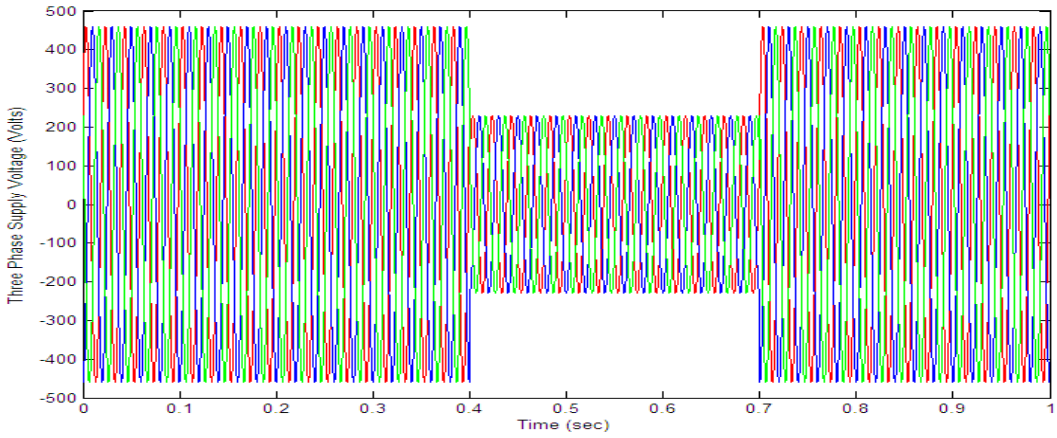

(a)

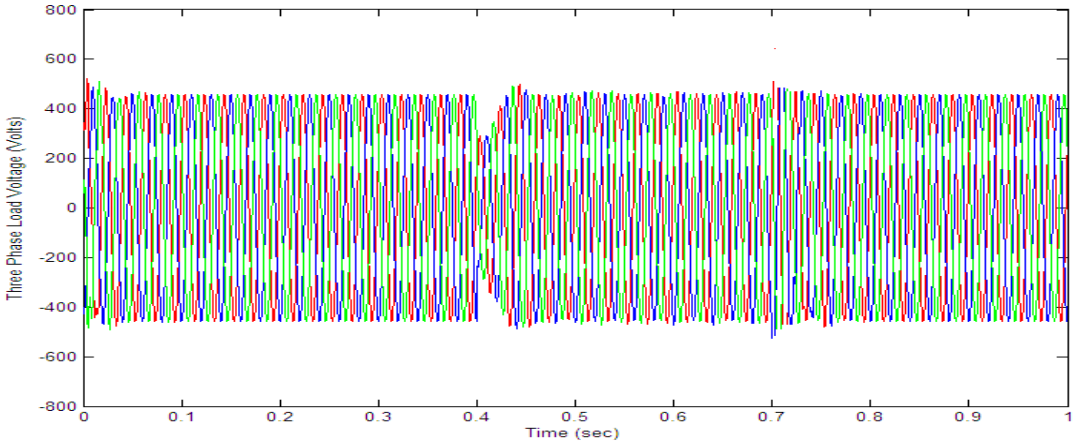

(b)

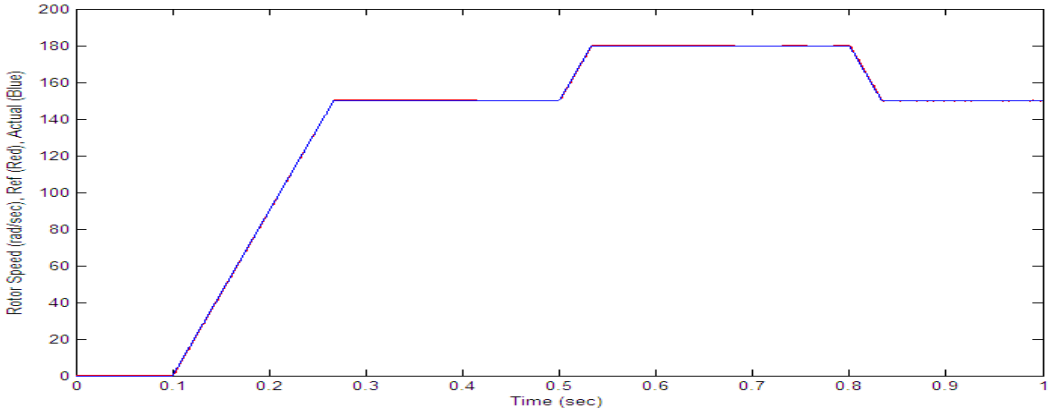

(c)

Fig.6.15: Performance analysis under three phase balanced voltage sag condition: (a) Three phase supply voltage, (b) Three phase load voltage and (c) Speed response of the IM drive.

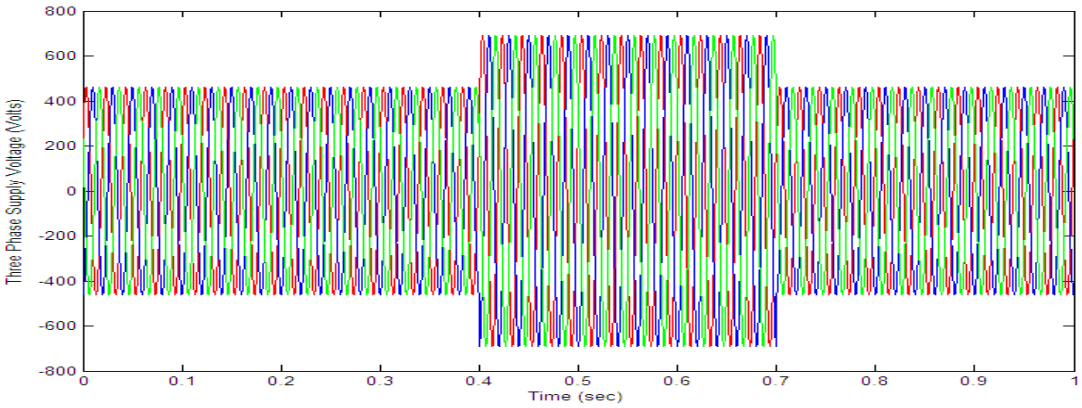

(a)

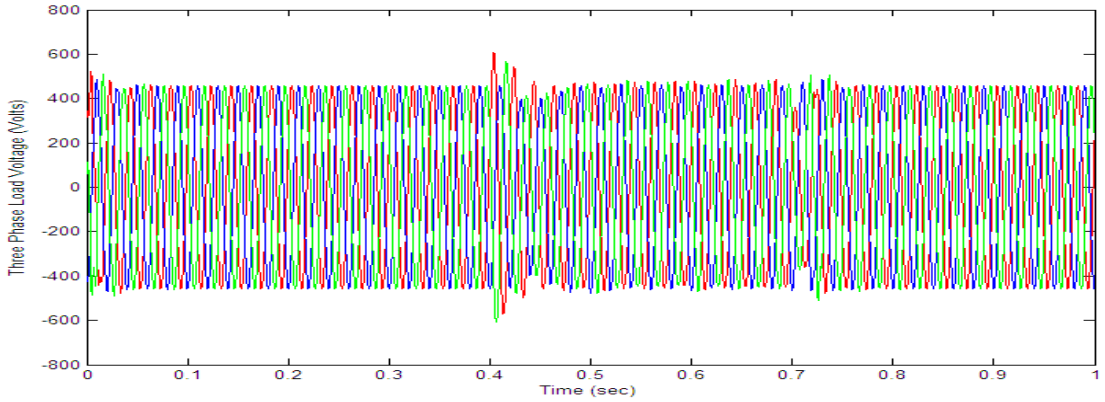

(b)

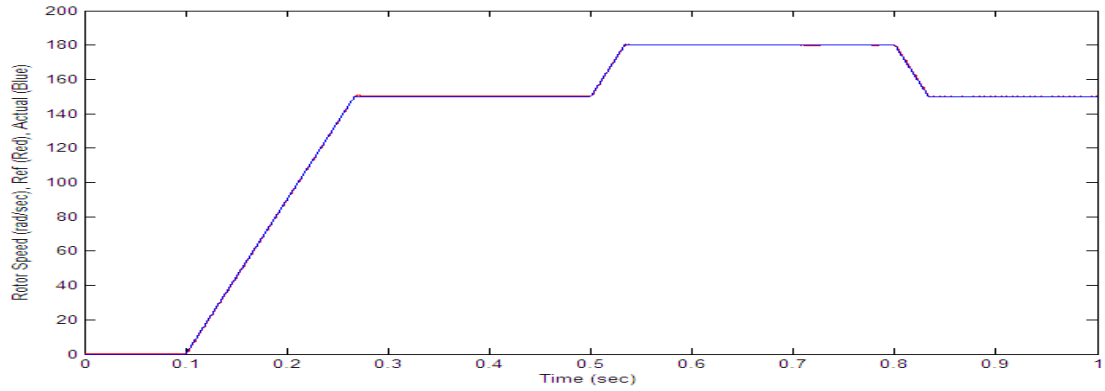

(c)

Fig.6.16: Performance analysis under three phase balanced voltage swell condition: (a) Three phase supply voltage, (b) Three phase load voltage and (c) Speed response of the IM drive.

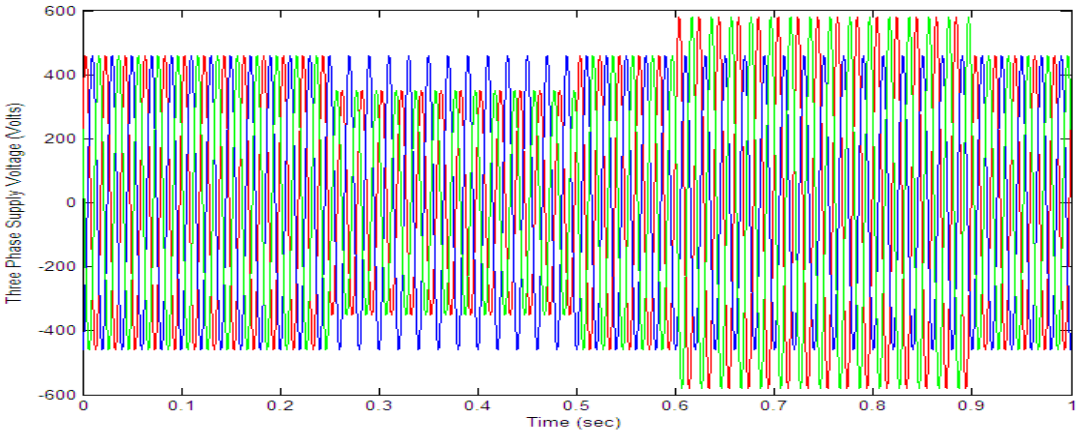

(a)

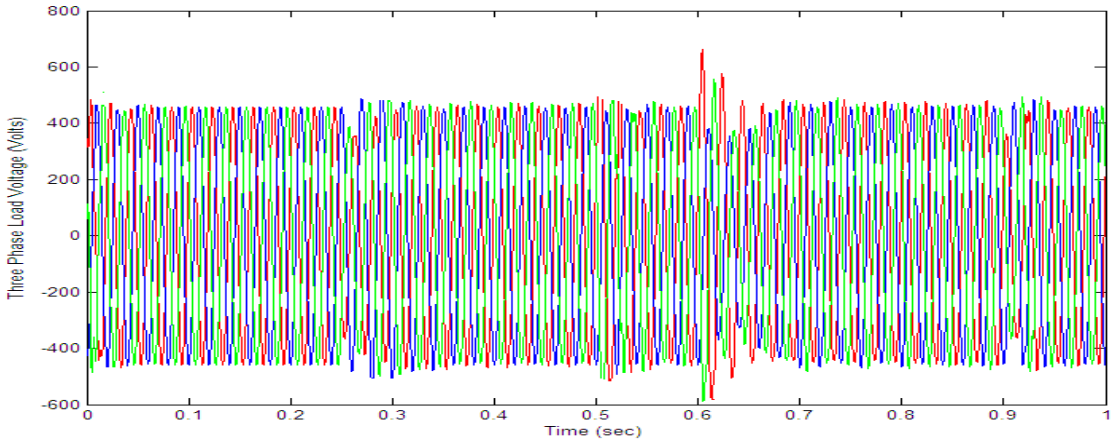

(b)

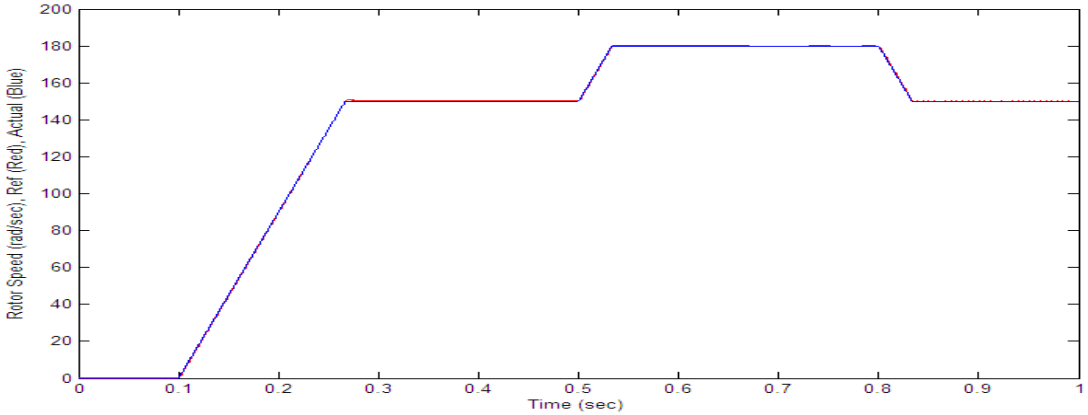

(c)

Fig.6.17: Performance analysis under consecutive voltage sag and swell condition: (a) Three phase supply voltage, (b) Three phase load voltage and (c) Speed response of the IM drive.

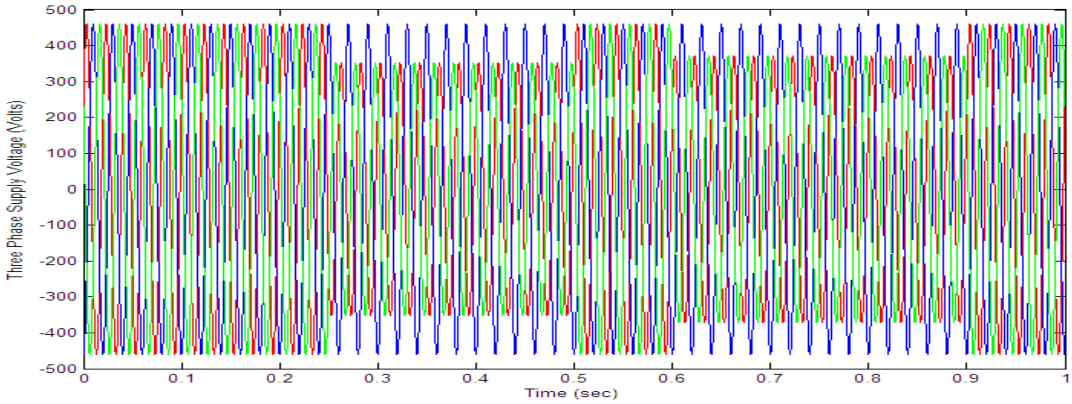

(a)

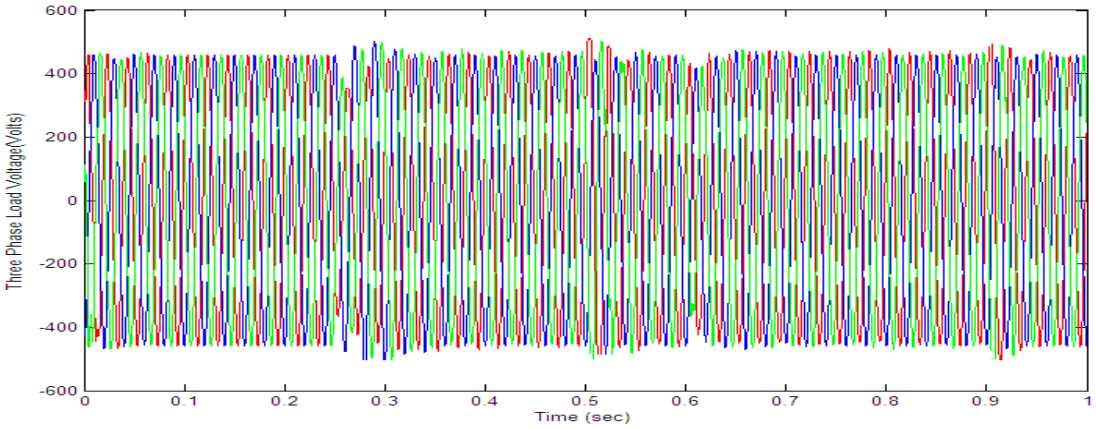

(b)

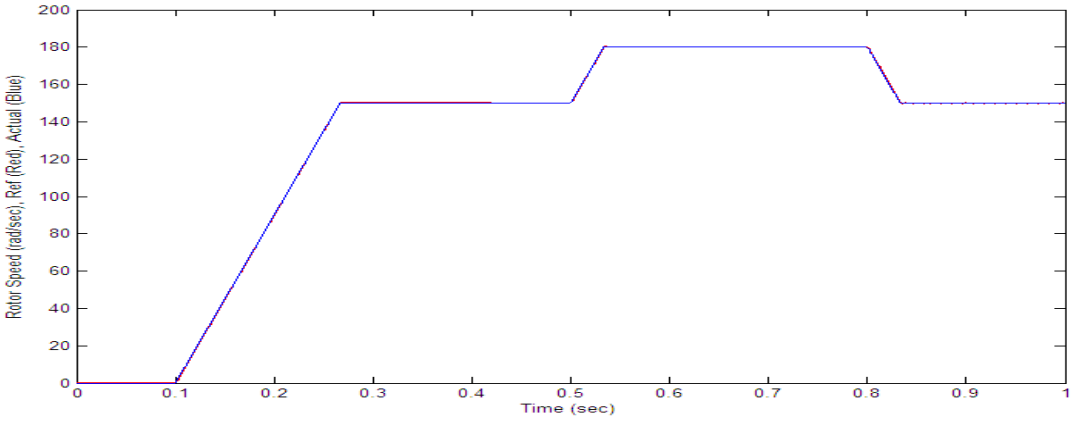

(c)

Fig.6.18: Performance analysis under multi-stage voltage sag condition: (a) Three phase supply voltage, (b) Three phase load voltage and (c) Speed response of the IM drive.

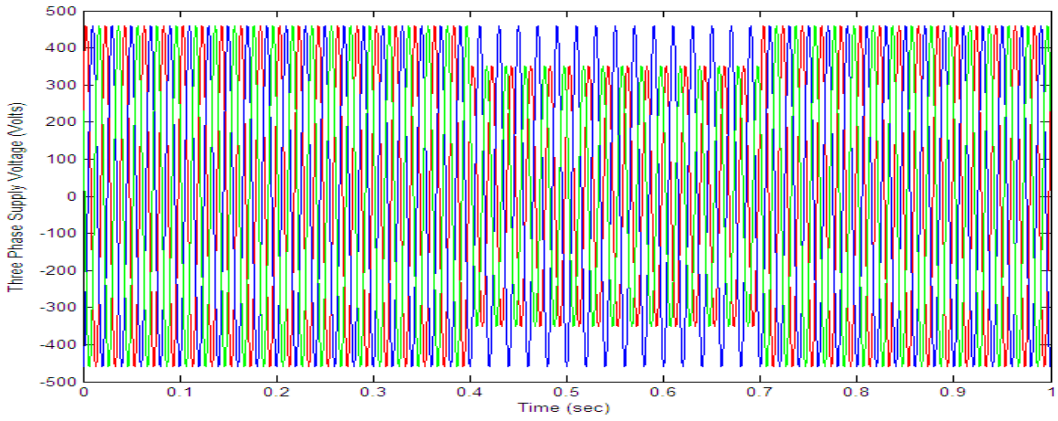

(a)

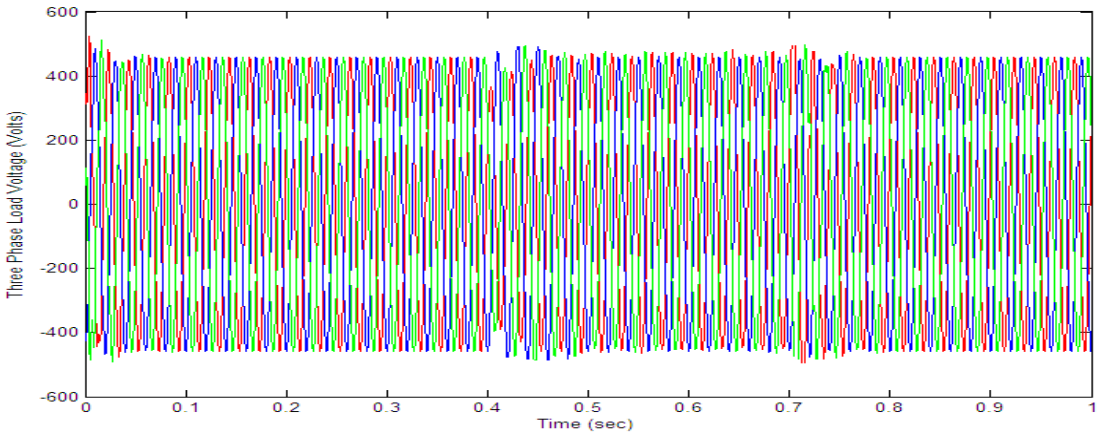

(b)

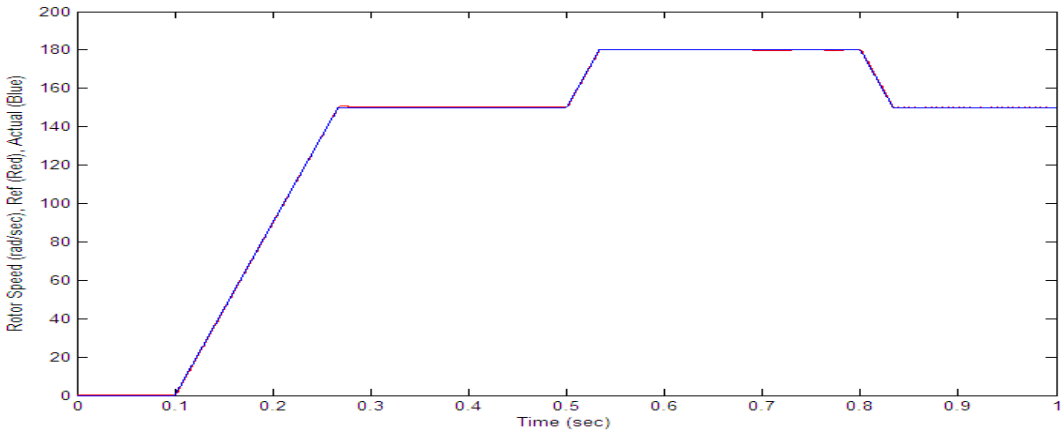

(c)

Fig.6.19: Performance analysis under unbalanced voltage sag condition: (a) Three phase supply voltage, (b) Three phase load voltage and (c) Speed response of the IM drive.

6.7. Conclusion

In this study, a simple, fast and efficient Dynamic Voltage Restorer (DVR) is proposed for mitigation of power quality problem associated with voltage sags/swells in industrial distribution systems with a large portion of its load comprising of induction motors drives. The proposed DVR employs the classical Fourier Transform technique for detection and quantification of voltage disturbances (sags/swells) events. Since induction motor drives are sensitive to changes in phase angle, pre-fault compensation method is used for calculation of the compensating voltage since it is fast and simple and finally a fuzzy logic based feedback controller is used to control the voltage injection of the proposed DVR system in case of voltage disturbances. The proposed DVR utilizes energy drawn from the supply line source during normal operation and stores in capacitors and which is converted to an adjustable three phase ac voltage suitable for mitigation of voltage sags/swells. The modeling and simulation of the proposed DVR using MATLAB/Simulink had been presented. The simulation shows that the DVR performance is efficient and satisfactory in mitigating voltage sags/swells. The DVR handles both balanced and unbalanced situations with sufficient efficiency and accuracy and injects the appropriate voltage component to correct rapidly any deviation in the supply voltage to keep the load voltage constant at the nominal value. The proposed DVR when used for maintaining the DTC based IM drive performance has shown promising results in overcoming both symmetrical and asymmetrical system faults and maintaining the drive performance at the desired level.

The main advantages of the proposed DVR are simple and efficient adaptive control and fast response. Future works will include a comparison with a laboratory experiments on a low voltage DVR in order to compare simulation and experimental results and estimate the cost of the practical system. Further issues associated with low pass filter construction and its parameters selection, injection transformer selection and its saturation and reduction in operational time of the entire DVR system will be investigated in future works.

The complete Simulink diagram for the proposed ANFIS based DTC of IM drive along with the Dynamic Voltage Restorer for the compensation of the power quality problems is shown in the Fig.6.20. The model for the DVR subsystem is shown in the Fig.6.21.

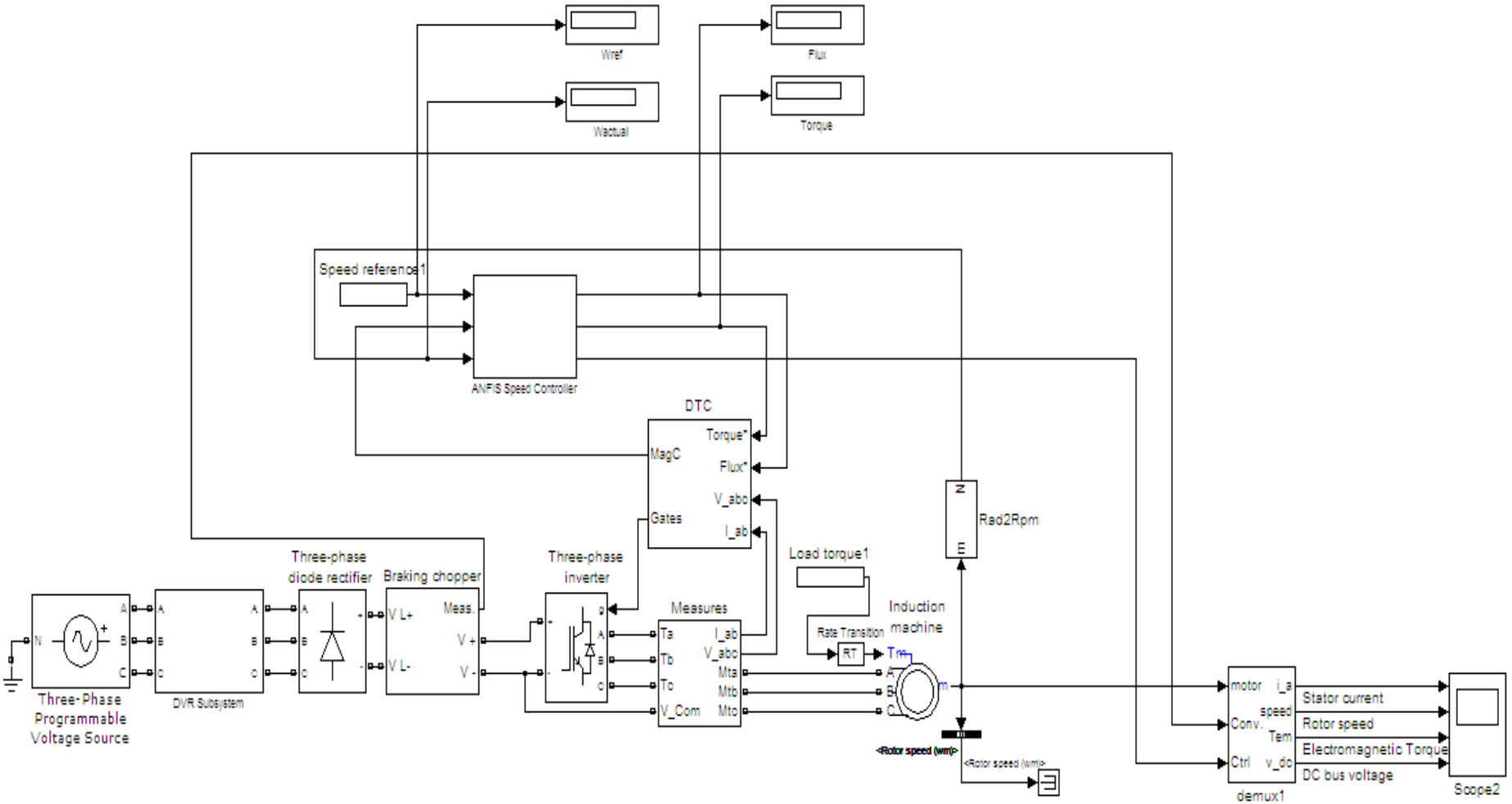

Fig.6.20: Proposed ANFIS Controller based DTC of IM Drive with Dynamic Voltage Restorer

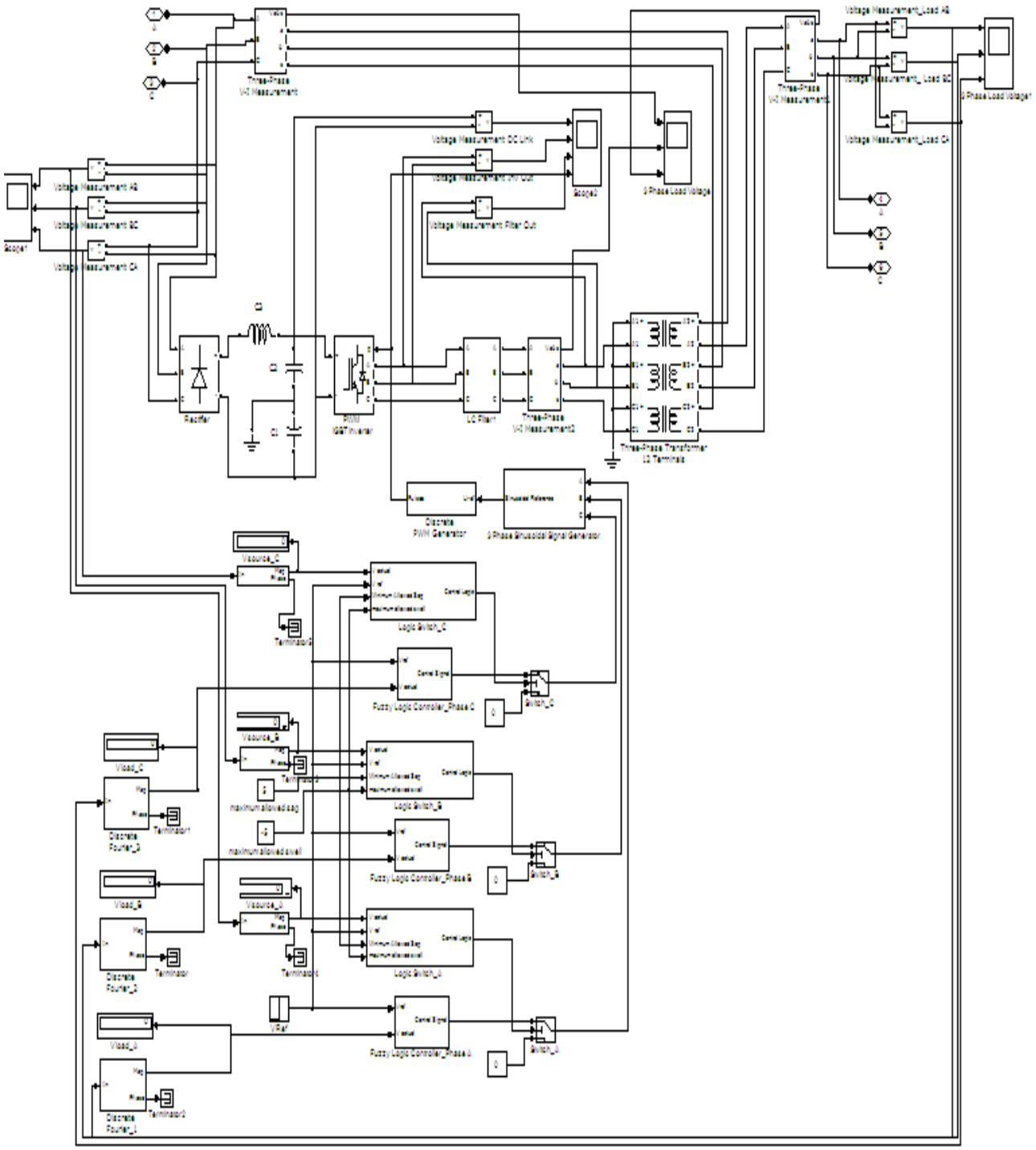

Fig.6.21: Simulink model for the fuzzy logic control dynamic voltage restorer for IM drives

Chapter 7

Summary and Conclusion

Direct torque control is supposed to be one of the best control schemes for driving any induction motor drive. Its principles and basic concepts have been introduced and thoroughly analyzed in this thesis. It is also demonstrated in the thesis that the method of direct torque control also allows the decoupled control of motor torque and motor stator flux. According to the analysis, the DTC strategy is simpler to implement than the vector control or field oriented control method because it does not require voltage modulators and co-ordinate transformations. However, it introduces undesired torque ripples.

In this thesis, fundamentals of induction motor drives have been studied thoroughly and the main topic of concern was speed control of induction motor drives. The focus was to develop an adaptive neuro-fuzzy inference system (ANFIS) based speed controller for IM drive so as to achieve precision in speed control. The artificial intelligence controllers (AICs) provide certain advantages over the conventional or classical controllers (like- Proportional Integral Controller). The most prominent of all the advantages of the proposed hybrid ANFIS controller is that it doesn't need any plant mathematical model to operate since the controller can attain a certain level of human intelligence by utilizing the linguistic variables of fuzzy logic instead of numerical ones and it also achieves the adaptability of human brain with the use of neural networks. Since it is completely independent of the mathematical model of the system that it will be driving, it relieves the designer from using cumbersome techniques.

In this research work, a simple hybrid adaptive neuro-fuzzy inference system based speed controller has been proposed which is employed in a direct torque control scheme based induction motor drive in order to achieve precise and efficient speed control. The proposed system was developed and simulated in MATLAB/ Simulink platform. The system was simulated for various operating conditions and results from each of the simulation were analyzed

concentrating on parameters such as rise time, settling time, percent overshoot, percent torque ripple, stator current ripple, ripples in stator flux linkage etc. The obtained simulation results were compared with the simulation results for classical PI controller under the same operating conditions. The comparison results yielded the followings advantages rendered by the proposed ANFIS controller over the conventional PI controller:

- The percent overshoot in the transient response has been reduced significantly.
- Significantly improved settling times have been observed.
- The speed tended to approach the reference speed even when it was higher than the base speed or very low as compared to the same, unlike the PI Controller.
- Improved IM torque response with lesser ripples both in steady state and transient state.
- Stator flux linkages have lesser ripples as compared to the conventional PI controllers.
- Fluctuations in stator currents are significantly reduced.

Although the proposed controller has shown signs of promising improvement in the DTC based speed control of IMs, much work is still needed to be done in order to fully test the proposed controller's functionality for any practical IM drives. The scope for further improvement in the proposed control system may include:

- Study of the ripples in the developed torque, stator current and flux linkages further and achieve any further ripple minimizations in the above mention quantities.
- Implementation of the system in real time in order to analyze its functionality in real time systems and to analyze the computational burden it applies on the processor.
- Study of the computational and processing time of the proposed system and work on any possible improvement.

In this thesis, a fuzzy logic controlled dynamic voltage restorer (DVR) for the IM drive has also been proposed. The proposed DVR system is capable of compensating for any possible system fault scenario associated with voltage sags and swells, and maintaining a constant voltage supply across the IM drive terminals. The proposed DVR also compensates for any possible phase angle jumps which may cause deterioration of the drive performance. The proposed system has also been developed and simulated using MATLAB/ Simulink platform and has been simulating for

several fault conditions including symmetrical and asymmetrical system faults. The proposed DVR has also been tested while used in conjunction with the DTC based IM drive system and the test results have been sufficiently accurate for considering the system for practical and real time implementation. Scope for further improvement in the proposed dynamic voltage restorer system may include reduction in the processing time, improved detection and compensation algorithms and may be in further development in the controller controlling the DVR injection. Further, it can be implemented in real time in order to verify its functionality both as a standalone system and in conjunction with the IM drives.

References

[1] R. Fei, E.F. Fuchs, and H. Huag, "Comparison of Two Optimization Techniques as applied to Three-Phase Induction Motor Design," IEEE Trans. Energy Conversion, vol. 4, no. 4, pp. 651-660, Dec 1989.

[2] Uddin M.N., Hao Wen, “Development of a Self-Tuned Neuro-Fuzzy Controller for Induction Motor Drives”, IEEE Transactions on Industry Applications, Vol. 43, Issue-4, pp. 1108-1116, July-August 2007.

[3] SJ. Chapman, Electric Machinery Fundamentals, New York: Mcgraw-Hill, 1999.

[4] A. M. Trzynadlowshi, The field orientation principle in control of induction motors, Kluwer Academic, 1994.

[5] I. Ludtke, and M.G. Jayne, "A comparative study of high performance speed control strategies for voltage sourced PWM inverter fed induction motor drives," 7th International Conference on Electrical Machines and Drives, 11-13 September 1995, university of Durham, UK.

[6] J. W. Finch, "Scalar and Vector: a simplified treatment of induction motor control performance", IEE colloguium on Vector Control Revisited, digest no. 1998/99, pp. 2/1- 2/4.

[7] Marek Stulrajter, Balería Hrabovcova and Mark Franks, "Permanent Magnets Synchronous Motor Control Theory," Journal of Electrical Engineering, vol. 58, no. 2, pp. 79-84, 2007.

[8] K.W. Ng, and CW. Poon, "Computer Simulation on a Typical VVVF Elevator drive- Scalar versus Vector"

[9] Sang Woo Nam, “Adaptive Back-stepping Based Online Loss Minimization Control and Induction Motor Drives”, M.Sc. Thesis, Lakehead University, 2006.

[10] B. K. Bose, “Power Electronics and AC Drives," Prentice Hall, 1986,

[11] F, Blasée, “The principle of Field Orientation as Applied to the New Trans-vector Closed Loop Control System for Rotating Field Machines," Seimens Review, vol. 34, pp. 2.7- 220, May 1972.

[12] N. P. Quang and ,A. D.ttnch, Vector Control of Three Phase Induction Machines, System Development in Practice, Springer Berlin Heidelberg, Jan 2010.

[13] D.W. Novotony and T.A. Lipo, “Vector Control and Dynamics of AC Drives”, Oxford University University Press, 1997.

[14] M. Ichiro, I. Aldo, and K. Talcahasht, “Recent Industrial Applications of Speed Sensorless Vector Control in Japan", IEEE 24th International Conference on Industrial Electronics, Control and Instrumentation, vol. 3, pp. 1573-1578, 1994.

[15] Takahashi, T. Nongnchi, "A New Quick Response and High Efficiency Control Strategy for an

Induction Motor," IEEE Trans. on Industrial Applications, vol. 22, no. 5, pp. 820- 827, 1986.

[16] M. Depenbrock., "Direct self-control (DSC) of inverter-fed induction machine", IEEE Trans. Power Electronics, vol. 3, no. 4, October 1988.

[17] Hang Le-Huy, "Comparison of Field-Oriented Control and Direct Torque Control for Induction Motor Drives," IEEE Industrial Application Conference, vol. 2 pp. 1245-125, 1999.

[18] M. P. Kazmierkowski, “Control Philosophies of PWM Inverter Fed Induction Motors”, IEEE Conf. on Industrial Electronics, vol. 1, pp. 16-26, 1997.

[19]. Peter Vas, “Sensorless Vector and Direct Torque Control”, Oxford University Press USA, 1998

[20] ABB, Technical Guide-1, Direct Torque Control, ABB-library [online]. Available: http://www05.abb.com/global/scot/scot201.nsf/veritydisplay/299c5d307cb78a34cl256d28003fedOc/$File/ABB_Technical_Guide_l_%20EN26042002.pdf.

[21] N. Minorshy, “Directional stability of automatically steered bodies”, Journal of the American Society for Naval Engineers, vol. 34, issue 2, pp. 280-309, 1922.

[22] K. H. Ang, G. C. Y. Chong, and Y. Li., “PID Control System Analysis Design and Technology”, IEEE Trans. on Control Systems Tech, vol. 13 no. 4, pp. 559-576, 2005.

[23] G. Espinosa-Perez, and R. Ortega, "Tuning of PI Gains for FOC of Induction Motors with Guaranteed Stability," IECON Proceedings, vol.2, pp. 569-574, 1997.

[24] G,W. Chang, G. Espinosa-Perez, E. Mendes, and R. Ortega, "Tuning rules for the PI gains of field-oriented controllers of induction motors," IEEE Trans. Industrial Electronics, vol. 47, no. 3, pp. 592-602, June 2000.

[25] R. D. Lorenz, and B.B. Lawson, "A simplified approach to continuous on-line tuning of field-oriented induction machine drives," IEEE-IAS Conference Record (Pittsburgh), pp. 444-449, 1988.

[26] Kuo -Kai Shyu, Hsiu-Jang Shieh, and Sheng-Shang Fu, "Model Reference Adaptive Speed Control for Induction Motor Drive using Neural Networks," IEEE Trans. Industrial Electronics, vol. 45, no. l,pp. 180-182, 1998.

[27] P. Santhosh, R. H. Chue, A.B. Patii, and D.R. Patii, "Model Reference Adaptive Technique for Sensorless Speed Control of Induction Motor," IEEE Conf. Emerging Trends in Engineering and Technology, pp. 893-898, 2008.

[28] K.B. Mohanty, "Sensorless Sliding Mode Control of Induction Motor Drives," TENCON, pp. 1-6, 2008,

[29] M. Rodic, K. Jezermk, and A. Sabanovic, "Speed Sensorless Sliding Mode Torque Control of Induction Motor," IEEE Conf. Industry Application, vol. 3 pp. 1820-1827, 2000.

[30] Z. Hakan Akpolat, G. M. Asher, and J. C. Clare, "A practical approach to the design of robust

speed controllers for machine drives," IEEE Trans. Industrial Electronics, vol. 47, no. 2, pp. 315-324, Apr 2000.

[31] P.V. Kokotovic, "The Joy of Feedback Nonlinear and Adaptive Control Systems," IEEE Control Systems Magazine, vol.12, no. 3, pp. 7-17, 1992.

[32] S. Shastry and M. Bodson, Adaptive Control: Stability, Convergence and Robustness, Prentice Hall, 1994

[33] H. Tan, and J. Chang,"Field Orientation and Adaptive Back-stepping for Induction Motor Control," IEE- IAS-1999, vol. 4, pp. 2357-2363.

[34] A. S. Morse, "Global Stability of Parameter Adaptive Control Systems," IEEE Trans Automatic Control", vol. AC-25, pp. 433-439, June 1980

[35] K. S. Narendra, Y. H. Lin, and I. S. Valavani, "Stable Apdaptive Controller Design- Part II: Proof of Stability," IEEE Tran. Automatic Control, vol. AC-25, pp. 440-448, June 1980.

[36] G. C. GoOdW1n, P. J. Ramadge, and P. E. Cames, "Discrete Time Multivariable Adaptive Control," IEEE Trans. Automatic Control, vol. AC-25, pp. 449-456, June 1980.

[37] C. E. Rohrs, L. Valavam, M. Äthans, and G. Stein, "Robustness of Continuous-Time Adaptive Control Algorithms m the Presence of Unmodeled Dynamics," IEEE Trans. on Automatic Control, vol. 30, no. 9, pp. 881-889, Sep 1985.

[38] L. Vandevelde, and J. A. A. Melkebeek, "Numerical Analysis of orations of Squirrel-Cage Induction Motors based on Magnetci Equivalent circuits and Structural Finite Element Models," IEEE Conf. on Industry Application, vol.4, pp. 2288-2295, 2001.

[39] Chm-Teng Lin, and C. S. G. Lee, "Neural Fuzzy Systems: A Neuro-Fuzzy Synergism to Intelligent Systems," NJ: Prentice Hall, 1996.

[40] Z. Ibrahim, And E. Levi. "A Comparative Analysis of Fuzzy Logic and PI Speed Control in High Performance AC Drives Using Experimental Approach," IEEE Trans. Industrial Application, vol. 38, no. 5, pp. 1210-1218, Sept./Oct 2002.

[41] Y. Tang, and L. Xu, "Fuzzy Logic Application for Intelligent Control of a Variable Speed Drive," IEEE Trans. Power Electronics, vol. 12, pp. 1028-1039, November 1997.

[42] C. C. Lee, " Fuzzy Logic in Control System: Fuzzy Logic Controller - Part I," IEEE Trans. on System, Man and Cybernetics, vol. 20, no. 2, pp. 404-435, 1990.

[43] L. A. Zadeh, "Fuzzy Sets", Information and Control, vol. 8, no. 3,pp. 338-353, 1965.

[44] D. Driankov, H. Hellendoorn, and M. Reinfrank, An Introduction to Fuzzy Control, 2nd edition, Springer-Verlag Berlin, 1996.

[45] Fatiha Zidani, and Rachid Nait Said, "Direct Torque Control of Induction Motor with Fuzzy Minimization Torque Ripple," Journal of Electrical Engineering, vol. 56, no. 7-8, 2005, pp. 183-

188.

[46] Hassan-Halleh, Meisam Rahmani, and Bahram Kimiaghalam, "Direct Torque Control of Induction Motors with Fuzzy Logic Controller," IEEE Conf. Control, Automation and Systems, Oct 14-17, 2008 in CEOX, Seoul, Korea, pp. 345-350.

[47] R. Toufouti, S. Meziane, and H. Benalla, "Direct Torque Control for Induction Motor using Intelligent Techniques," Journal of Theoretical and Applied Information Technology, pp. 35-44, 2007.

[48] L. Youb, and A. Craciunescu, "Direct Torque Control of Induction Motors with Fuzzy Minimization Torque Ripple," WESCO 2009, vol. 2, pp. 713-717.

[49] M. N. Uddin, T. S. Radwan, and M. A. Rahman, "Performance of fuzzy-logic based indirect vector control· for induction motor drive," IEEE Transaction on Industry Applications, vol. 38, no. 5, pp. 1219-1225, September/October 2002.

[50] T. C. Huang, and M. A. El-Sharkawi, "High performance speed and position tracking of induction motors using multi-layer fuzzy control," IEEE Trans. Energy Conversion, vol.11, no. 2, pp. 353-358, June 1996.

[51] Y. Tang, and L. Xu, "Fuzzy Logic Application for Intelligent Control of a Variable Speed Drive," IEEE Trans. on Energy Conversion, vol. 9, pp. 679-685, December 1994.

[52] F. F. Cheng, and S. N. Yeh, "Application of Fuzzy Logic in the Speed Control of AC Servo System and an Intelligent Inverter," IEEE Trans. Energy Conversion, vol. 8, no. 2, pp. 312-318, June 1993.

[53] A. Engel, and C. Van Den Broech, Statistical Mechanics of Learning, Cambridge University Press, 2001.

[54] B. Kosco, "Neural Networks and Fuzzy Systems: A Dynamic Systems Approach to Machine Intelligence," Englewood Cliffs, NY: Prentice Hall, 1992.

[55] R. Kumar, R. A. Gupta, S. V. Bhangale, and Himanshu Gothwal, "Artificial Neural Network Based Direct Torque Control of Induction Motor Drives," IETECH Journal of Electrical Analysis, vol. 2, no. 3, pp. 159-165, 2008.

[56] Y. V. S. Reddy, M. Vijayakumar, and T. Brahmananda Reddy, “Direct Torque Control of Induction Motor Using Sophisticated Lookup Tables Based on Neural Networks," AIML Journal, vol. 7, no. 1, June 2007.

[57] Yen-Shin La1, and Juo-Chiun Lm, “New Hybrid Fuzzy Controller for Direct Torque Control Induction Motor Drives," IEEE Trans. on Power Electrons, vol. 18, no. 5, pp. 1211-1219, September 2003.

[58] P. C. Krause, and C. H. Thomas, “Simulation of Symmetrical Induction Machinery”, IEEE Trans.

Power Apparatus System, vol. PAS-84, no. 11, pp. 1038-1053, 1965.

[59] N.R.N. Idris and A.H.M. Yatim, “Direct Torque Control of Induction Machine with Constant Switching Frequency and Reduced Torque Ripple”, IEEE Trans. Industrial Electronics, vol.51, no.4, pp.758-767, Aug. 2004.

[60] A. E. Fowkes, “Hardware efficient algorithm for trigonometric functions," IEEE Trans. Computers, vol. 42 no. 2, pp. 235-239, February 1993.

[61] Marin P. Kazmierdowski, “Improved direct torque and flux vector control of PWM inverter fed induction motor drives”, IEEE Trans. Ind. Electronics, vol. 42, no. 4, August 1995.

[62] Matlab, Simulink User Guide, the Math Works Inc., 2004.

[63] B. Kosko, Fuzzy Engineering, Prentice-Hall Inc., 1997.

[64] David M. Skapura, Building Neural Networks, ACM Press, Addison-Wesley, 1996

[65] H. Dmathur, and S. Ghosh, "A Comprehensive Analysis of Intelligent Controllers for Load Frequency Control," Power India Conference, IEEE, 10-12 April, 2006. pp.5.

[66] D. Dnankov, H. Hellendoorn, and M. Reinfrank, "An introduction to fuzzy control," 2nd ed., Springer-Verlag, Berlin. 1996.

[67] Peter Vas, Artificial-Intelligence-Based Electrical Machines and Drives, Oxford University Press, 1999.

[68] M. N. Uddin, and Hao Wen, “Development of a Self-Tuned Neuro-Fuzzy Controller for Induction Motor Drives," IEEE transaction on Industrial Electronics, vol. 42, no. 4, July/August 2007.

[69] Akio Yamamoto, Yosunori Kitamura, and Yoshihiro Yamane, "Computational Efficiencies of Approximated Exponential Functions for Transport Calculations of the Characteristics Method," Annals of Nuclear Energy, vol. 31, pp. 1027-1037, 2004. Available: www.Sciencedirect.com

[70] N.G. Hingorani, 1995, "Introducing Custom Power in IEEE Spectrum", 32p, pp 41-48.

[71] IEEE Std. 1159-2001R, IEEE Recommended Practice for Power Quality Monitoring

[72] IEC 1000-4-30, Testing and Measurement Techniques - Power Quality Measurement Methods

[73] Bingham, R., 1998, “SAGs and SWELLs”. New Jersey: Dranetz-BMI

[74] Dugan, R., McGranaghan, M., Santoso, S., and Beaty, H.W. 2004. Electrical Power Systems Quality (2nd ed.). New York: McGraw-Hill.

[75] Bollen, M., 1996, Fast assessment methods for voltage sags in distribution systems. IEEE Trans. Ind. Appli., 32: 1414-1423.

[76] G. Yalcinkaya, M.H.J. Bollen and P.A. Crossley, July/Aug 1998, “Characteristics of voltage sags in industrial distribution systems,” IEEE Trans on Industry Appl,, vol. 34, no. 4, pp. 682-688.

[77] E.R.Collins Jr and S.W.Middlekauff, Jan 1998, System and customer impact: considerations for series custom power devices,” IEEE Trans on Power Delivery, vol. 13, no. 1, pp. 278-282.

[78] Djokic, S. and J. Milanovic, 2006, Advanced voltage sag characterization. Part I: Phase shift. IEEE Proc. Generation. Transmission, Distribution, 153: 423-430. DOI: 10.1049/ip-gtd:20050350

[79] ElShennawy, T., M. El-Gammal and A. Abou-Ghazala, 2009. Voltage sag effects on the process continuity of a refinery with induction motors loads. Am. J. Applied Sci., 6: 1626-1632.

[80] Woodley, N., R. Morgan and A. Sundaram, 1999. Experience with an inverter-based dynamic voltage restorer. IEEE Trans. Power Delivery, 14: 1181-1185.

[81] Etxeberria-Otadui, I., U. Viscarret, S. Bacha, M. Caballero and R. Reyero, 2002. Evaluation of different strategies for series voltage sag compensation. Proceeding of the IEEE 33rd Annual Power Electronics Specialists Conference, June 23-27, Cairns, Queensland, Australia, pp: 1797-1802.

[82] C. Zhan, V.K. Ramachandaramurthy, A. Arulampalam, C. Fitzer, S. Kromlidis, M. Barnes, N. Jenkins, 2001, "Dynamic voltage restorer based on voltage space vector PWM control" in Proc. Applied Power Electronics Conference and Exposition, pp. 1301- 1307

[83] J. H. Han, II D. Seo, l. G. Shon, H. j. jeon, 2007, 'Development of On-line type Dynamic Voltage Compensation System Using Supercapacitor', The 7th International Conference on Power Electronics October 22-26, EXCO, Daegu, Korea.

[84] Y. Li, Y. l. Wang, B. h. Zhang, C. x. Mao, 2008, 'Modeling and Simulation of Dynamic Voltage Restorer Based on Super Capacitor Energy Storage' International Conference on Electrical Machines and Systems (ICEMS), 17-20 Oct., pp.2064-2066, Wuhan, China.

[85] P. Jayaprakash, B. Singh, D. P. Kothari, A. Chandra, K. Al- Haddad, 2008,'Control of Reduced Rating Dynamic Voltage Restorer with Battery Energy Storage System', IEEE Power India Conference, 12-15 Oct., pp: 1-8, New Delhi, India.

[86] C. Zhan, M. Barnes, V.K. Ramachandarmurthy, N. JenkinsJ, 2000, Dynamic Voltage Restorer with Battery Energy Storage for Voltage Dip Mitigation, Power Electronics and Variable Speed Drives, 18-19 September, Conference Publication No. 475 0 IEE 2000

[87] W. J. Xu, A. S. Yueyue, 2008, 'A Survey on Control Strategies of Dynamic Voltage Restorer' 13th International Conference on Harmonics and Quality of Power (ICHQP), Sept. 28 -Oct. 1, pp: 1-5, Wollongong, NSW.

[88] J. G. Nielsen, F. Blaabjerg, 2005, A Detailed Comparison of System Topologies for Dynamic Voltage Restorers' IEEE transactions on industry applications, vol. 41, No.5, September October.

[89] H. Kim, J. H. Kim, S. K. Sul, 2004, "A design consideration of output filters for dynamic voltage restorers," Power Electronics Specialists Conference. PESC 04.2004 IEEE 35th Annual, Volume 6, 20-25 June 2004 Page(s):4268 - 4272 Vo1.6

[90] ElShennawy, Abdel-Mon'em Moussa, M. El-Gammal and A. Abou-Ghazala, 2010. "A Dynamic

Voltage Restorer for Voltage Sag Mitigation in a Refinery with Induction Motor Loads", Am. J. Applied Sci. 3(1): 144-151, 2010.

[91] Jing, W., X. Aiqin and S. Yueyue, 2008. A survey on control strategies of dynamic voltage restorer.Proceeding of the IEEE 13th International Conference Harmonics and Quality of Power (ICHQP), Sept. 28-Oct. I, Wollongong, NSW., pp: 1-5. DOI: 10.1109/ICHQP.2008.4668845

[92] Meyer, C. Romaus, C. Doncker, R. W., 2005, “Optimized Control Strategy for a Medium-Voltage DVR”. Power Electronics Specialists Conference, IEEE, pp: 1887-1993.

[93] Nielsen, J. G. Blaabjerg, F. and Mohan, 2005, N. “Control Strategies for Dynamic Voltage Restorer Compensating Voltage Sags with Phase Jump”. Applied Power Electronics Conference and Exposition, IEEE, Vol.2 pp: 1267-1273.

[94] Kim, H., 2002, “Minimal energy control for a dynamic voltage restorer”. Proceedings of PCC Conference, IEEE, vol. 2, Osaka (JP), pp: 428–433.

[95] V.K. Ramachandaramurthy, A. Arulampalam, C. Fitzer, C. Zhan, M. Barnes and N. Jenkins, July 2004 “Supervisory control of dynamic voltage restorers “IEEE Proc.- Gener. Transm. Distrib. Vol. 151, No. 4, pp. 509-516.

[96] Benachaiba, C. and B. Ferdi, 2008. Voltage quality improvement using dynamic voltage restorer. Elect. Power Quality Utiliz. J., 14: 39-46.

Appendix - A

Induction Motor Parameters

Name of the Parameter	**Simulation Model**
Number of Phases	3
Number of Pole Pairs (P)	2
Rated Frequency (Hz)	50
Rated Speed (rad/sec)	150
Rated Power (HP)	10
Rated Input Line to Line Voltage (V)	460
Mutual Inductance, L_m (H)	10.46e-3
Stator Leakage Inductance, L_{ls} (mH)	0.3027
Rotor Leakage Inductance, L_{lr} (mH)	0.3027
Stator Resistance per Phase, R_s (Ω)	14.85e-3
Rotor Resistance per Phase, R_r (Ω)	9.295e-3
Inertia Constant, J ($K\text{-}m^2$)	3.1
Rotor Damping Constant, Bm (N.m.s)	0.08

Appendix - B

Subsystems for MATLAB/ Simulink Model

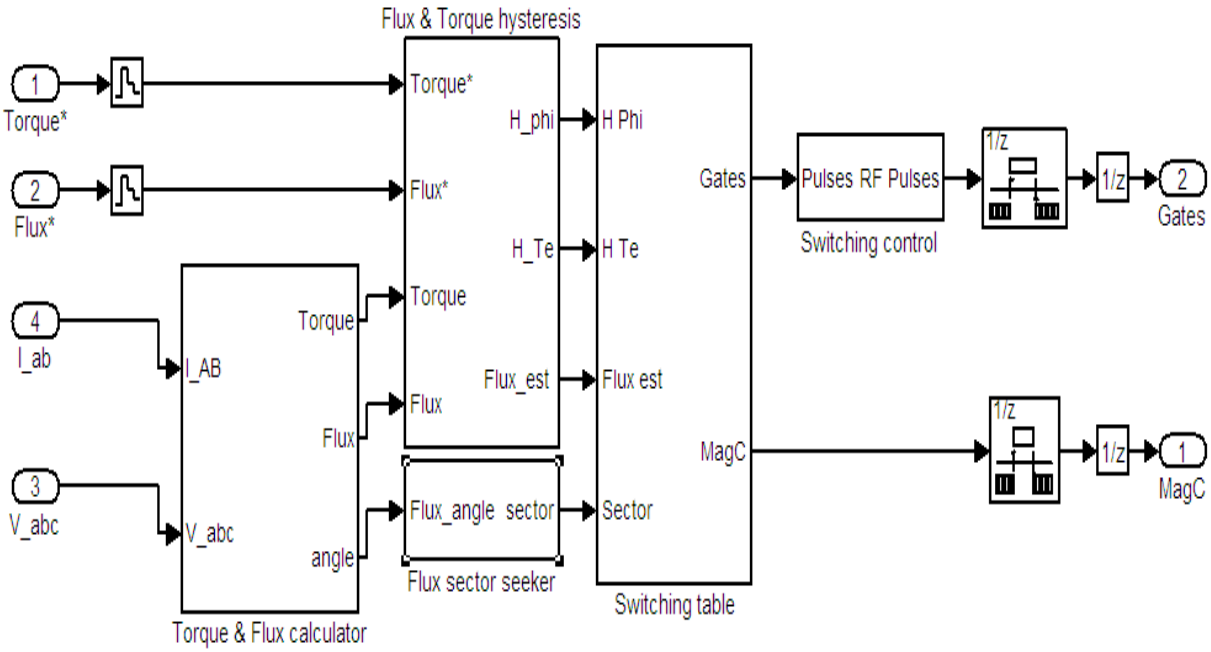

B.1: Direct Torque Control (DTC) Subsystem

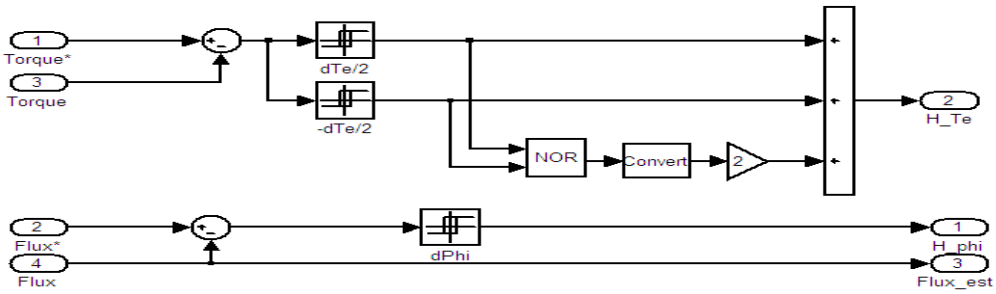

B.2: Torque and Flux Hysteresis Subsystem

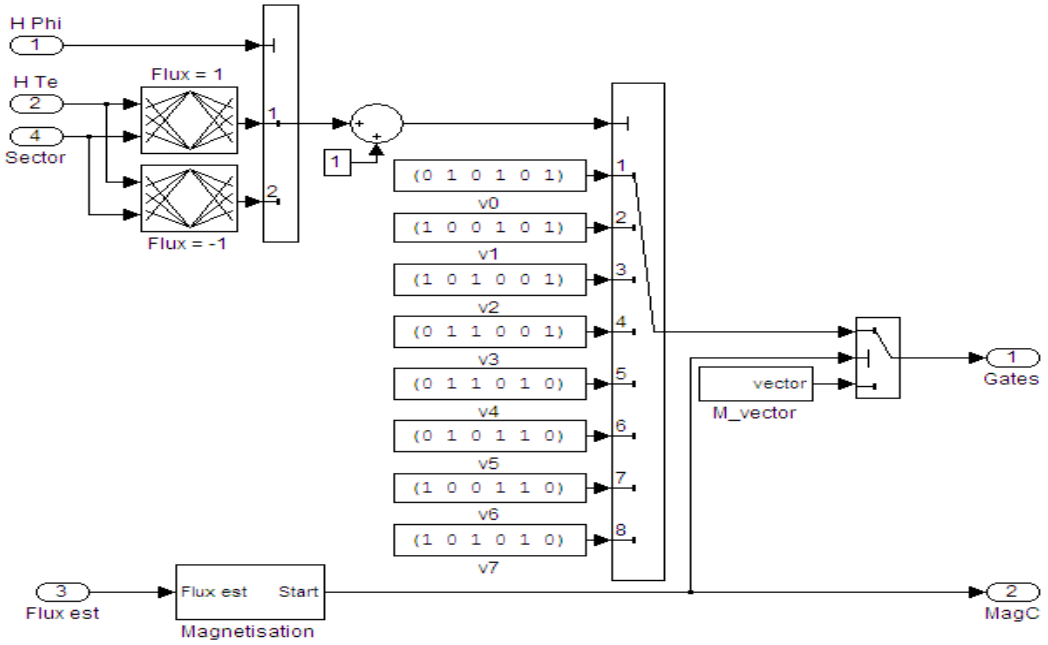

B.3: Subsystem for 'Switching Table'

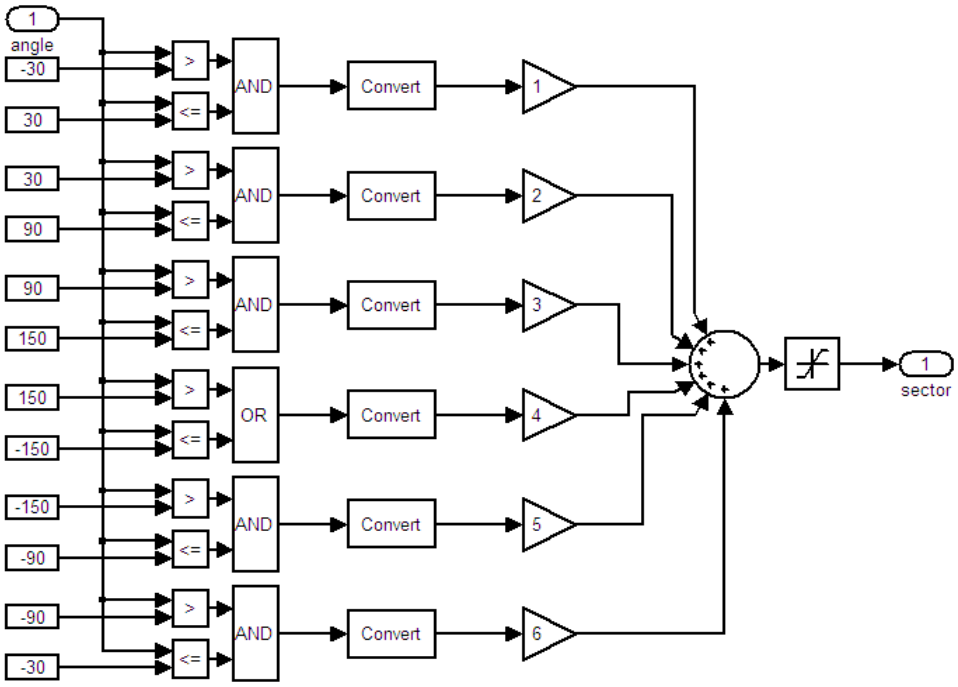

B.4: Subsystem for 'Flux Sector Selector'

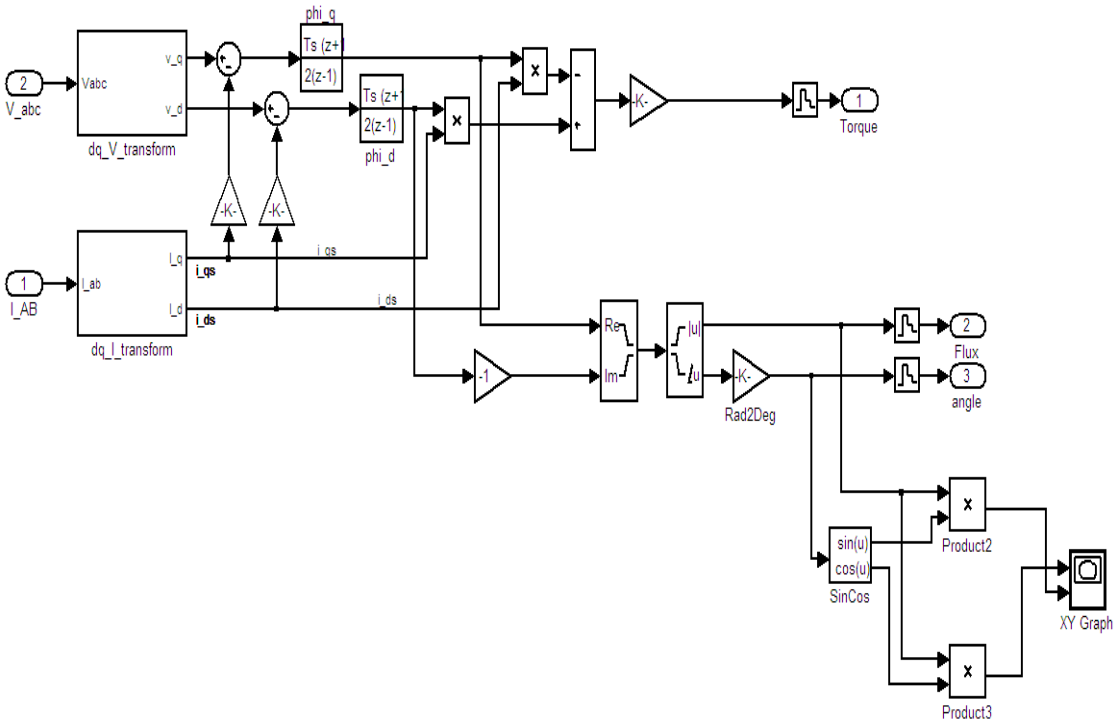

B.5: 'Flux and Torque Estimation' Subsystem

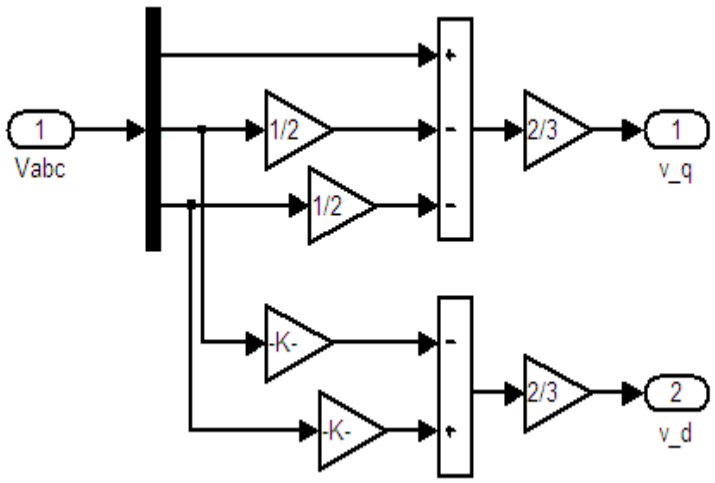

B.6: Subsystem for 'Stator Voltage abc to dq Transformation'

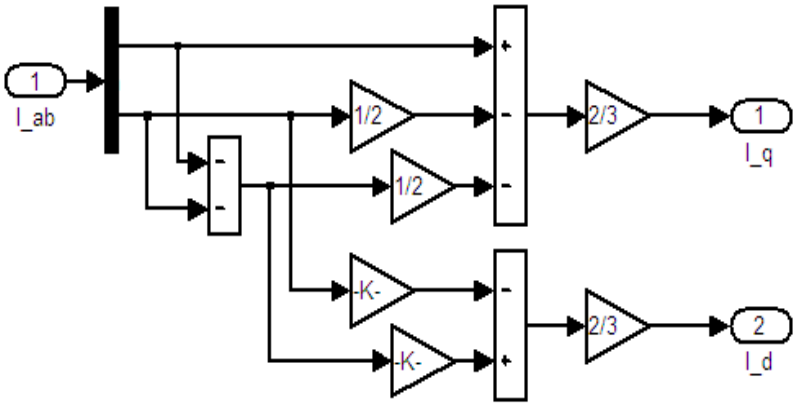

B.7: Subsystem for ‘Stator Current abc to dq Transformation’

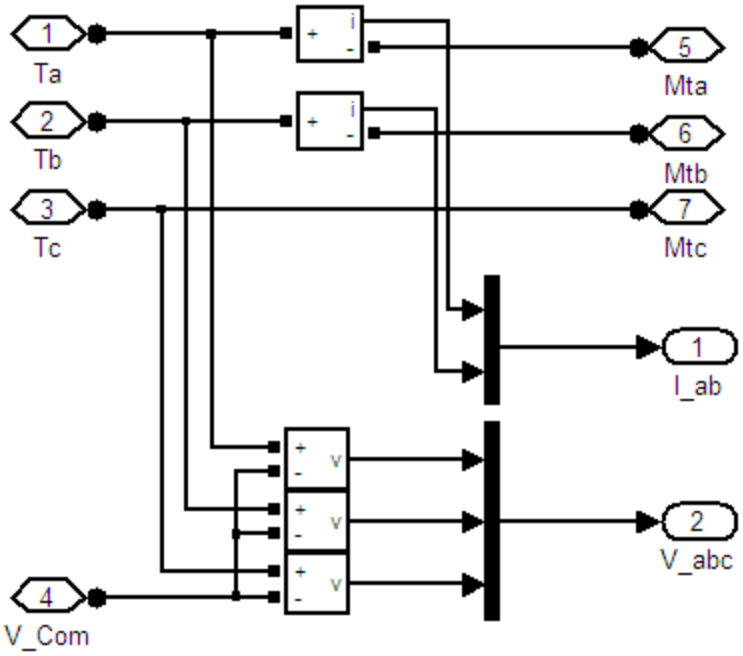

B.8: Subsystem for Electrical Measurements

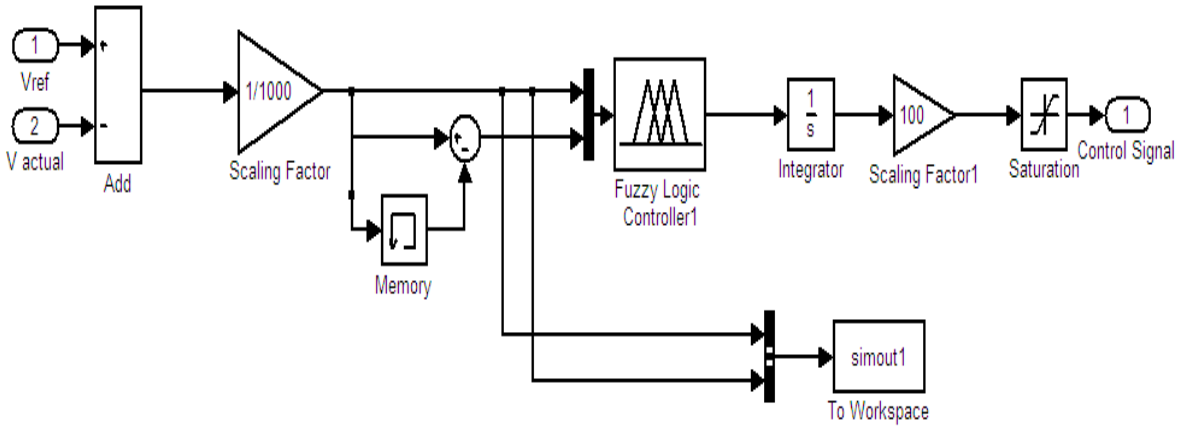

B.9: Fuzzy Logic Controller Subsystem for Dynamic Voltage Restorer (DVR)

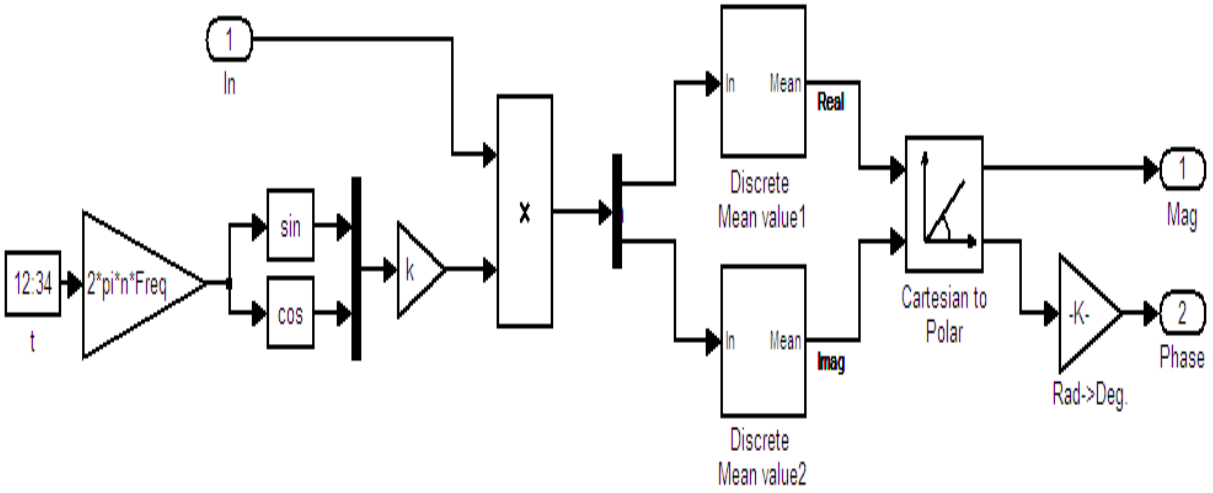

B.10: Subsystem for DVR Supply Voltage Phase and Magnitude Calculation

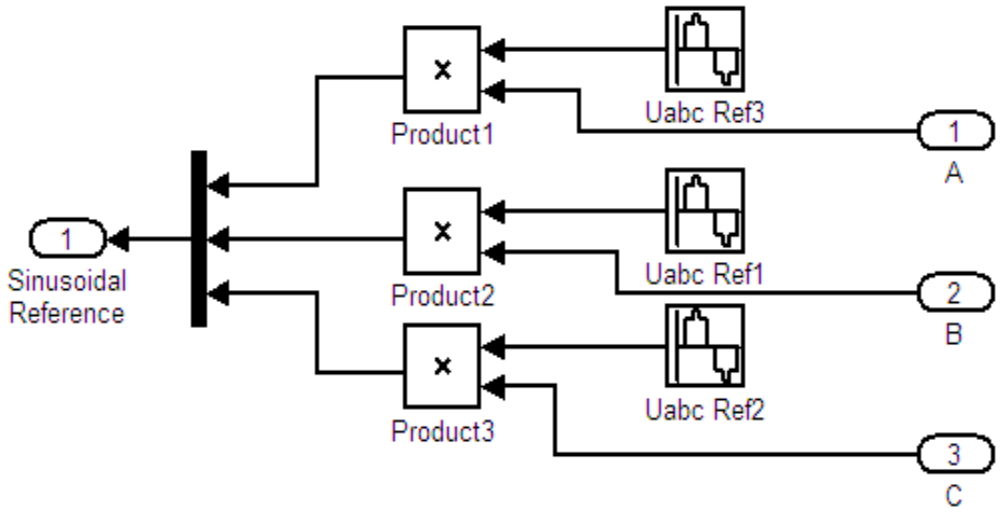

B.11: 'Sinusoidal Reference Generation' Subsystem for Sine Pulse Width Modulation in Dynamic Voltage Restorer (DVR)

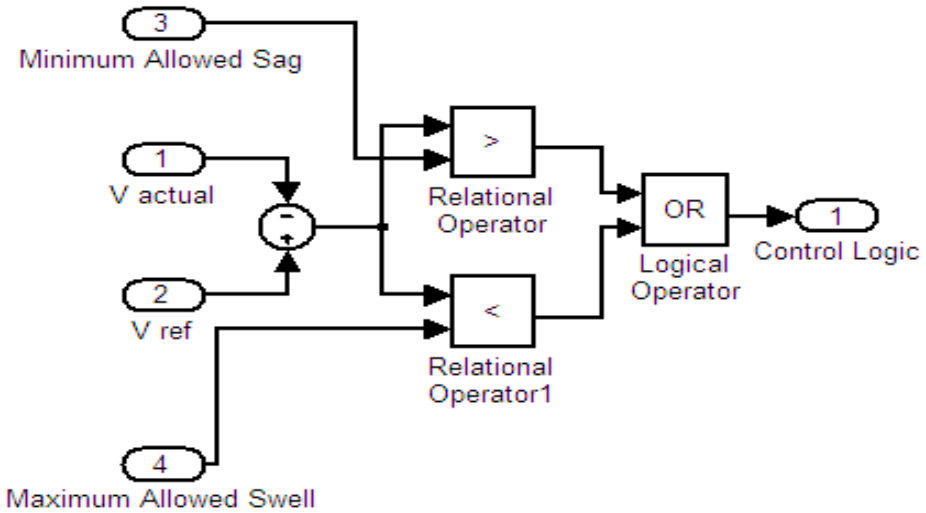

B.12: Subsystem for DVR Triggering Circuit

Appendix – C

Fuzzy Rule Base for the Proposed ANFIS Controller

1. If (speed error is NB) and (change in error is NB) then (output1 is NS) (1)
2. If (speed error is NB) and (change in error is NM) then (output1 is NS) (1)
3. If (speed error is NB) and (change in error is NS) then (output1 is NS) (1)
4. If (speed error is NB) and (change in error is NS) then (output1 is NS) (1)
5. If (speed error is NB) and (change in error is PS) then (output1 is NM) (1)
6. If (speed error is NB) and (change in error is PM) then (output1 is NS) (1)
7. If (speed error is NB) and (change in error is PB) then (output1 is Z) (1)
8. If (speed error is NM) and (change in error is NB) then (output1 is NS) (1)
9. If (speed error is NM) and (change in error is NM) then (output1 is NS) (1)
10. If (speed error is NM) and (change in error is NS) then (output1 is NB) (1)
11. If (speed error is NM) and (change in error is Z) then (output1 is NM) (1)
12. If (speed error is NM) and (change in error is PS) then (output1 is NS) (1)
13. If (speed error is NM) and (change in error is PM) then (output1 is Z) (1)
14. If (speed error is NM) and (change in error is PB) then (output1 is PS) (1)
15. If (speed error is NS) and (change in error is NB) then (output1 is NS) (1)
16. If (speed error is NS) and (change in error is NM) then (output1 is NB) (1)
17. If (speed error is NS) and (change in error is NS) then (output1 is NM) (1)
18. If (speed error is NS) and (change in error is Z) then (output1 is NS) (1)
19. If (speed error is NS) and (change in error is PS) then (output1 is Z) (1)
20. If (speed error is NS) and (change in error is PM) then (output1 is PS) (1)

21. If (speed error is NS) and (change in error is PB) then (output1 is PM) (1)
22. If (speed error is Z) and (change in error is NB) then (output1 is NB) (1)
23. If (speed error is Z) and (change in error is NM) then (output1 is NM) (1)
24. If (speed error is Z) and (change in error is NS) then (output1 is NS) (1)
25. If (speed error is Z) and (change in error is PB) then (output1 is PB) (1)
26. If (speed error is Z) and (change in error is Z) then (output1 is Z) (1)
27. If (speed error is Z) and (change in error is PS) then (output1 is PS) (1)
28. If (speed error is Z) and (change in error is PM) then (output1 is PM) (1)
29. If (speed error is PS) and (change in error is NB) then (output1 is NM) (1)
30. If (speed error is PS) and (change in error is NM) then (output1 is NS) (1)
31. If (speed error is PS) and (change in error is NS) then (output1 is Z) (1)
32. If (speed error is PS) and (change in error is Z) then (output1 is PS) (1)
33. If (speed error is PS) and (change in error is PS) then (output1 is PM) (1)
34. If (speed error is PS) and (change in error is PM) then (output1 is PB) (1)
35. If (speed error is PS) and (change in error is PB) then (output1 is PS) (1)
36. If (speed error is PM) and (change in error is NB) then (output1 is NS) (1)
37. If (speed error is PM) and (change in error is NM) then (output1 is Z) (1)
38. If (speed error is PM) and (change in error is NS) then (output1 is PS) (1)
39. If (speed error is PM) and (change in error is Z) then (output1 is PM) (1)
40. If (speed error is PM) and (change in error is PS) then (output1 is PB) (1)
41. If (speed error is PM) and (change in error is PM) then (output1 is PS) (1)
42. If (speed error is PM) and (change in error is PB) then (output1 is PB) (1)
43. If (speed error is PB) and (change in error is NB) then (output1 is Z) (1)
44. If (speed error is PB) and (change in error is NM) then (output1 is PS) (1)
45. If (speed error is PB) and (change in error is NS) then (output1 is PM) (1)

46. If (speed error is PB) and (change in error is Z) then (output1 is PB) (1)

47. If (speed error is PB) and (change in error is PS) then (output1 is PB) (1)

48. If (speed error is PB) and (change in error is PM) then (output1 is PB) (1)

49. If (speed error is PB) and (change in error is PB) then (output1 is PB) (1)

Back Propagation Algorithm for Training the Neural Network of the Proposed ANFIS Controller

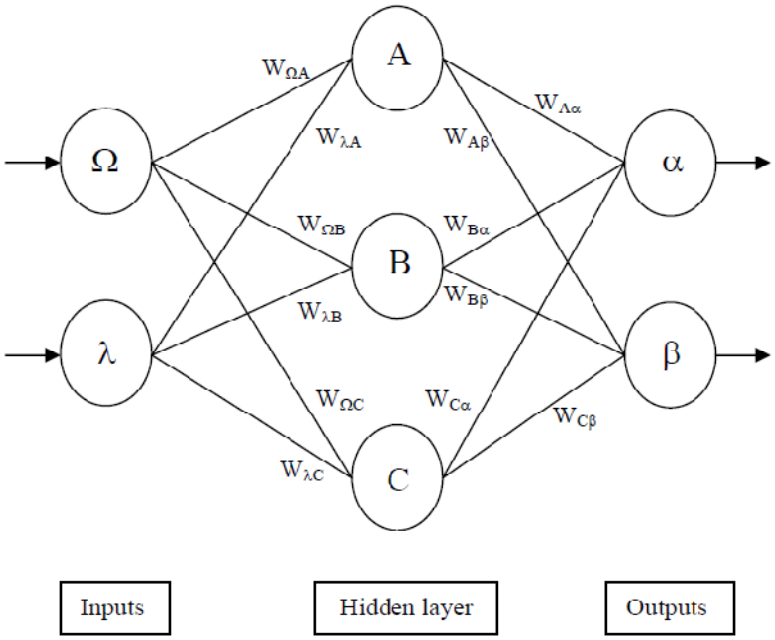

C.1: An example of a Back Propagation NN with two input neurons and two output neurons

The Back Propagation algorithm works as follows:

Step-1: The inputs to the network are applied and the outputs are worked out. This initial output can be anything since the initial weights are random numbers.

Step-2: Then the errors for each of the output neurons are calculated as follows:

$$\delta_\alpha = out_\alpha (1 - out_\alpha) (Target_\alpha - out_\alpha)$$

$$\delta_\beta = out_\beta (1 - out_\beta) (Target_\beta - out_\beta)$$

Where, out_α and out_β are the outputs of the output layer neurons α and β respectively.

$Target_\alpha$ and $Target_\beta$ are the desired output of the output layer neurons α and β respectively.

Step-3: The weights of the output layer neurons are updated as follows:

$$W_{A\alpha}^{+} = W_{A\alpha} + \eta\delta_{\alpha}\, out_{A}$$

$$W_{A\beta}^{+} = W_{A\beta} + \eta\delta_{\beta}\, out_{A}$$

$$W_{B\alpha}^{+} = W_{B\alpha} + \eta\delta_{\alpha}\, out_{B}$$

$$W_{B\beta}^{+} = W_{B\beta} + \eta\delta_{\beta}\, out_{B}$$

$$W_{C\alpha}^{+} = W_{C\alpha} + \eta\delta_{\alpha}\, out_{C}$$

$$W_{C\beta}^{+} = W_{C\beta} + \eta\delta_{\beta}\, out_{C}$$

The constant η (called the learning rate, and nominally equal to one) is put in to speed up or slow down the learning if required.

Step-4: Errors for the hidden layer neurons are calculated. Since, these errors unlike the output layer can't be calculated directly, so back propagation from the output layer (hence the name of the algorithm) is done. This is done by taking the errors from the output layer neurons and running them back through the weights to get the hidden layer errors. Mathematically it can be expressed as:

$$\delta_{A} = out_{A}(1 - out_{A})\,(\delta_{\alpha}W_{A\alpha} + \delta_{\beta}W_{A\beta})$$

$$\delta_{B} = out_{B}\,(1 - out_{B})\,(\delta_{\alpha}W_{B\alpha} + \delta_{\beta}W_{B\beta})$$

$$\delta_{C} = out_{C}\,(1 - out_{C})\,(\delta_{\alpha}W_{C\alpha} + \delta_{\beta}W_{C\beta})$$

Step-5: In this step, having obtained the errors for the hidden layer neurons, now the hidden layer weights are updated in a way similar to that of the output layer neurons. The hidden layer weight change can be expressed as:

$$W_{\lambda A}^{+} = W_{\lambda A} + \eta\delta_{A}\, in_{\lambda}$$

$$W_{\Omega A}^{+} = W_{\Omega A} + \eta\delta_{A}\, in_{\Omega}$$

$$W_{\lambda B}^{+} = W_{\lambda B} + \eta\delta_{B}\, in_{\lambda}$$

$$W_{\Omega B}^{+} = W_{\Omega B} + \eta \delta_B \, in_{\Omega}$$

$$W_{\lambda C}^{+} = W_{\lambda C} + \eta \delta_C \, in_{\lambda}$$

$$W_{\Omega C}^{+} = W_{\Omega C} + \eta \delta_C \, in_{\Omega}$$

The flow chart of the complete process is given below.

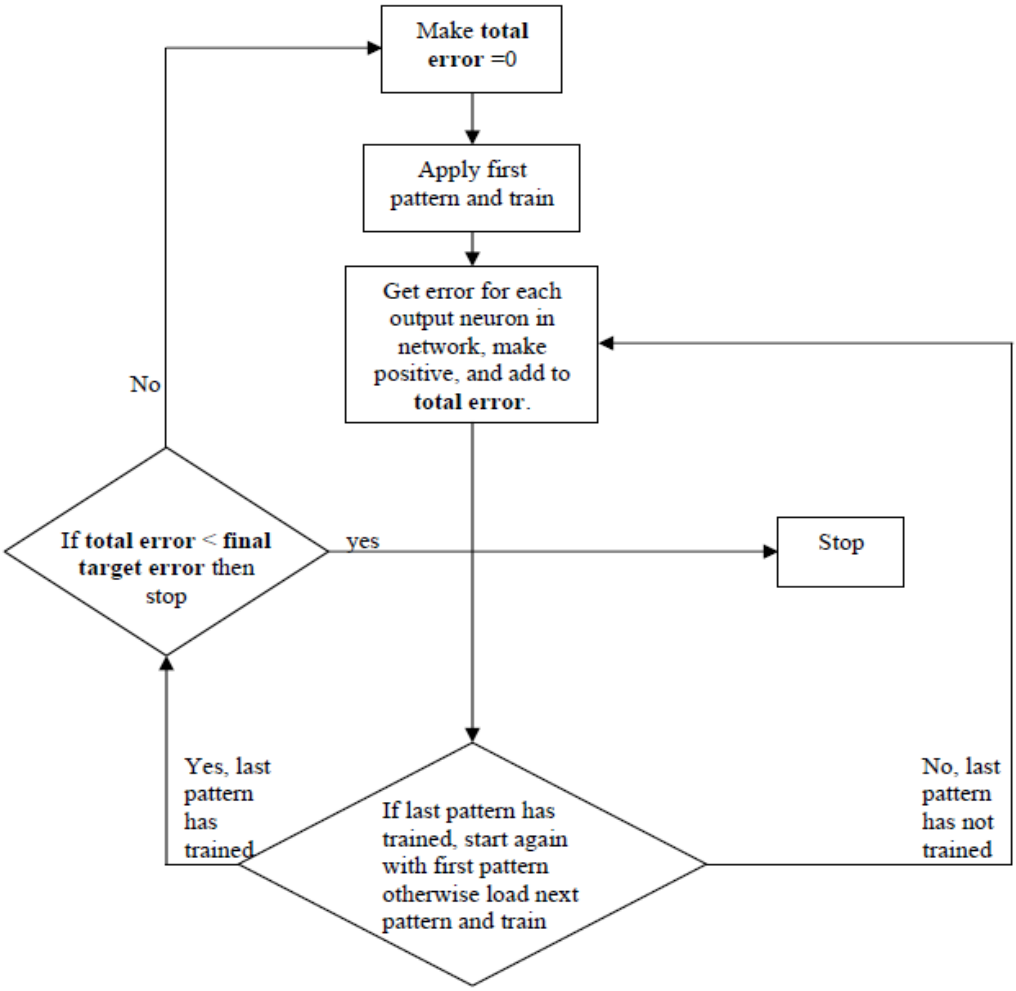

C.2: Flow chart for back propagation algorithm

By repeating this method network of any number of layers can be trained.